



TECHNICAL UNIVERSITY OF CRETE
SCHOOL OF ENVIRONMENTAL ENGINEERING
ENERGY MANAGEMENT IN THE BUILT ENVIRONMENT
LABORATORY

«Analysis of Nature-based Solutions in urban areas»

Master Thesis
Submitted in the
School of Environmental Engineering
from
Dimitrios E. Xilas
Environmental Engineer
Chania,
March, 2021

«Analysis of Nature-based Solutions in urban areas»

Dimitrios E. Xilas

Examination committee:

Advisor Professor:

Dionysia Kolokotsa, *Professor in the School of Environmental Engineering*

Members:

Mihalis Lazaridis, *Professor, Dean of the School of Environmental Engineering*

Nikolaos Nikolaidis, *Professor in the School of Environmental Engineering*

Date of examination:

*"Η παιδεία, καθάπερ
ευδαίμων χώρα, πάντα
τ' αγαθά φέρει."*

Σωκράτης (469 -399 π.Χ, Φιλόσοφος)

ACKNOWLEDGMENTS

This master thesis was based on the ideas of my supervisor Professor, Kolokotsa Dionysia, whom I would like to thank for our productive and pleasant collaboration, her constant interest, as well as for the opportunity she gave me to deal with a topic of my interest. The most important thing in our social interaction beyond the academic issues is that next to her I evolved and improved as a person, so I would like to thank her from the bottom of my heart.

At the same time I would like to make a special mention to my colleague environmental engineer, Ms Georgopoulou Maria who with selflessness, patience and constant encouragement when the time was pressing, played a catalytic role in the elaboration of my diploma thesis. Warm thanks to my colleagues from Energy Management in the Built Environment Research laboratory, Environmental Engineers Mr Konstantino Gobaki and Ms Katerina Lilli for their constant encouragement and catalytic assistance.

Finally, I would like to warmly thank my parents Emmanuel Xylas and Garyfallia Panousi-Vogeli and my brother Panagiotis Xylas for always willing to help and support me.

At last but not least I would like to say that I am grateful to my wife, Ms Kalogeropoulou Styliani for the patience and understanding she has shown. Also the psychological and spiritual support he gave me was crucial in order to finalize my master thesis.

ABSTRACT

In the last decades, the urbanization of city centers combined with the intense degradation of their natural greenery has inevitably led to the development of new sustainable and eco-friendly man-made solutions to increase greenery areas. Nature-based Solutions (NBS) seem to be a viable and innovative strategy towards climate change mitigation with direct impact in socio-economic and ecological conditions and functions of urban life. Studies shows that the city of Chania, Crete, Greece, experiences problems of urban overheating. The case study area examined is the Municipal Garden of Chania, located in the centre of the city and its surrounding area. The aim of the current study is to evaluate the Cool Island Effect of the case study area and also to utilize ENVI-met software to simulate and characterize the influence of the spatial arrangement of different NBS and cool materials on local temperature reduction. The cooling capacity of different green infrastructure elements (i.e. urban parks, street trees, green pavements), as well as the effect of vegetation cover and tree diversity are assessed. The evaluated scenarios include the replacement of the conventional pavement material by cool material and different types of tree planting along the sidewalks or by the combination of them, the application of a green canopy in a pedestrian road, as well as the application of greenery and cool materials separately in specific areas of Chania, Crete, Greece.

Contents

1.	Introduction and State of the Art.....	1
1.1	Definition of Urban Heat Island Effect	2
1.2	Nature Based Solutions	5
1.3	Cool Materials	9
1.4	Impact Evaluation Framework for Planning and Evaluation of NBS Projects.....	10
1.4.1	Contribution of NBS to Climate Resilience and Green Space Management ..	11
2.	Materials and Methods	15
2.1	Description of the case study area	15
2.2	Environmental simulation of study area	17
2.3	ENVI-met – Mathematical considerations of the Atmospheric Model	18
2.3.1	Description of the Mean Air Flow.....	18
2.3.2	Temperature and Humidity.....	19
2.3.3	Atmospheric turbulence.....	20
2.3.4	Radiative Fluxes	22
2.4	ENVI-met – Mathematical considerations of the Soil Model	24
2.5	ENVI-met – Mathematical considerations of the Vegetation Model	25
2.5.1	Turbulent fluxes of heat and vapour.....	26
2.5.2	Stomatal resistance	27
2.5.3	Energy balance of the leaf	28
2.5.4	Water balance of the plant/soil system.....	29
2.6	ENVI-met – Mathematical considerations of Ground Surface and Building Surfaces 29	
2.6.1	Radiative fluxes	30
2.6.2	Turbulent fluxes of sensible heat and vapor	31
2.6.3	Soil heat flux and heat flux through building walls.....	32
2.7	Methodology and Input data of study.....	33
2.8	Numerical aspects and simulation techniques	15
3.	Scenarios description.....	46
3.1	CS1-Cool Pavements.....	46
3.2	CS2-Green Pavements.....	47

3.3	CS3-Combination Cool and Green Pavements	48
3.4	F2 Street Trees Scenario.....	48
3.5	K2 Street Trees Scenario	48
3.6	Green Canopy Scenario.....	49
4.	Simulation Results.....	51
4.1	Baseline senario results	51
4.2	Cool Pavement scenario results.....	52
4.3	Green Pavements scenario results	55
4.4	Combination of Cool and Green Pavements scenario results.....	58
4.5	F2 Street Trees Scenario.....	65
4.6	K2 Street Trees Scenario	69
4.7	Green Canopy Scenario.....	72
5.	Discussion	80
	References	85

List of Figures

Figure 1:	NBS examples, categorized based on building, local and region scale.	6
Figure 2:	Map of case study area (left). Municipal Garden of Chania (right).	16
Figure 3:	Separation of the case study area.	16
Figure 4:	Temperature and humidity data from a reference weather station at the center of the town of Chania.	34
Figure 5:	Basic meteorological settings.	35
Figure 6:	Summary of initial settings.	35
Figure 7:	Full forcing data.	36
Figure 8:	Input parameters values of asphalt road database.	37
Figure 9:	Input parameters values of concrete pavement grey database.	37
Figure 10:	Input parameters values of cool pavement database.	38
Figure 11:	Input parameters values of red tarta database.	38
Figure 12:	Input parameters values applied in vegetation scenario GA.	39
Figure 13:	Input parameters values applied in vegetation scenario K2.	39
Figure 14:	Input parameters values applied in vegetation scenario F2.	40
Figure 15:	Input parameters values applied in vegetation scenario K1.	40
Figure 16:	Input parameters values applied in vegetation scenario F1.	41
Figure 17:	Input parameters values of green canopy database.	15
Figure 18:	Modelization of case study area.	15
Figure 19:	Implementation of cool pavements in the case study area.	46
Figure 20:	Example on green pavements and its implementation.	47
Figure 21:	Implementation of green pavements in the case study area.	48

Figure 22: Implementation of street trees in the case study area.....	49
Figure 23: Implementation of green canopy in the case study area.	49
Figure 24: Baseline Scenario - Air Temperature (Time 14:00).....	51
Figure 25: Baseline Scenario - Surface Temperature (Time 14:00).....	52
Figure 26: Cool Pavement Scenario - Air temperature (Time 14:00).	53
Figure 27: Comparison Cool Pavement Scenario-Baseline Scenario Air Temperature (Time 14:00).....	54
Figure 28. Cool Pavement Scenario - Surface Temperature (Time 14:00).	54
Figure 29: Comparison Cool Pavement Scenario-Baseline Scenario Surface Temperature (Time 14:00).....	55
Figure 30: Green Pavement Scenario - Air temperature (Time 14:00).	56
Figure 31: Green Pavement Scenario - Surface Temperature (Time 14:00).....	57
Figure 32: Comparison Green Pavement Scenario - Baseline Scenario Surface Temperature (Time 14:00).....	57
Figure 33: Cool and Green Pavement Scenario - Air temperature (Time 14:00).....	58
Figure 34: Comparison Cool and Green Pavement Scenario - Baseline Scenario Air Temperature (Time 14:00).	59
Figure 35: Cool and Green Pavement Scenario - Surface Temperature (Time 14:00).....	60
Figure 36: Comparison Cool and Green Pavement Scenario - Baseline Scenario Surface Temperature (Time 14:00).	60
Figure 37: Cool Pavement Scenario - Air temperature (Time14:00).	62
Figure 38: Cool and Green Pavement Scenario - Air temperature (Time14:00).....	62
Figure 39: Comparison Cool Pavement Scenario - Cool and Green Pavement Scenario Air Temperature (Time 14:00).	63
Figure 40: Cool Pavement Scenario - Surface Temperature (Time 14:00).....	64
Figure 41: Cool and Green Pavement Scenario - Surface Temperature (Time 14:00).....	64
Figure 42: Comparison Cool Pavement Scenario - Cool and Green Pavement Scenario Surface Temperature (Time 14:00).	65
Figure 43: F2 Trees Scenario - Air Temperature (Time 14:00).	66
Figure 44: Comparison F2 Trees Scenario - Baseline Scenario Air Temperature (Time 14:00).	67
Figure 45: F2 Trees Scenario - Surface Temperature (Time 14:00).	68
Figure 46: Comparison F2 Trees Scenario - Baseline Scenario Surface Temperature (Time 14:00).....	68
Figure 47: K2 Trees Scenario - Air temperature (Time 14:00).	70
Figure 48: Comparison K2 Trees Scenario - Baseline Scenario Air Temperature (Time 14:00).	70
Figure 49: K2 Trees Scenario - Surface Temperature (Time 14:00).....	72
Figure 50: Comparison K2 Trees Scenario - Baseline Scenario Surface Temperature (Time 14:00).....	72
Figure 51: Green Canopy Scenario - Air Temperature (Time 14:00).	73
Figure 52: Comparison Green Canopy Scenario - Baseline Scenario Air Temperature (Time 14:00).....	74
Figure 53: Green Canopy Scenario - Surface Temperature (14:00).....	75
Figure 54: Comparison Green Canopy - Baseline Scenario Surface Temperature (Time 14:00).....	75

Figure 55: F2 Trees Scenario - Air Temperature (Time 14:00).	77
Figure 56: K2 Trees Scenario - Air Temperature (Time 14:00).....	77
Figure 57: Comparison K2 Trees Scenario - F2 Trees Scenario Air Temperature (Time 14:00).....	77
Figure 58: F2 Trees Scenario - Surface Temperature (Time 14:00).	78
Figure 59: K2 Trees Scenario - Surface Temperature (Time 14:00).....	79
Figure 60: Comparison K2 Trees Scenario - F2 Trees Scenario Surface Temperature (Time 14:00).....	80

List of Tables

Table 1: Adaptation and mitigation strategies and technologies against UHI effect, based on green and cool technologies.	4
Table 2: Examples of indicators and metrics for assessing the impact of climate mitigation and adaptation actions (CHALLENGE 1), green space management (CHALLENGE 4) and urban regeneration (CHALLENGE 6).	12
Table 3. Categorization of vegetation	36
Table 4. Technical materials' features	36
Table 5. Comparison of different material pavement scenarios to the baseline scenario.....	80
Table 6. Comparison of different tree planting scenarios to the baseline scenario.	82

Chapter 1st

1. Introduction and State of the Art

Cities, representing 2% of the planet's surface and more than 50% of the population (Gaitani et al., 2011; Akbari et al., 2016), serve not only as extensive systems of buildings and transportation, but also as manifestation of economic, social and environmental processes, intimately connected to the changing needs of society, having the potential to protect and ensure quality of life, offering income and employment, and providing hubs for innovation and economic growth (Drahansky Martin et al., 2016). However, cities produce pollution and waste, provoking local scale climate alterations. It is considered that the consumption of resources and energy, which take place to meet the needs of large urban centers, result to up to 75% production of CO₂ emissions (Bai et al., 2018). CO₂ emissions, the anthropogenic heat (Shahmohamadi et al., 2011b; Wang et al., 2018) and the high rise buildings combined with the loss of urban green spaces, due to the excessive urbanization (Mensah, 2014) (Lin et al., 2015), lead to a significant heat stress in the city center comparing to the suburban and rural areas, enhancing the urban heat island (UHI) phenomenon (Lee et al., 2014; Nuruzzaman, 2015; Qiu et al., 2017). Worth to note that the increase rate during the early summer is more intense than the decrease rate of temperatures during autumn (Kolokotsa et al., 2009; Shahmohamadi et al., 2011b). Thus, considering that about half of the human population globally lives in urban areas, it is evident that local climate change and urban heat island present the greatest challenges of cities worldwide (Akbari et al., 2016).

In the last decade, new mitigation and rehabilitation approaches supporting the transition to sustainable urbanization have been proposed to reverse and/or reduce the negative effects of the UHI phenomenon (Filho et al., 2017). These approaches include low carbon infrastructures, green infrastructures or Nature-based Solutions (NBS) and incorporation of cool materials within cities (Christopher M. Raymond et al., 2017; Seddon et al., 2020).

In particular, NBS, which are mainly divided in two major categories: natural and man-made, include provision of urban forms of greenery, such as parks, nature reserves, rooftop gardens, vertical greeneries, street trees (Kabisch et al., 2016). The aforementioned forms of greenery have the potential to ameliorate high temperature

in cities or regulate air and water flows, or the allocation of natural habitat space in floodplains that may buffer impacts of flood events (Kabisch et al., 2016; Watkin et al., 2019). Thus, main benefits of NBS application is that they use natural flows of matter and energy (i.e. natural processes and cycles), taking advantage of local solutions and following the seasonal and temporal changes of the ecosystems (Meli et al., 2014). Moreover, in many cases, NBS could be the answer for cities to help them improving the quality of life, mental and physical health and achieving their commitments towards the Sustainable Development Goals (SDGs), as result to contributing to global sustainability agenda (Christopher M. Raymond et al., 2017).

Additionally, towards the development of more effective urban planning solutions, application of cool materials could also reduce temperature and save energy, ameliorating the buildings' indoor environmental quality and the well-being of citizens in open spaces (Santamouris et al., 2012; Raven et al., 2018). Cool materials appear higher solar reflectance and infrared emittance compared to conventional building and paving materials, therefore can dissipate the absorbed heat, maintaining lower temperatures. Furthermore, they can be easily applied to new and existing surfaces, extending their lifetime (Santamouris et al., 2008; Gaitani et al., 2011; Calautit et al., 2017; Santamouris et al., 2017).

The current study utilizes ENVI-met model to characterize the influence of the spatial arrangement of different NBS and cool materials on local temperature reduction of the Municipal Garden of Chania, located in Chania, Crete, Greece. The cooling capacity of different green infrastructure elements (i.e. urban parks, street trees, green pavements), as well as the effect of vegetation cover and tree diversity were assessed. The evaluated scenarios include the replacement of the conventional pavement material by cool material and different types of tree planting along the sidewalks or by the combination of them, the application of a green canopy in a pedestrian road, as well as the application of greenery and cool materials separately in specific areas.

1.1 Definition of Urban Heat Island Effect

The expansion of highly dense built environments and the resulting increase in

human activities have led to significant temperature differences between urban and rural areas; this phenomenon has come to be known as “Urban Heat Island” (UHI) (Kolokotsa et al., 2013).

The UHI is considered as a multiparametric phenomenon, affected by many different factors (Lee et al., 2017). In general, UHI is caused by the stored heat from radiative imbalances, anthropogenic heat emissions, production of “waste heat” because of energy use (e.g. heating, traffic), lowered wind speeds, a lack of green surfaces that encourage evaporation, and the material properties of buildings and pavement (Santamouris et al., 2011).

To be specific, cities development and building construction lead to wide loss of vegetation as more surfaces are paved or covered. Those ground coverage alterations result in creation of impervious areas which evaporate less water, provide less shade and moisture, to keep urban areas cool, because of deforestation, contributing to elevated surface and air temperatures. Worth to note that, in built environments, the relative influence of UHI on the level of heat stress depends on regional climate conditions and different atmospheric chemical constituents over the city (US EPA, 2008; Nuruzzaman, 2015). In addition, urban areas are densely populated and simultaneously densely constructed, meaning that a lot of people are gathered together in places where buildings are also constructed very close together. People and their tools, such as cars and factories, are always burning off energy which usually escapes in the form of “waste heat” that also contributes to appearance of UHI (Nuruzzaman, 2015).

UHI cause an increase in the risk of heat stress, a condition that is significantly related to human health and life quality in cities (Tomlinson et al., 2011). UHI can affect communities by increasing summertime peak energy demand (Li et al., 2019), air conditioning costs (Arifwidodo and Chandrasiri, 2015; Lundgren-Kownacki et al., 2018), air pollution and greenhouse gas emissions (Li et al., 2018), heat-related illness and mortality (Lai and Cheng, 2010), and water quality (Shahmohamadi et al., 2011a). For instance, UHI can worsen air and water quality of city centers than their rural neighbors because there are more pollutants (waste products from vehicles, industry, and people) being pumped into the air (Rao, 2014). These pollutants are not blocked from scattering and becoming more toxic. In addition, water quality also

suffers, as when warm water from the UHI ends up flowing into local streams, it stresses the native species that have adapted to life in a cooler aquatic environment (Hathway and Sharples, 2012; YUE Wenze and XU Lihua, 2013). UHIs also contribute to energy demands in the summer, straining energy resources. UHIs are often subject to “rolling blackouts,” or power outages. Utility companies start rolling blackouts when they do not have enough energy to meet their customers’ demands. The energy used in electric fans and air conditioning ends up contributing to an even hotter UHI (Li et al., 2019).

Because of these negative impacts, the scientists, who are studying how UHI effect might contribute to global warming, strongly believe that citizens, engineers and city designers have to co-work to reduce anthropogenic impact on urban areas and the heat impact of the surrounding areas (Kabisch et al., 2017). The main available mitigation strategies, against UHI effect, consist of a technologic employment of vegetation (e.g. green technology) in urban areas and the application of materials with peculiar radiative features for roofs and pavements (e.g. cool technology) (Nuruzzaman, 2015; Kabisch et al., 2016).

Table 1: Adaptation and mitigation strategies and technologies against UHI effect, based on green and cool technologies.

Adaptation and mitigation strategies and technologies	Trees and Vegetation	Increasing tree and vegetation cover lowers surface and air temperatures by providing shade and cooling through evapotranspiration. Trees and vegetation can also reduce stormwater runoff and protect against erosion.
	Green Roofs	Growing a vegetative layer (i.e. plants, shrubs, grasses, and/or trees) on a rooftop reduces temperatures of the roof surface and the surrounding air and improves stormwater management. Also called “rooftop gardens” or “eco-roofs,” green roofs achieve these benefits by providing shade and removing heat from the air through evapotranspiration.
	Cool Roofs	Installing a cool roof – one made of materials or coatings that significantly reflect sunlight and heat away from a building – reduces roof temperatures, increases the comfort of occupants, and lowers energy demand.
	Cool Pavements	Using paving materials on sidewalks, parking lots, and streets that remain cooler than conventional pavements (by reflecting more solar energy and enhancing water evaporation) not only cools the pavement surface and surrounding air, but can also reduce stormwater runoff

	and improve nighttime visibility.
Smart Growth	These practices cover a range of development and conservation strategies that help protect the natural environment and at the same time make our communities more attractive, economically stronger, and more livable.

The above table (Table 1) presents some examples of cool materials and green infrastructure involvement and incorporation within cities, as well as their advantages. These solutions provide different benefits not only related to the mitigation potential but also regarding the economic trade-offs of an installation.

1.2 Nature Based Solutions

Adaptation to climate change effects involves a range of measures or actions that can be taken to reduce the vulnerability of society and to improve the resilience capacity against expected changing climate. Possible adaptation measures and solutions to handle climate change can take many forms and be effective at a range of spatial and temporal scales, proactively planned or as a result of socio-political drivers, such as new planning regulations, market demand or even social pressure (Kabisch et al., 2017).

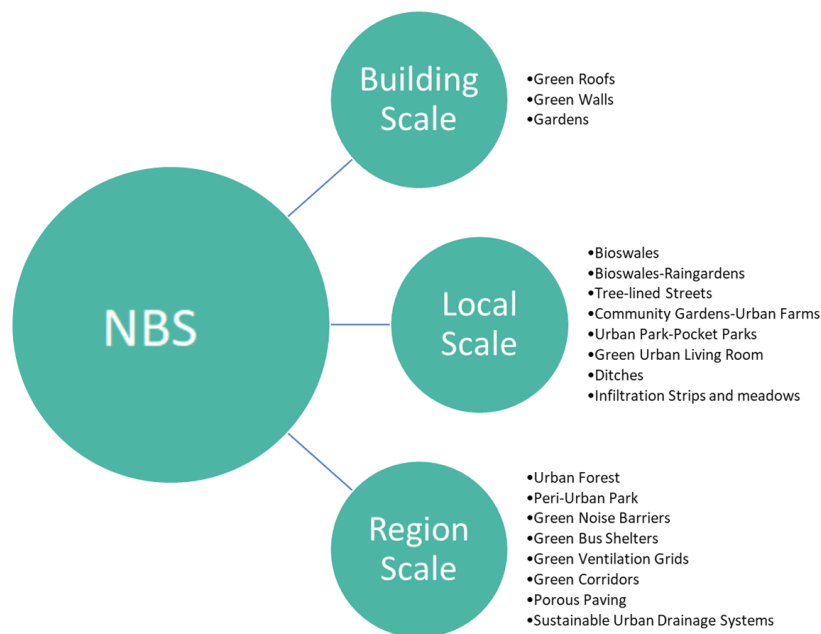


Figure 1: NBS examples, categorized based on building, local and region scale.

Nature Based Solutions (NBS) are solutions inspired and supported by nature in order to tackle challenges such as climate change, food security, water resources, or disaster risk management (Pauleit et al., 2017). In particular, NBS promote the sustainable management (van Ham and Klimmek, 2017), restoring natural or modified ecosystems in urban and rural areas and at the same time they are cost effective (Kronenberg et al., 2017). Thus, NBS provide simultaneous environmental, social and economic benefits, helping build resilience, including stormwater mitigation, biodiversity enhancement, and human well-being (Cohen-Shacham, E; Walters, G; Janzen, C; Maginnis, 2016).

The concept has been adopted by the European Commission, in its research programme EKLIPSE – Horizon 2020, to promote its uptake in urban areas and establish Europe as a world leader of NBS (see 1.4). However, the concept has been defined vaguely and the relationships with already existing concepts and approaches, to enhance nature and its benefits in urban areas, require clarification (Pauleit et al., 2017).

Some representative building and local scale NBS examples in urban areas include incorporation of green roofs and walls, provision of urban green spaces, such as parks and street trees (see Table 1). Small-scale NBS, such as infiltration trenches

and rain gardens, can benefit stormwater management by reducing runoff, flooding, and transport of pollutants (Stovin, 2010; Mak et al., 2017). In addition, individual urban trees, as NBS solution, can have an effect on urban temperatures by contributing to reducing UHI as well (Emilsson and Ode Sang, 2017). For instance, a high plant cover could lead to reduced solar radiation uptake due to high albedo, shading and evapotranspiration of the vegetation system. Worth to mention that the temperature reduction potential through the use of vegetation has been shown to be larger in densely built-up area as compared to more sparse developments, with variation due to prevailing wind direction and time of the day (Emilsson and Ode Sang, 2017). Besides that, the climatic performance of vegetation systems are also dependent on the design and the characteristics of the urban fabric such as the structure and the type of building (Lehmann et al., 2014).

Novel types of vegetation systems such as green roofs and green walls, included in NBS framework, can also alter the energy balance of urban areas. The advantage of these systems is that they can be incorporated as a complement to existing blue and green infrastructure and that they make it possible to utilize spaces that normally are not green.

Particularly, green roofs can serve to temperature reduction and incensement of related energy savings, through reduced cooling loads, as well as to air quality improvement (Alexandri and Jones, 2008). Similarly, development of urban green spaces leads to amelioration of high temperature in cities (Gill et al., 2007). Furthermore, it has been confirmed that green walls present strong ability to reduce wall temperatures (Cameron et al., 2014) and street canyon temperatures with close to 10 °C during the day in hot and dry climates (Alexandri and Jones, 2008).

However, the performance of the urban vegetation also depends on the tree characteristics (i.e. leaf organization and canopy shape), where sparse crowns with large leaves have higher cooling capacity (Leuzinger et al., 2010), the species composition, with different species having varied cooling capacity and different modes of cooling (i.e. evaporative or shade cooling) (Cameron et al., 2014), the management variables (i.e. irrigation and water levels) in the substrate (Song and Wang, 2015) , as well as the substantial seasonality, with stronger effects in summer than early spring. While the aforementioned parameters may cause broad differences

in urban vegetation cooling efficiency, there is also cooling effect variation linked to the level of soil sealing and amount of vegetation, which could explain microclimatic effects (Lehmann et al., 2014).

It is important to remember that a changing climate will have conflicting consequences on the existing plant material. Unfortunately, in many cases, it has been shown that plants experience increasing stress and consequently lower survival and performance rates. Thus, the current selection of the right tree material, like plants with limited maintenance needs, which at the same time fulfill other ecosystem services such as habitat creation and delivering aesthetical values, plays a critical role to achieve high temperature efficiency and the planting design has to be adjusted to accommodate a changing climate (Rahman et al., 2015).

Also, in region scale, NBS are showing great potential in mitigating the effects of extreme weather events (Andersson et al., 2017), slowing and storing stormwater which reduces downstream flooding (Oral et al., 2020). Thus, NBS could act as flexible and adaptable solutions to hydro-meteorological risk, while they have the added potential to be combined with grey infrastructure, which are often referred to as hybrid measures, to provide a range of benefits and cobenefits (Depietri and McPhearson, 2017).

The cobenefits of NBS in urban landscapes are being increasingly recognized as a result of increased provisioning and improved availability of urban green spaces. Despite the important environmental benefits, like reduction of heat and noise, and limitation of water, soil, and air pollution, from a sociocultural perspective, the incorporate vegetation like grasses, shrubs, and trees is capable of improving the quality of life, mental and physical health (e.g. amelioration of waterborne illnesses, respiratory diseases and level of stress), and reinforcing cultural identity through supporting a sense of belonging (Keniger et al., 2013; Hartig et al., 2014).

From economical perspective, the high adaptation ability of NBS solutions to different extreme events can save up great amounts of money when compared to implementation of grey infrastructure alone, and simultaneously NBS with water storage and reuse capabilities can increase agriculture production and incomes of farming communities (Kabisch et al., 2017).

Taking this aspect of multifunctionality into account and considering the cobenefits produced in different domains and contexts, NBS often represent more efficient and cost-effective solutions to climate change threats than more traditional approaches, such as conventional sewage or air conditioning systems (European Commission, 2015), but systematic evaluation frameworks that can assess their full potential, as well as their possible side effects, are still lacking.

Specifically, the findings show that more investigations are required on the assessment of large scale NBS, hybrid measures that combine large and small scale NBS, and catchment scale NBS. Such frameworks are needed in order to quantify the benefits so that decision makers have a better understanding of their advantages and disadvantages. Up to date, most of the available assessing methods, proposed in the literature, such as hydrological and hydraulic modelling, water balance, rainfall runoff estimates, cost-benefit analysis, life cycle costing, and multi-criteria analysis, aim to evaluate potential benefits of future NBS or focus on their hydro-meteorological benefits (Christopher M Raymond et al., 2017; Huthoff et al., 2018). Note that it is recommended the above methods to be combined with interviews and fieldwork so that qualitative and quantitative benefits to be assessed. However, only limited existing frameworks address the evaluation of implemented NBS, providing only qualitative assessments (Christopher M Raymond et al., 2017; Huthoff et al., 2018). Hence, integrated frameworks for quantitative evaluation of implemented NBS are still needed (Watkin et al., 2019).

1.3 Cool Materials

Houses, shops, and industrial buildings could also contribute to the UHI effect arise when they are constructed and located close together. Building materials are usually very good at insulating and holding of heat, making the areas around buildings warmer. In addition, the change of urban surface albedo by the building materials and pavements leads to a significant difference in the thermal balance of cities versus their surroundings (Taha, 1997; Zaragoza and Bartolom, 2012). Building materials and pavements absorb solar and infrared radiation, part of which is dissipated to the atmosphere, resulting in an increase of the ambient temperature (Shahmohamadi et al., 2011b). Thus, it is evident that the selection of buildings' and pavements'

materials influences the energy consumption and indoor environmental quality of buildings as well as the users' well-being in open spaces.

However there are specific materials, known as cool materials, presenting higher solar reflectance and infrared emittance (i.e. higher emissivity factor), which can dissipate the absorbed heat (Santamouris et al., 2011; Santamouris et al., 2012), while their use is also related to energy benefits as the cooling load of buildings is significantly reduced (Santamouris et al., 2008). Therefore, cool materials can maintain lower temperatures compared to conventional building and paving materials (Santamouris et al., 2008; Gaitani et al., 2011). Thus, such materials could be used in paths, roads and other urban structures and be easily applied to new and/or existing building rooftops, significantly contributing to the reduction of surface temperatures, up to several degrees, as well as the extending of the lifetime of the surfaces they are applied to (Santamouris et al., 2011; Karlessi and Santamouris, 2013; Santamouris et al., 2011). Worth to note that, although highly reflective materials have been extensively tested in cool roof applications, existing data on their potential to mitigate UHI effect when used in pavements and other urban structures is very limited.

1.4 Impact Evaluation Framework for Planning and Evaluation of NBS Projects

The European Commission requested the EKLIPSE project in order to help building up an evidence and knowledge base on the benefits and challenges of applying NBS. The aim of EKLIPSE Expert Working Group (EWG) activity is to devise an impact evaluation framework that can guide the design, development, implementation and assessment of NBS demonstration projects in urban contexts. The framework takes into account insights from recent studies into the mapping and assessment of ecosystems and their services, ecosystem- based adaptation projects, and relevant information on climate adaptation, natural water retention, green infrastructure, and greening. The EWG methodological approach involved a quick scoping review of the literature combined with expert consultation within and outside the EWG. The EWG selected the following ten (10) challenges from the expert report on NBS supported by DG Research and Innovation (European Commission, 2016, 2015) and a recent review of NBS frameworks (Kabisch et al., 2017, 2016):

- 1) Climate mitigation and adaptation;
- 2) Water management;
- 3) Coastal resilience;
- 4) Green space management (including enhancing/conserving urban biodiversity);
- 5) Air/ambient quality;
- 6) Urban regeneration;
- 7) Participatory planning and governance;
- 8) Social justice and social cohesion;
- 9) Public health and well- being;
- 10) Potential for new economic opportunities and green jobs, cities and other European Commission based initiatives (Christopher M Raymond et al., 2017)

Among the above mentioned, the two challenges that were mainly considered in the present study were the “Contribution of NBS to Climate Mitigation and Adaptation” and the “Green Space Management”.

1.4.1 Contribution of NBS to Climate Resilience and Green Space Management

Climate resilience is based on two interacting concepts, the “adaptation”, that is the capacity to react and respond to an external stimulus or stress such as climate change, and “mitigation”, that is the potential of improving the current status of a parameter or driver through active or passive behavior, in this case through reducing greenhouse gas emissions or sequestering carbon. In the case of NBS, which involve elements of ecosystems, the two concepts are closely linked as any adaptation of an ecosystem can further influence the mitigation potential (e.g. by sequestering carbon in vegetation), with an overall dramatic effect on climate resilience (Calfapietra et al., 2015; van Vuuren et al., 2011).

One of the major issues in implementing NBS for urban climate resilience and in understanding their potential impact and effectiveness is related to the scale of intervention. Action on climate mitigation can span the micro level of a single building, the meso level of the whole city or country and the macro level of the entire planet, though it has essentially a macro (global) scale effect through affecting global concentrations of greenhouse gases. Climate adaptation is more often planned and implemented at the meso (national) to micro (local) level, and the impacts are also at these levels. There are some common actions and indicators, but also some that are

specific to the different scales of climate action to be addressed, as identified below (see Table 2).

Table 2: Examples of indicators and metrics for assessing the impact of climate mitigation and adaptation actions (CHALLENGE 1), green space management (CHALLENGE 4) and urban regeneration (CHALLENGE 6).

CHALLENGES	TYPE OF INDICATORS	EXAMPLES OF METRICS
CHALLENGE 1: Climate mitigation & adaptation	Carbon savings per unit area (environmental, chemical) Carbon storage and sequestration in vegetation and soil (Davies et al., 2011; Demuzere et al., 2014).	Tonnes of carbon removed or stored per unit area per unit time (Zheng et al., 2013), total amount of carbon (tonnes) stored in vegetation (Davies et al., 2011). Comparison with calculations of carbon consumption of equivalent non-NBS actions (e.g. through Life Cycle Assessment). Allometric forest models of carbon sequestration, developed using proxy data obtained from Lidar data (Giannico et al., 2016). Growth rates derived from Forest Inventory Analysis (Zheng et al., 2013).
	Carbon savings per unit area (economic) Value of carbon sequestration by trees (Baró et al., 2014).	Measurements of gross and net carbon sequestration of urban trees based on calculation of the biomass of each measured tree (i-Tree Eco model), translated into avoided social costs of CO ₂ emissions (USD t-1 carbon).
	Temperature reduction (environmental, physical)	Decrease in mean or peak daytime local temperatures (°C) (Demuzere et al., 2014). Measures of human comfort e.g. ENVIMET PET – Personal Equivalent Temperature, or PMV – Predicted Mean Vote. Heatwave risks (number of combined tropical nights (>20°C) and hot days (>35°C)) following Fischer, Schär, 2010, cited by (Baró et al., 2015).
	Energy and carbon savings from reduced building energy consumption (environmental, physical)	kWh/y and t C/y saved.
CHALLENGE 4: Green Space Management	Social indicators (benefits)	Distribution of public green space – total surface or per capita (Badiu et al., 2016; Gómez-Baggethun and Barton, 2013; La Rosa et al., 2016). Accessibility (measured as distance or time) of urban green spaces for population (Tamosiunas et al., 2014). Recreational (number of visitors, number of recreational activities) or cultural (number of cultural events, people involved, children in educational activities) value (Kabisch and Haase, 2014).
	Environmental (biological)	Changes in the pattern of structural and

		functional connectivity (Iojă et al., 2014).	
		Species richness and composition in respect to indigenous vegetation and local/national biodiversity targets (M. Cohen et al., 2012; Krasny et al., 2013).	
CHALLENGE 6: Urban Regeneration	Urban green indicators (environmental, biological)	Urban green: Index of biodiversity, provision and demand of ecosystem services.	
		Ecological connectivity (Pino and Marull, 2012).	
		Accessibility (Schipperijn et al., 2010): distribution, configuration, and diversity of green space and land use changes (multi-scale; (Goddard et al., 2010)	
			Ratio of open spaces to built-form.
			Reclamation of contaminated land: percentage of contaminated area reclaimed.
	Building efficiency and environmental design indicators		Reclamation of building materials: percentage reclaimed from existing buildings.
			Energy efficiency: building materials/construction methods based on points awarded according to energy efficiency checklist.
			Incorporation of environmental design: percentage of total building stock.
			Land devoted to roads: percentage of site area occupied by roads.
	Socio-cultural indicators		Conservation of built heritage resources: percentage of built from retained for culture.
			Land dedicated to pedestrians: percentage of road network.
			Public transport links: walking distance to nearest facilities.
		Access to open space: average journey time for residents/employees by foot or average distance to sports center, recreation area, or green space.	
		Access to cultural facilities: average journey time for residents on foot or average distance to cultural center.	
		Access to housing: affordability and choice.	
		Level of devices contributing to the safety of users in the neighborhood: lighting of common areas, access control, presence of technical, or specialized staff, etc.	

Chapter 2nd

2. Materials and Methods

This chapter describes the basic characteristics (i.e., climatic and vegetation conditions) of the study area, presents the microscale atmospheric model ENVI-met Version 4.4 (Bruse, 2004; Bruse and Fleer, 1998) and its basic mathematical considerations, which are generally used in environmental simulations, analyses the methodology developed in the present study, as well as the input data which were provided in the model, to simulate and characterize the influence of the spatial arrangement of different NBS and cool materials on local temperature reduction of the study area based on different scenarios.

2.1 Description of the case study area

Chania is a north oriented coastal town defined by the Aegean Sea at its northeast border and located in a plain, at the base of a large circular shaped peninsula named Akrotiri. The southern part of the plain is constricted by the White Mountains with more than 2000 m altitude. The city's population is about 53910 inhabitants. The climatic conditions are typical Mediterranean with mild rainy winters and hot dry summers. The atmosphere is always warm, but fierce heat waves (temperatures above 38 °C) are not very common, since the prevailing Etesian winds blow from northern directions and pleasantly moderate the conditions. However, in recent years there has been a strong impact of climate change on the microclimate conditions of the city. Thus, urban heat island and outdoor comfort conditions in Chania have been thoroughly studied by various researchers (Kolokotsa et al., 2009; Maragkogiannis et al., 2014; Tsitoura et al., 2014) showing a maximum UHI intensity of almost 8K. The high rise buildings and the anthropogenic heat combined with the limited green spaces lead to a significant heat stress in the city center comparing to the suburban and rural areas.



Figure 2: Map of case study area (left). Municipal Garden of Chania (right).

In the case study area preeminent is the role of the Municipal Garden of Chania, as it covers a big portion of the area and providing cool island benefits (Figure 1). The Municipal Garden was designed in 1870 and is the first public benefit project in the city. The Garden was planted with evergreen trees and its paths were laid with thick sand. In 1918 the Garden was rebuilt. New trees and plants are being planted, creating a labyrinth with an entrance to the western part of the Garden to enter the visitors. Today, the Garden hosts a wide variety of trees, shrubs, fruit and ornamental plants. To facilitate the case study analysis process, the selected area has been separated into three different areas, as illustrated in the figure below (Figure 3).



Figure 3: Separation of the case study area.

2.2 Environmental simulation of study area

Prediction of the cooling effect of green spaces and cool materials on the three different examined areas was based on the holistic, three-dimensional (3D) and non-hydrostatic ENVI-met 4.4 simulation software which very often used to simulate urban environments and to assess the effects of green architecture visions. ENVI-met is freeware but is not Open Source. ENVI-met is designed for microscale, with a typical horizontal resolution from 0.5 to 5 metres and a typical time frame of 24 to 48 hours and a time step of 1 to 5 seconds. This resolution allows to analyze small-scale interactions between individual buildings, surfaces and plants. The last available version of the prognostic model (i.e. v.4.4. ENVI-met) takes under consideration the fundamental laws of fluid dynamics and thermodynamics, including simulation of several phenomena: heat flux around and between buildings; heat and steam exchange at soil level and between walls, turbulence, thermo-hygrometric exchange in vegetation, bioclimatology, fluid dynamics of small particles and polluting species.

The calculating model includes:

- Shortwave and longwave radiation fluxes with respect to shading, reflection and re-radiation from building systems and the vegetation;
- Transpiration, evaporation and sensible heat flux from the vegetation into the air including full simulation of all plant physical parameters (e.g., photosynthesis rate);
- Surface and wall temperature for each grid point and wall;
- Water- and heat-exchange inside the soil system;
- Calculation of biometeorological parameters like Mean Radiant Temperature or Fanger's Predicted Mean Vote (PMV) Value;
- Dispersion of inert gases and particles including sedimentation of particles on leaves and surfaces.

The simulation results can be analyzed from a multitude of perspectives with the software tool LEONARDO, which comes with plenty of illustration facilities. The ENVI-MET database provides a wide variety of different vegetation and materials for walls, roofs and surfaces and can easily be extend by the user to fit the individual demands (source: envimet website).

2.3 ENVI-met – Mathematical considerations of the Atmospheric Model

This section describes the calculation method of the main prognostic variables, such as main wind flow, temperature, humidity and turbulence, which are taken into account in the atmospheric model.

2.3.1 Description of the Mean Air Flow

The three-dimensional turbulent air flow in the model is given by the following non-hydrostatic incompressible Navier-Stokes equations (1a-c), where all three-dimensional advection and diffusion terms are written in Einstein summation (i.e., $u_i = (u, v, w)$; $x_i = (x, y, z)$, for $i = 1, 2, 3$):

$$\frac{\partial u}{\partial t} + u_i \frac{\partial u}{\partial x_i} = -\frac{\partial p}{\partial x} + K_m \left(\frac{\partial^2 u}{\partial x_i^2} \right) + f(v - v_g) - S_u \quad (1a)$$

$$\frac{\partial v}{\partial t} + u_i \frac{\partial v}{\partial x_i} = -\frac{\partial p}{\partial y} + K_m \left(\frac{\partial^2 v}{\partial x_i^2} \right) + f(u - u_g) - S_v \quad (1b)$$

$$\frac{\partial w}{\partial t} + u_i \frac{\partial w}{\partial x_i} = -\frac{\partial p}{\partial z} + K_m \left(\frac{\partial^2 w}{\partial x_i^2} \right) + g \frac{\theta(z)}{\theta_{ref}(z)} - S_w \quad (1c)$$

$$\frac{\partial u}{\partial x} + \frac{\partial v}{\partial y} + \frac{\partial w}{\partial z} = 0 \quad (2)$$

Where:

- $f (=10^4 \text{ sec}^{-1})$ is the Coriolis parameter,
- p is the local pressure perturbation, and
- θ the potential temperature at level z .

Note that the reference temperature θ_{ref} , which represents the larger scale meteorological conditions, is calculated as an average temperature over all grid cells of height z , excluding those occupied by buildings. In addition, the *Boussinesq*

Approximation is used in order to be removed the air density ρ from the original compressible Navier-Stokes equations. This replacement leads to one additional source term in the equation (1c) to include thermal forced vertical motion and one continuity equation (2) which has to be satisfied for each time step in order to keep the flow field mass conserving. Furthermore the effect of the local source and/or sink terms (i.e. S_u , S_v and S_w), which describe the loss of wind speed due to drag forces occurring at vegetation elements, can be parameterized, following (Liu et al., 1996) and (Yamada, 1982), as:

$$S_{u(i)} = \frac{\overline{\partial p'}}{\partial x_i} = c_{d,f} LAD(z) \cdot W \cdot u_i \quad (3)$$

Where:

- $W = (u^2 + v^2 + w^2)^{0.5}$ is the mean wind speed (at height z),
- $LAD(z)$ is the leaf area density, in [$m^2 m^{-3}$], of the plant in this height (z).
- $c_{d,f}$ is the mechanical drag coefficient at plant elements, set to 0.2.

For all solid surfaces, a no-slip condition is applied, where the inflow profile is obtained from the one-dimensional reference model and a zero-gradient Neumann condition is used at the outflow and lateral boundaries. At the top boundary all vertical motions are assumed to be zero. Note that special boundary conditions are used for the pressure perturbation on all outflow boundaries to keep the model mass conserving.

2.3.2 Temperature and Humidity

The distribution of the air temperature θ and specific humidity q is described and simulated by the combined advection-diffusion equation including possible internal source/sinks terms:

$$\frac{\partial \theta}{\partial t} + u_i \frac{\partial \theta}{\partial x_i} = K_h \left(\frac{\partial^2 \theta}{\partial x_i^2} \right) + \frac{1}{c_p \rho} \frac{\partial R_{n,lw}}{\partial z} + Q_h \quad (4)$$

$$\frac{\partial q}{\partial t} + u_i \frac{\partial q}{\partial x_i} = K_q \left(\frac{\partial^2 q}{\partial x_i^2} \right) + Q_q \quad (5)$$

The quantities Q_h and Q_q , which are provided by the vegetation model (see section 2.5), are used to link the exchange of heat and vapour which takes place at plants with the atmospheric model. Note that the partial derivative $\partial R_{n,lw}/\partial z$ represents the vertical divergence of longwave radiation taking into account the cooling and heating effect of radiative fluxes. In addition, the surface temperature of the ground surfaces, of roofs and of walls are used as real physical boundaries. Dirichlet, Neuman or cyclic boundary conditions could be applied for the inflow profile. At the outflow and lateral boundaries a zero-gradient condition is used, while the values for the top of the three dimensional model are obtained from the one dimensional boundary layer model, which extends up to 2500 m.

2.3.3 Atmospheric turbulence

When the air flow is sheared at building walls or vegetation elements leads to production of turbulence effect. It is expected that under windy conditions, the magnitude of local turbulence production surpasses its dissipation, as a result the turbulent eddies to be transported by the mean air flow. Depending on the structure of the flow, this leads to an increased turbulence away from the original source of disturbance. To simulate the turbulent effect, a so-called 1.5 order turbulence closure model is used in ENVI-met. Based on the work of Mellor and Yamada (Yamada and Mellor, 1975) two additional prognostic variables, i.e., the local turbulence (E) and its dissipation rate (ε) are added to the model. Their distribution is given by the following prognostic equations (6) and (7):

$$\frac{\partial E}{\partial t} + u_i \frac{\partial E}{\partial x_i} = K_E \left(\frac{\partial^2 E}{\partial x_i^2} \right) + Pr - Th + Q_E - e \quad (6)$$

$$\frac{\partial \varepsilon}{\partial t} + u_i \frac{\partial \varepsilon}{\partial x_i} = K_\varepsilon \left(\frac{\partial^2 \varepsilon}{\partial x_i^2} \right) + r_1 \frac{\varepsilon}{E} Pr - c_3 \frac{\varepsilon}{E} Th - c_2 \frac{\varepsilon^2}{E} + Q_\varepsilon \quad (7)$$

Where:

- Pr, Th terms describe the production and dissipation of turbulent energy due to wind shear and thermal stratification,
- Q_e , Q_ε denote the local source terms for turbulence production and dissipation at vegetation.

The mechanical production Pr is described using the three-dimensional deformation tensor of the local wind field as seen in equation (8), while the production of buoyancy Th is given by equation (9) as follows:

$$Pr = K_m \left(\frac{\partial u_i}{\partial x_j} + \frac{\partial u_j}{\partial x_i} \right) \frac{\partial u_i}{\partial x_j} \quad \text{with } i, j = 1, 2, 3 \quad (8)$$

$$Th = \frac{g}{\theta_{ref}(z)} K_h \frac{\partial \theta}{\partial z} \quad (9)$$

To calibrate the ε -equation, the standard values $c_1=1.44$ $c_2=1.92$ and $c_3=1.44$, given by Launder and Spalding (Launder and Spalding, 1974), have been used. It has to be noted, that the application of the 1.5 order closure model to the atmospheric boundary layer induces some uncertainty in the simulation process. Thus, depending on the specific situation, different calibration values might be used and the production of turbulent energy normally needs to be restricted in the higher layers of the atmosphere. Following the results of Liu et al. (1996) (Liu et al., 1996) and Wilson (1988) , (Wilson, 1988) two extra source terms are added to equations (6) and (7) in order to consider the additional turbulence produced at vegetation as well as the turbulence destruction due to the cascade from larger shear-induced eddies to smaller and waker eddies:

$$Q_E = c_{d,f} LAD(z) \cdot W^3 - 4c_{d,f} LAD(z) \cdot |W| \cdot E \quad (10)$$

$$Q_\varepsilon = 1.5c_{d,f} LAD(z) \cdot W^3 - 6c_{d,f} LAD(z) \cdot |W| \cdot \varepsilon \quad (11)$$

Where, W is the mean wind speed (see description of equation (3)). Note that the source term for the dissipation equation (11) is based on the Kolmogorov relation (Launder and Spalding, 1974). Thus it should be adjusted in cases where measured data are available (see e.g. Liu et al., 1996). Moreover from the calculated E - ε field the turbulent exchange coefficients are calculated assuming local turbulence isotropy based on the following relationships (12a-12d), where $c_\mu=0.09$, $\sigma_E=1$ and $\sigma_\varepsilon=1.3$:

$$K_m = c_\mu \frac{E^2}{\varepsilon} \quad (12a)$$

$$K_H, K_q = 1.35 \cdot K_m \quad (12b)$$

$$K_E = \frac{K_m}{\sigma_E} \quad (12c)$$

$$K_\varepsilon = \frac{K_m}{\sigma_\varepsilon} \quad (12d)$$

At all solid surfaces, variables E and ε are calculated as a function of local tangential friction velocity (u^*), which is calculated using the flow components tangential to the concerned surface. In equations (13a) and (13b) with k is denoted the von-Kármán constant which is equal to 0.4 and z_0 is the microscale roughness length of the surface.

$$E(z=0), E_w = \frac{(u_*^2)^{\tan}}{\sqrt{c_\mu}} \quad (13a)$$

$$\varepsilon(z=0), \varepsilon_w = \frac{(u_*^3)^{\tan}}{\kappa \cdot z_0} \quad (13b)$$

2.3.4 Radiative Fluxes

The incoming shortwave and longwave fluxes are applied as boundary condition at the top of the model. For the longwave fluxes a two-stream radiative flux approximation is provided while a set of empirical equations is used for the calculation of shortwave wavelength spectra (Bruse, 2004; Bruse and Fleer, 1998). In

case of the three-dimensional model, the radiative fluxes are modified by plants and buildings. In order to estimate their effect on the radiative conditions, flux reduction coefficients (σ) are used, ranging from 1 for undisturbed fluxes to 0 in case of total absorption (Bruse, 2004; Bruse and Fleer, 1998). In total, the five different reduction coefficients are defined based on equations (14a – e), as follows:

$$\sigma_{sw,dir}(z) = \exp(-F \cdot LAI^*(z)) \quad (14a)$$

$$\sigma_{sw,dif}(z) = \exp(-F \cdot LAI(z, z_p)) \quad (14b)$$

$$\sigma_{lw}^{\downarrow}(z) = \exp(-F \cdot LAI(z, z_p)) \quad (14c)$$

$$\sigma_{lw}^{\uparrow}(z) = \exp(-F \cdot LAI(0, z)) \quad (14d)$$

$$\sigma_{svf}(z) = 1 / 360 \sum_{\pi=0}^{360} \cos \lambda(\pi) \quad (14e)$$

The coefficients $\sigma_{sw,dir}$, $\sigma_{sw,dif}$, $\sigma_{lw,down}$ and $\sigma_{lw,up}$ describe the influence of vegetation on direct shortwave radiation, diffuse shortwave radiation, downward and upward flux of longwave radiation, respectively. Coefficient σ_{svf} parameterises the local obstruction of the sky by buildings and ranges from 1 (in case of free sky) to 0 (for no sky visible). Note that parameter λ is the maximum shielding angle found by the ray-tracing module in direction π and LAI is the one-dimensional vertical leaf area index of the plant from level z to the top of the plant at z_p or the ground ($z=0$), given from equation (15) :

$$LAI(z, z + \Delta z) = \int_z^{z + \Delta z} LAD(z') dz' \quad (15)$$

The three-dimensional index LAI^* is used instead of the one-dimensional vertical LAI for the estimation of the decrease of the direct solar radiation. In particular, LAI^* is calculated with respect to the angle of incidence from the incoming sun rays and analyses the model environment for objects intersecting with the ray path. If a building is found to lie between the point of interest and the sun, $\sigma_{sw,dir}$ is set to zero immediately, while if vegetation is found, the intensity is adjusted as shown in

equation (14a). Based on the aforementioned, the direct and diffuse shortwave radiation fluxes can be calculated at any point of interest based on equations (16a) and (16b), where $R_{sw,dir}^0$ and $R_{sw,dif}^0$, are the direct and diffuse shortwave radiative fluxes at the model top and the additional last term (\bar{a}) for the diffuse component considers the reflection of shortwave radiation inside the environment using the average wall albedo as reflectivity indicator.

$$R_{sw,dir}(z) = \sigma_{sw,dir}(z) R_{sw,dir}^0 \quad (16a)$$

$$R_{sw,dif}(z) = \sigma_{sw,dif}(z) \sigma_{svf}(z) R_{sw,dif}^0 + (1 - \sigma_{svf}(z)) R_{sw,dir}^0 \cdot \bar{a} \quad (16b)$$

$$R_{lw}^{\downarrow}(z) = \sigma_{lw}^{\downarrow}(z) R_{lw}^{\downarrow,0} + \left(1 - \sigma_{lw}^{\downarrow}(z)\right) \varepsilon_f \sigma_B \bar{T}_{f+}^{-4} \quad (16c)$$

$$R_{lw}^{\uparrow}(z) = \sigma_{lw}^{\downarrow}(z) \varepsilon_s \sigma_B T_0^4 + \left(1 - \sigma_{lw}^{\downarrow}(z)\right) \varepsilon_f \sigma_B \bar{T}_{f-}^{-4} \quad (16d)$$

$$R_{lw}^{\leftrightarrow}(z) (1 - \sigma_{svf}(z)) \varepsilon_w \sigma_B \bar{T}_w^{-4} \quad (16e)$$

In the case of the longwave radiation, the longwave fluxes at level z are given by equations (16c-e) using the concept of reduction coefficients and assuming that shielding vegetation layers will absorb parts of the flux and replace it with their own longwave radiation. Horizontal longwave radiation fluxes from building walls (16e) are calculated by weighting the emitted radiation of the walls with the sky-view factor. It is noted that \bar{T}_{f+}^4 and \bar{T}_{f-}^4 are the average foliage temperatures of the overlying (+) and underlying (-) vegetation layer, respectively, T_0 is the ground surface temperature, \bar{T}_w is the average surface temperature of building walls, the parameters ε_f , ε_s , ε_w denote the emissivity of foliage, the ground surface and of the walls and σ_B is the Stefan-Boltzman constant.

2.4 ENVI-met – Mathematical considerations of the Soil Model

A wide range of different soil and surface types, varying from natural soils to completely artificial materials, is usually found in urban environments. To simulate soil heterogeneity, individual soil properties such as thermodynamic and hydraulic

conductivity or albedo, can be assigned to each grid cell of the surface/soil model. The soil model is organised in 14 layers between the surface and its lower boundary in 2 m depth. The vertical resolution varies between 0.01 m for depths close to the surface and 0.5 m in the deeper layers and the exchange processes are simulated in terms of heat and water transfer between the layers. Except of the uppermost soil layer in which the heat transfer is calculated in three dimensions, the soil is treated as a one dimensional vertical column. The distribution of heat (T) and soil volumetric moisture content (η) are given by the one dimensional prognostic equations (17) and (18) as follows:

$$\frac{\partial T}{\partial t} = \kappa_s \frac{\partial^2 T}{\partial z^2} \quad (17)$$

$$\frac{\partial \eta}{\partial t} = D_\eta \frac{\partial^2 \eta}{\partial z^2} + \frac{\partial K_\eta}{\partial z} - S_\eta(z) \quad (18)$$

The thermal diffusivity κ_s of natural soils is a function of the available soil moisture (η) and is calculated based on equation proposed by Tjernström (1989) (Tjernström, 1989). In equation (18), as hydraulic parameters are used the volumetric water content η , its saturation value η_s , the hydraulic conductivity K_η and the hydraulic diffusivity D_η . All coefficients are calculated using the equations given by Clapp and Hornberger (1978) (Clapp and Hornberger, 1978). In addition, the factor describes water uptake by the plant roots (S_η) provided by the vegetation model has to be considered as an internal sink of moisture. Furthermore, the evaporation of the soil surface as given by (26 c) has to be considered as an external sink (or source in the case of condensation) at the top layers of the soil model.

2.5 ENVI-met – Mathematical considerations of the Vegetation Model

To meet the model requirements, vegetation is treated as a one-dimensional column with height z_p . The profile of leaf area density (LAD) is used to describe the

amount and the distribution of leafs. Thus, following the same conceptualization which used during soil system simulation, the distribution of roots is represented by the root area density (RAD) profile stretching from the surface down to the root depth $-z_r$. This scheme is universal and can be used for small plants like grass or crop as well as for huge trees, if z_p and $-z_r$ are adjusted accordingly.

2.5.1 Turbulent fluxes of heat and vapour

Terms of sensible heat flux ($J_{f,h}$), evaporation flux of liquid water on the leafs ($J_{f,evap}$) and transpiration flux controlled by the leaf stomata ($J_{f,trans}$) are used to express the interactions between the plant leafs and the surrounding air.

$$J_{f,h} = 1.1 r_a^{-1} (T_f - T_a) \quad (19a)$$

$$J_{f,evap} = r_a^{-1} \Delta q \delta_c f_w + r_a^{-1} (1 - \delta_c) \Delta q \quad (19b)$$

$$J_{f,trans} = \delta_c (r_a + r_s)^{-1} (1 - f_w) \Delta q \quad (19c)$$

In equations (19a-c) T_a and q_a are the temperature and the specific humidity of the air around the leaf, Δq is the leaf-to-air humidity deficit given from equation (20). T_f symbolizes the foliage temperature and q^* is the saturation value of q at the leaf surface.

$$\Delta q = q \cdot T_f - q_a \quad (20)$$

In addition, the aerodynamic resistance r_a is given as function of the leaf geometry and wind speed, by equation (21) following Barden (1982):

$$r_a = A \sqrt{\frac{D}{\max(W, 0.05)}} \quad (21)$$

Where:

- W is the wind speed at the leaf surface,
- Parameter A is equal to $87 \text{ sec}^{0.5} \text{ m}^{-1}$ for conifers and grass and $200 \text{ sec}^{0.5} \text{ m}^{-1}$ for deciduous trees,

- D is the typical leaf diameter, ranging from 0.02 m for conifers up to 0.5 m or more for tropical plants (Schilling, 1991). The max condition ensures that no invalid values appear in the case of very low winds.
- δ_c is a factor set to 1 if evaporation and transpiration can occur ($\Delta q \geq 0$), otherwise δ_c is equal to 0 and only condensation is possible.

Assuming that only wet parts of the vegetation can evaporate and that only dry parts will transpire, the fraction of wet leaves inside one grid box is needed which can be calculated by equation (22), following Deardorff (1978), where W_{dew} is the actual amount of dew on the leave surfaces and $W_{\text{dew,max}}$ is the maximum possible value ($=0.2 \text{ kg m}^{-2}$).

$$f_w = \left(\frac{W_{\text{dew}}}{W_{\text{dew,max}}} \right)^{2/3} \quad (22)$$

2.5.2 Stomatal resistance

As described by Deardorff (1978) (Deardorff, 1978), the stomatal resistance of a vital plant r_s can be calculated by equation (23) with respect to actual and maximum shortwave radiation input (R_{sw} and $R_{\text{sw,max}}$) and of the available soil water content inside the root zone (η).

$$r_s = r_{s,\text{min}} \left[\frac{R_{\text{sw,max}}}{0.03 R_{\text{sw,max}} + R_{\text{sw}}} + \left(\frac{\eta_{\text{wilt}}}{\eta} \right)^2 \right] \quad (23)$$

Note that, the minimum stomatal resistance $r_{s,\text{min}}$ depends on the type of plant and ranges from $200 \text{ s}^{0.5} \text{ m}^{-1}$ for grass up to $400 \text{ s}^{0.5} \text{ m}^{-1}$ for deciduous leafs. Alternatively to the simple Deardorff-approach, the stomata resistance can also be calculated using a photosynthesis model that allows a more dynamic description of the plant processes (Jacobs and De Bruin, 1997).

2.5.3 Energy balance of the leaf

In cases where the internal energy storage inside the leaf can be neglected, the foliage temperature T_f can be obtained from the steady-state leaf energy budget, given by equation (24) as follows:

$$0 = R_{sw,net}(z) + R_{lw,net}(z) - c_p \rho J_{f,h} - \rho L (J_{f,evap} + J_{f,tran}) \quad (24)$$

where c_p is the specific heat of the air and ρ the air density, L is the latent heat of vaporization and $R_{sw,net}$ is the net shortwave radiation absorbed by the leaf surface calculated by equation (25):

$$R_{sw,net}(z) = (F \cdot R_{sw,dir}(z) + R_{sw,dif}(z))(1 - a_f - tr_f) \quad (25)$$

F is a non-dimensional parameter describing the orientation of the leafs towards the sun (=0.5 for randomly orientated leafs), a_f is the albedo of the foliage and tr_f is a transmission factor (set to 0.3). The longwave radiation budget for equation (24) is given by:

$$R_{lw,net}(z, T_f) = \varepsilon_f R_{lw}^{\downarrow}(z) + R_{lw}^{\leftrightarrow}(z) + \varepsilon_f R_{lw}^{\uparrow}(z) - 2\varepsilon_f \sigma_B T_f^4 - (1 - \sigma_{svf}(z)) \sigma_B T_f^4 \quad (26)$$

The source/sink terms for the atmospheric model can finally be computed using (19a-c) with T_f value obtained by solving equation (24):

$$Q_h(z) = LAD(z) J_{f,h} \quad (27)$$

$$Q_q(z) = LAD(z) (J_{f,evapo} + J_{f,trans}) \quad (28)$$

The equations (27) and (28) assume, that only one side of the leaf is participating in the turbulent exchange processes of heat and vapour (the luv side) and absorbs shortwave radiation, whereas in the longwave radiation spectra, both sides of the leaf take part in the radiative exchange process.

2.5.4 Water balance of the plant/soil system

To ensure a realistic simulation of the feedback mechanisms between water transpiration by the plant and water supply by the soil, the water transpired by the plant must be taken from the soil via root water uptake, resulting in a loss of soil water content. If the soil fails to supply enough water, the stomatal resistance will be increased and the transpiration rate decreases. The total mass of water (m_{trans}) transpired by the plant is given by equation (29) which describes the vertical integral over the transpiration fluxes in the different plant layers:

$$m_{trans} = \rho \int_0^{z_p} L A D(z) J_{f,trans}(z) dz \quad (29)$$

Following Pielkes' suggestion (Pielke, 2013), the water is taken from different soil layers inside the root zone of the plant depending on the amount of roots in the layer ($RAD(z)$ value) and the hydraulic diffusivity of the soil layer ($D_\eta(z)$). Thus, the parameter $S_\eta(-z)$ is calculated as follows:

$$S_\eta(-z) = \frac{m_{trans}}{\rho_w} (RAD(-z) D_\eta(-z)) \left(\int_{-z_r}^0 RAD(-z) D_\eta(-z) dz \right)^{-1} \quad (30)$$

2.6 ENVI-met – Mathematical considerations of Ground Surface and Building Surfaces

The temperature T_0 of the ground surface in equilibrium can be calculated from the energy balance, given by equation (31):

$$0 = R_{sw,net} + R_{lw,net} - c_p \cdot \rho \cdot J_h^0 - \rho \cdot L \cdot J_v^0 - G \quad (31)$$

in which $R_{sw,net}$ and $R_{lw,net}$ are the net radiative energy fluxes, J_h and J_v are the turbulent fluxes of heat and vapour and G is the soil heat flux. In the case of building

surfaces (walls, roofs), the soil heat flux is replaced by the heat transmission through the wall or the roof (Q_w).

2.6.1 Radiative fluxes

Using the radiative fluxes scheme introduced in section 2.2.4, the shortwave net flux can be written in form of equation (32):

$$R_{sw,net} = (R_{sw,dir}(z=0) \cdot \cos(\beta) + R_{sw,dif}(z=0))(1 - a_s) \quad (32)$$

where β is the angle of incidence of the incoming shortwave radiation relative to the surface exposition and a_s is the surface albedo. The calculation of the longwave net radiation must take in account the influence of potential vegetation layers above the surface as well as the longwave fluxes from buildings and reflection of radiation between buildings and the surface. For simplicity, the longwave budget is split into a fraction that is unshielded by buildings ($R_{lw,net}^{us}$) and a fraction obstructed by buildings ($R_{lw,net}^s$):

$$R_{lw,net}(T_0) = \sigma_{svf} R_{lw,net}^{us}(T_0) + (1 - \sigma_{svf}) R_{lw,net}^s \quad (33)$$

where the sky-view-factor σ_{svf} is used to weight the energy budget for the shielded and unshielded fraction according to the situation. Based on Deardorff (1978) (Deardorff, 1978) the exchange of longwave radiation between the ground and the vegetation (first term) and between the ground and buildings (second term) can be written as:

$$R_{lw,net}^{us} = \sigma_{lw}^{\downarrow}(0) (R_{lw}^{\downarrow,0} - \epsilon_s \sigma_B T_0^4) + (1 - \sigma_{lw}^{\downarrow}(0)) \frac{\epsilon_f \epsilon_s}{\epsilon_f + \epsilon_s - \epsilon_f \epsilon_s} (\sigma_B \bar{T}_f^4 - \sigma_B T_0^4) \quad (34a)$$

$$R_{lw,net}^s = \frac{\epsilon_w \epsilon_s}{\epsilon_w + \epsilon_s - \epsilon_w \epsilon_s} \left\{ \max(\sigma_B \bar{T}_w^4, \sigma_B T_0^4) - \sigma_B T_0^4 \right\} \quad (34b)$$

In equation (34b) T_w is the average temperature of the building walls and ε_w the walls' emissivity. For the shielded fraction of the energy balance (second term) it is assumed, that the energy flux from the walls is only relevant if the walls are warmer than the ground surface. If the ground surface is warmer, the reflection of the longwave radiation of the surface at the walls is the dominating effect. In the case of building walls, the radiative scheme is less complex. The effects of vegetation are neglected because only few information are available about the horizontal longwave fluxes from the vegetation layers. For vertical walls, it is assumed, that the unshielded fraction will receive 50% of the longwave radiation from the sky and the other 50% from the ground. For the shielded fraction, 2/3 of the longwave radiation are supposed to come from the emission of other walls and the remaining 1/3 of the radiation is assumed to be radiation from the ground reflected by the walls. For roofs the radiative components are the same as for the ground surface except that $z \neq 0$ and that additional vegetation layers above the roof are not taken into account.

2.6.2 Turbulent fluxes of sensible heat and vapor

The turbulent fluxes of heat J_h^0 and vapor J_v^0 at the ground surface and at building walls and roofs are calculated as:

$$J_h^0 = -K_h^0 \left. \frac{\partial T}{\partial z} \right|_{z=0} = -K_h^0 \left. \frac{\theta(\kappa=1) - T_0}{0.5 \Delta z(\kappa=1)} \right| \quad (35a)$$

$$J_v^0 = -K_v^0 \left. \frac{\partial q}{\partial z} \right|_{z=0} = -K_v^0 \left. \frac{q(\kappa=1) - q_0}{0.5 \Delta z(\kappa=1)} \right| \quad (35b)$$

where $k=1$ indicates the first calculation layer above or adjacent to the surface and K_h^0 , K_v^0 are the exchange coefficients for heat and vapour between the surface and the air which are both calculated with respect to the thermal stratification between the surface and the overlying air layer (Asaeda and Ca, 1993). In the case of walls, the notations in (35a,b) have to be adopted according to the orientation of the wall. In the case low wind speeds leading to free convection conditions, the so-called $z^{-1/3}$ law is used to describe vertical transport by thermals. The Surface humidity q_0 can be

obtained from the soil moisture content at level $z=-1$ using the β -approach from (Deardorff, 1978) described by equations (36a,b):

$$q_0 = \beta_{q^*} (T_0) + (1 - \beta) q (z = 1) \quad (36a)$$

$$\beta = \min (1, \eta (z = -1) / \eta_{fc}) \quad (36b)$$

Where:

- η is the volumetric soil water content in the first soil layer,
- η_{fc} is its value at field capacity.

Noted that the water flux is linked to the soil hydraulic model using an additional sink term $S_{\eta,0}$ which is related to the evaporation at the surface through equation (37):

$$S_{\eta,0} (k = -1) = - \frac{\rho}{\rho_w} J_v^0 \frac{1}{\Delta z (k = -1)} \quad (37)$$

Where:

- $k=-1$ is the first layer of the soil model,
- Δz is the thickness of the soil layer
- ρ_w is the density of water.

Practical application have shown that it is more realistic to distribute the water loss over the upper two layers of soil and also use these two layers to estimate parameter β in equation (36b) rather than using only the uppermost layer. Otherwise, because of the layers thinness, it will dry out too fast.

2.6.3 Soil heat flux and heat flux through building walls

The soil heat flux is calculated based on the surface temperature and the temperature of the first level of the soil model below the surface, applying equation (38), where λ_s is the heat conductivity of the first soil layer which depends on the soil material and the water content.

$$G = \lambda_s (k = -1) \frac{T_0 - T (k = -1)}{0.5 \Delta z (k = -1)} \quad (38)$$

However, for buildings, G is replaced by Q_w approach, which is given by equation (39) and in which k is the heat transmission coefficient of the wall material and $T_{a,i}$ is the air temperature inside the building. This approach is rather simple and does not take into account the heat storage inside the wall material.

$$Q_w = k (T_w - T_{a,i}) \quad (39)$$

2.7 Methodology and Input data of study

To approach the most realistic results at the analysis, the following methodology steps were used:

- Case study area data selection (weather data, building and constructions materials characteristics, local vegetation types).
- Data categorization.
- Linking selected data to ENVI-met library data.
- Modelization of the case study area using ENVI-met (**Error! Reference source not found.**).

The initial conditions of the model are the average meteorological conditions of temperature, wind speed and humidity, extracted by the meteorological station in the centre of the town of Chania.

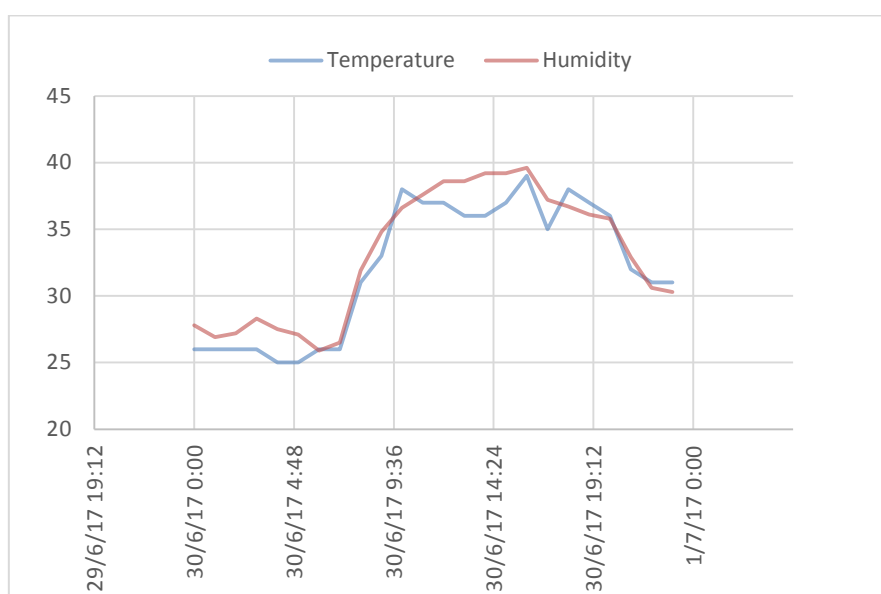


Figure 4. Temperature and humidity data from a reference weather station at the center of the town of Chania.

The initial conditions of the model, considering a typical summer day, were the following (see Figure 5 and Figure 6):

- ✓ Wind speed: 1.48 m/s
- ✓ Wind direction: 200 Degrees
- ✓ Starting time and date of simulation: 18:00; 29/6/2017
- ✓ Ending time and date of simulation: 01:00; 30/6/2017
- ✓ Average temperature: 32.08 °C
- ✓ Average Humidity: 36.79 %

The 3D model in ENVI-met was developed using in-situ measurements of the urban layout, maps, and photos. Two types of files (input file and configuration file) were developed to support the simulation. The model area consists of 213 x 220 x 25 cells and the real dimensions of the area are 420m x 450m. Full forcing was used for the air temperature, relative humidity and solar radiation simulation. This means that the diurnal variation of the atmospheric boundary conditions is defined in each simulation step (

Figure 7). The buildings in the model have common walls with a height between 3m and 20m. The categorization of the vegetation was based on the types of the vegetation inside the Garden of Chania (see Table 3 and Figure 8, Figure 9, Figure 10 and Figure 11). The technical materials' features are presented in Table 4 and in

Figure 12, Figure 13, Figure 14, Figure 15 and Figure 16. Final modelization of case study area considering all aforementioned parameters and input statements is illustrated in Figure 18.

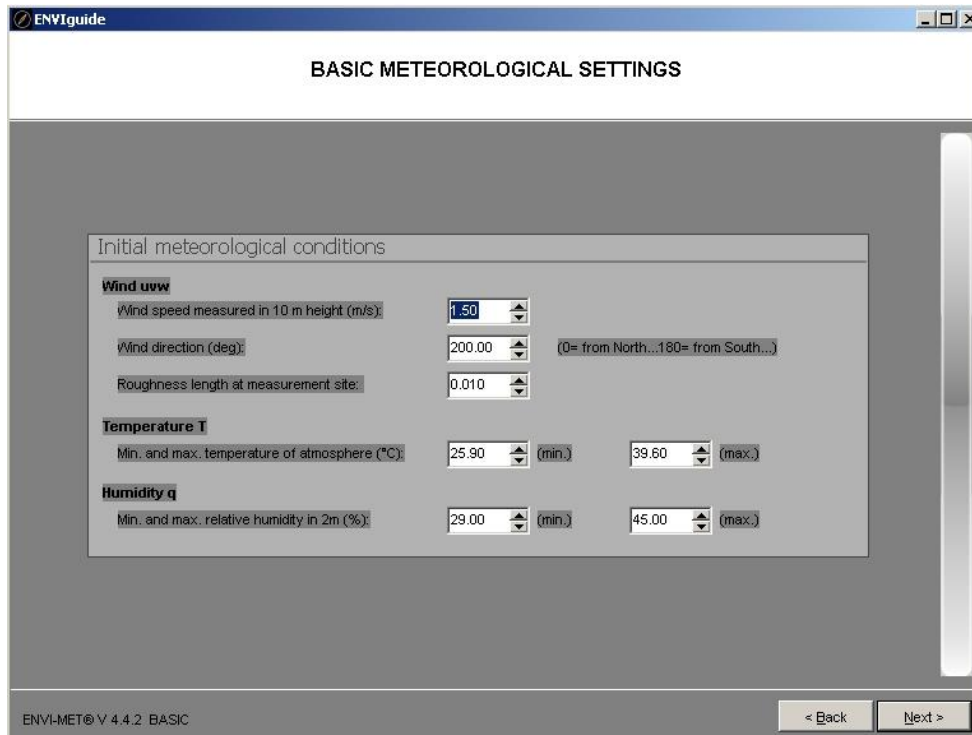


Figure 5: Basic meteorological settings.

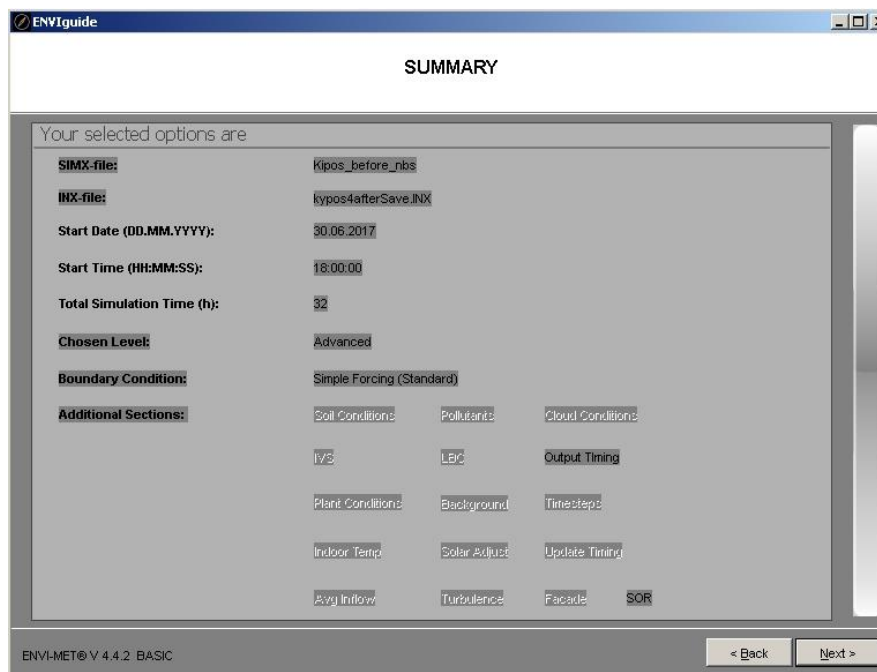


Figure 6: Summary of initial settings.



Figure 7: Full forcing data.

Table 3. Categorization of vegetation

Code	Details	Leaf Type
GA	Grass 10cm aver, dense	Grass
K2	Tree 10m very dense, free stem crown layer	Conifer
F2	Tree 10m very dense, leafless base	Deciduous
K1	Tree 5m dense, distinct crown layer	Conifer
F1	Tree 5m dense, distinct crown layer	Deciduous

Table 4. Technical materials' features

Code	Details	Albedo
RT	Red tartan	0.25
ST	Asphalt road	0.20
PG	Concrete pavement gray	0.50
CP	Cool Pavements	0.69

2. Case study area & Methodology development

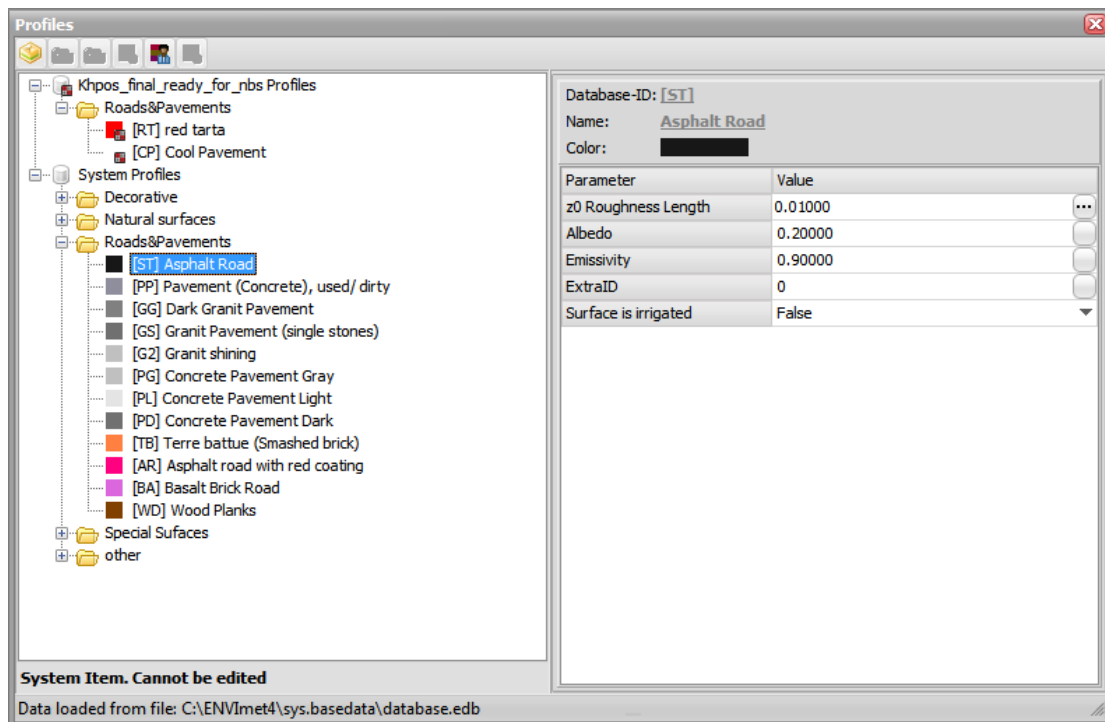


Figure 8: Input parameters values of asphalt road database.

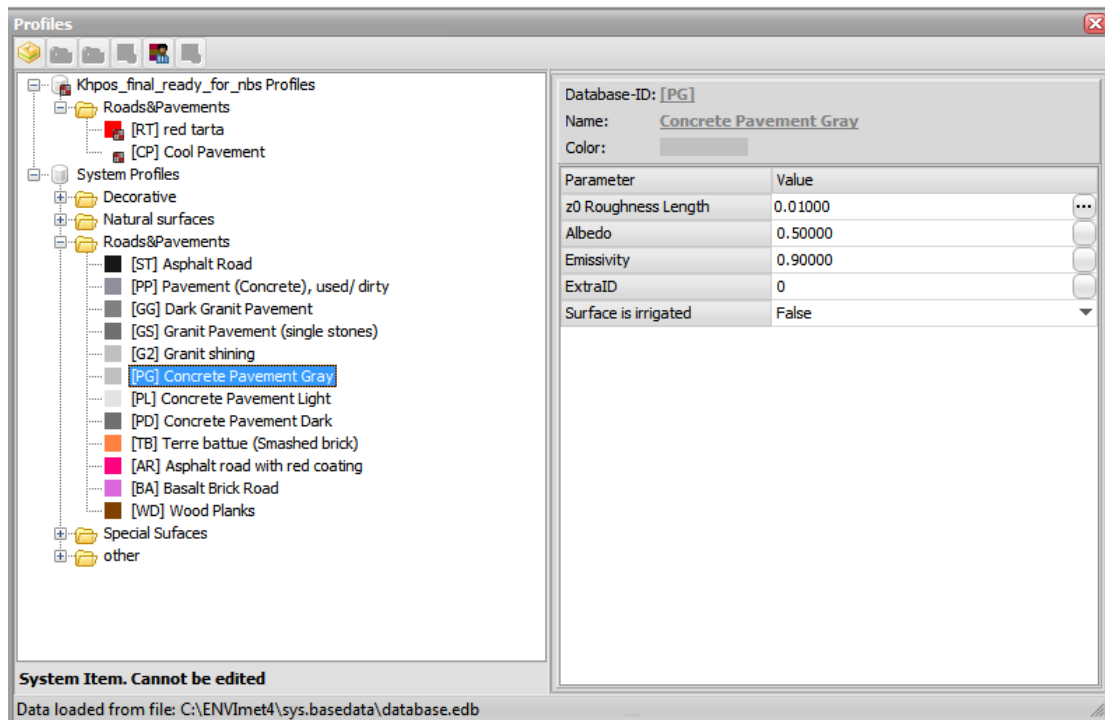


Figure 9: Input parameters values of concrete pavement grey database.

2. Case study area & Methodology development

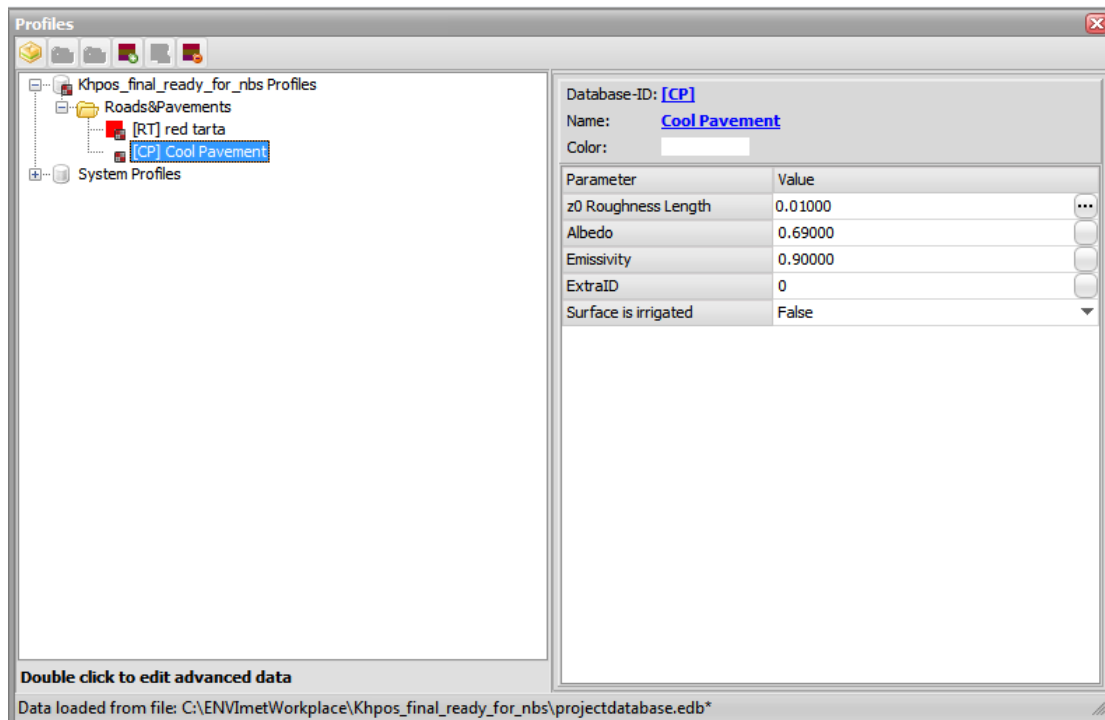


Figure 10: Input parameters values of cool pavement database.

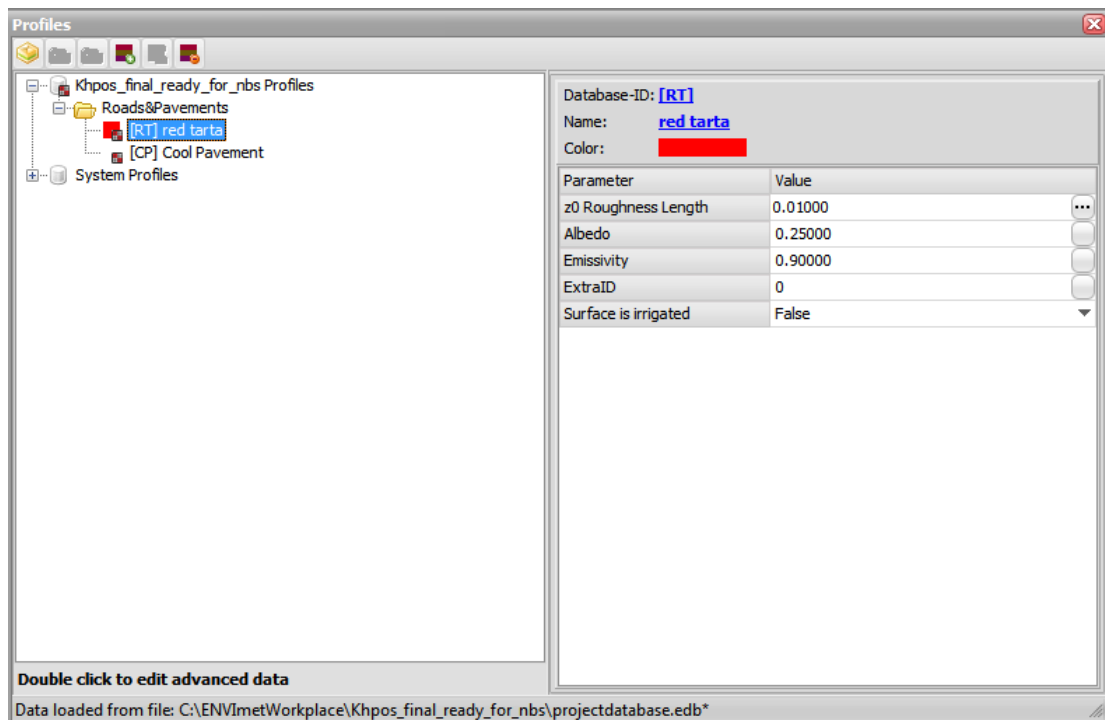


Figure 11: Input parameters values of red tarta database.

2. Case study area & Methodology development

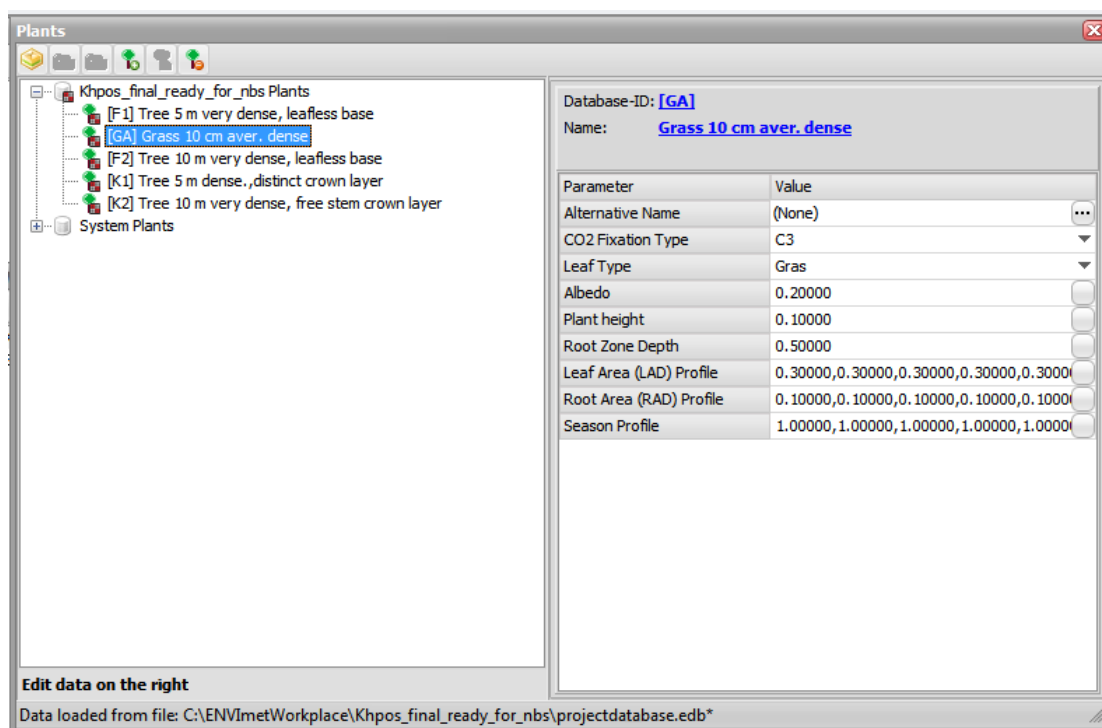


Figure 12: Input parameters values applied in vegetation scenario GA.

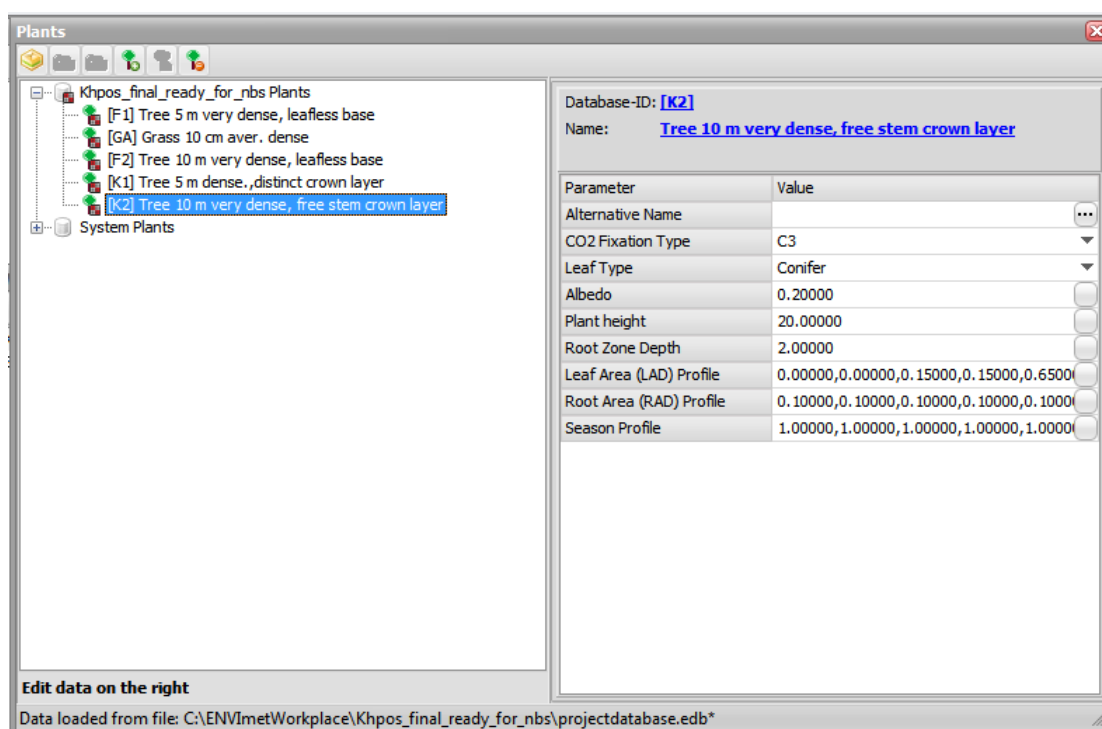


Figure 13: Input parameters values applied in vegetation scenario K2.

2. Case study area & Methodology development

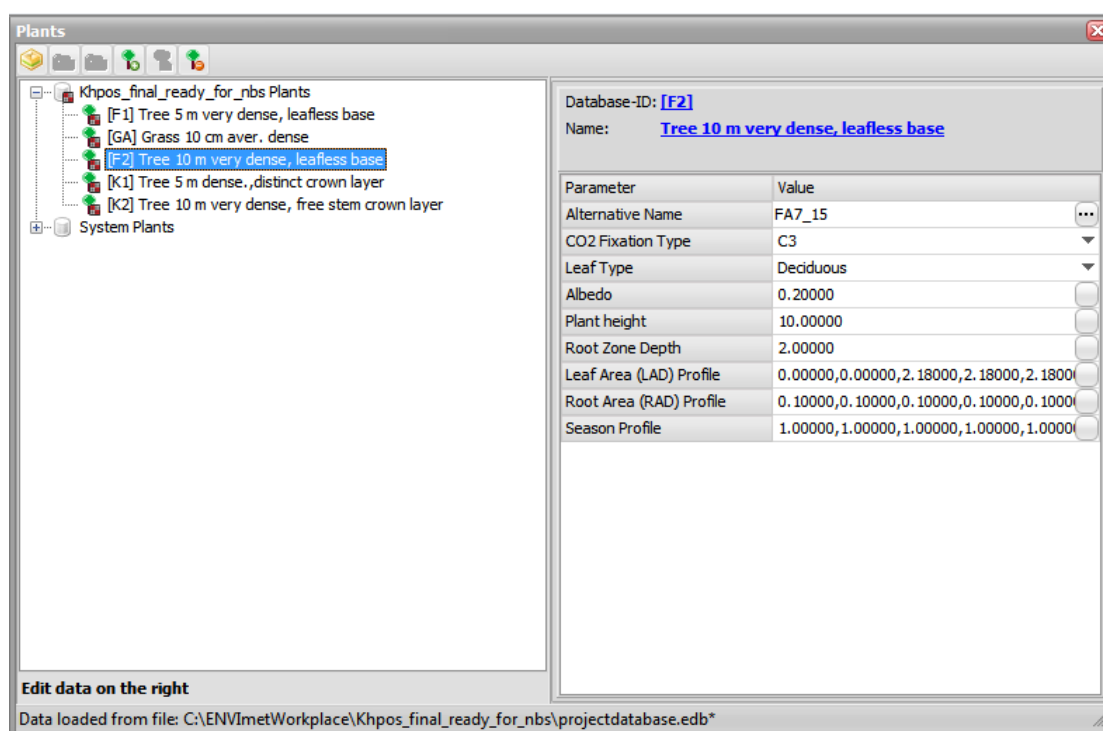


Figure 14: Input parameters values applied in vegetation scenario F2.

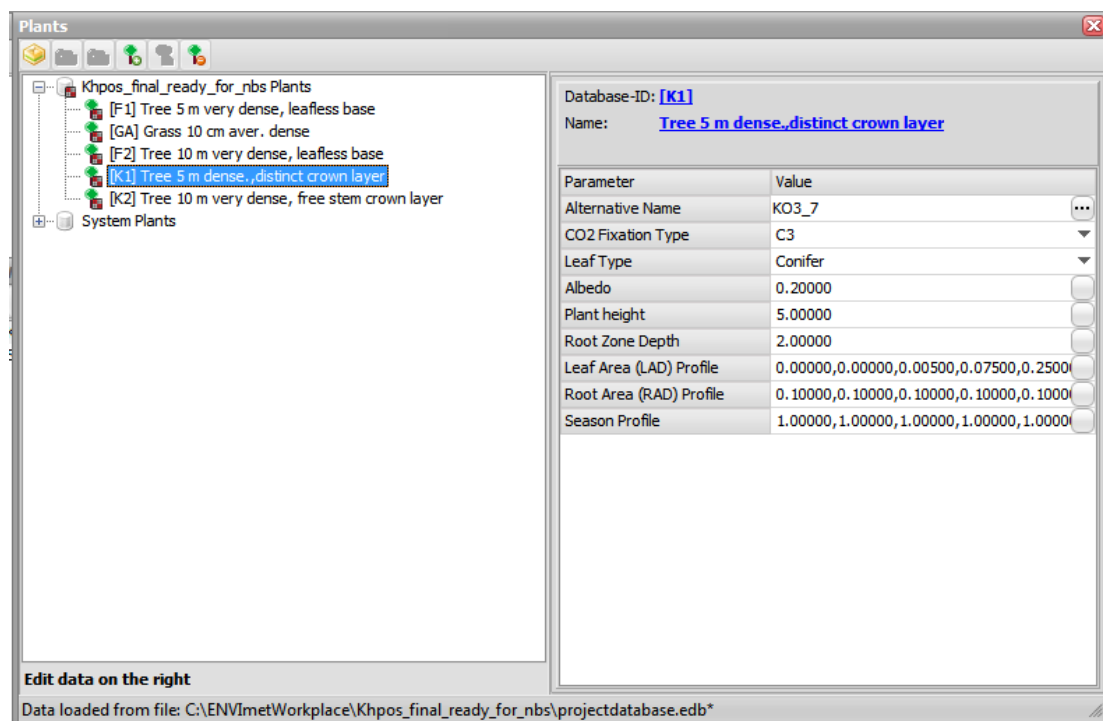


Figure 15: Input parameters values applied in vegetation scenario K1.

2. Case study area & Methodology development

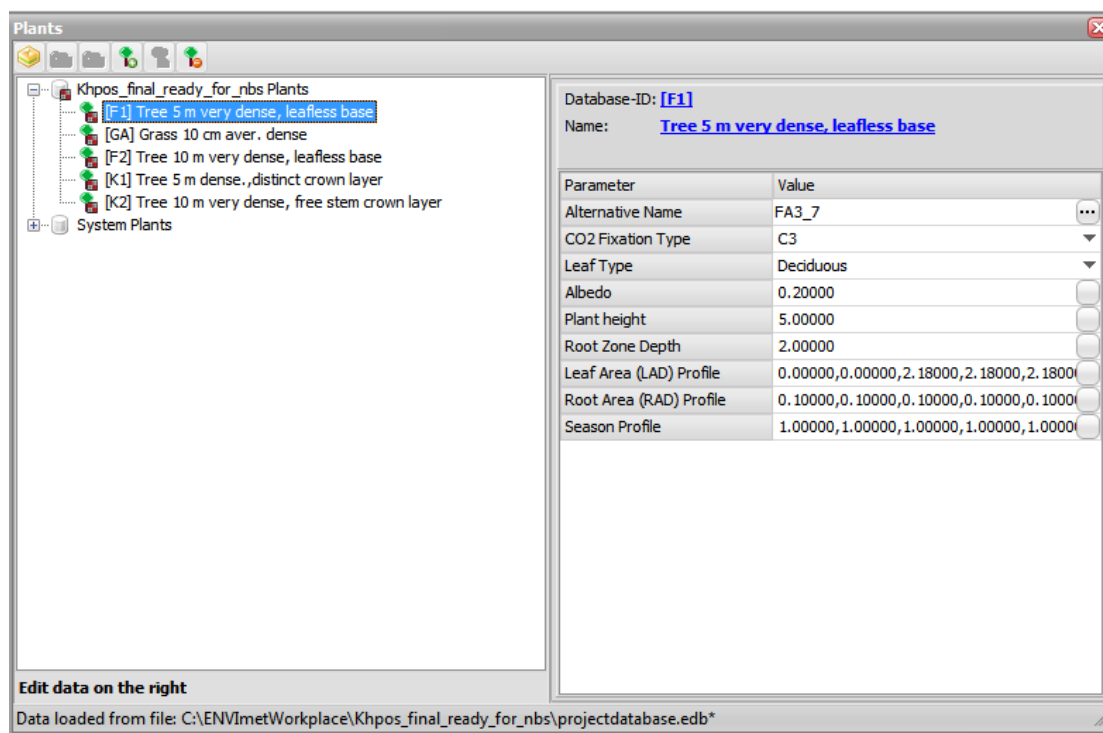


Figure 16: Input parameters values applied in vegetation scenario F1.

2. Case study area & Methodology development

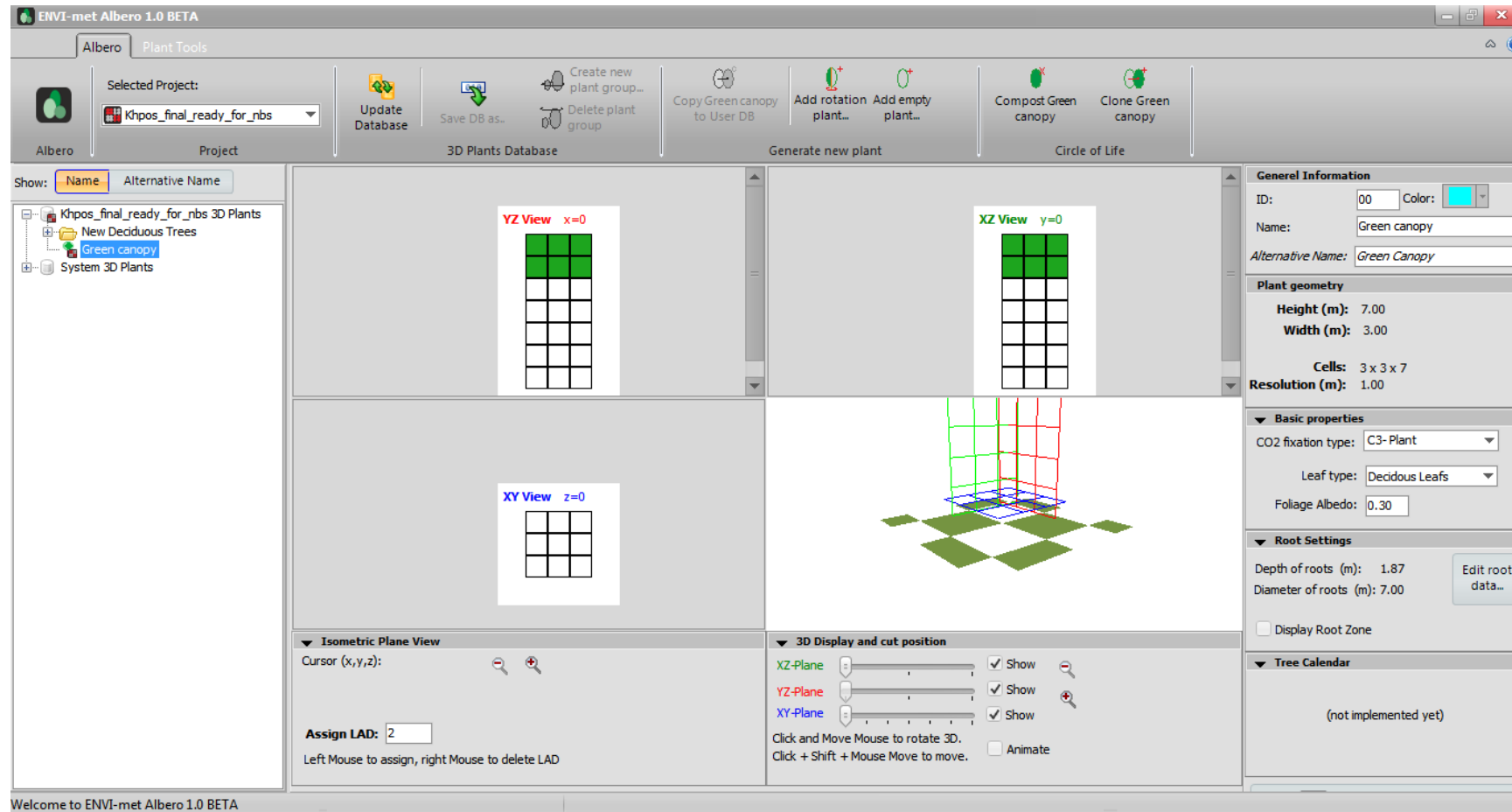


Figure 17: Input parameters values of green canopy database.

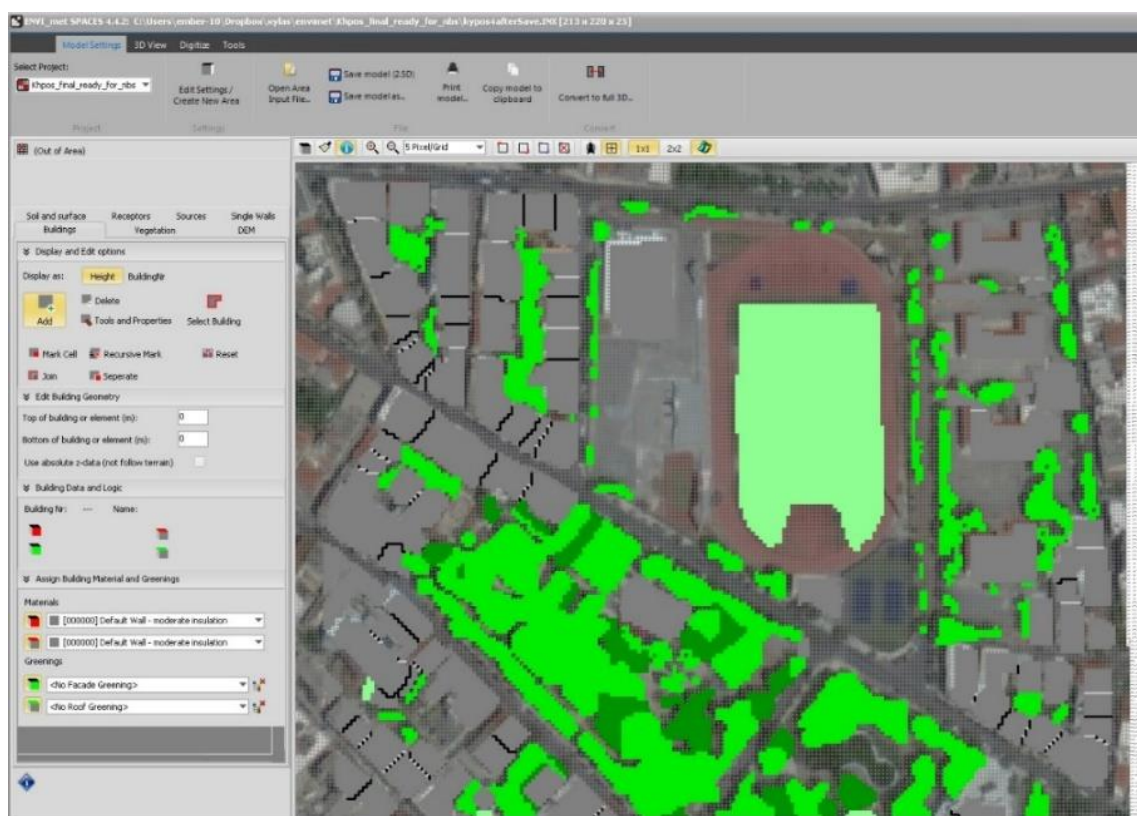


Figure 18: Modelimgn of case study area.

2.8 Numerical aspects and simulation techniques

The differential equations in the model are solved on a staggered grid system using the finite difference method. The three dimensional advection-diffusion equations are de-coupled using the Alternating Directions Implicit (ADI) method in combination with an upstream advection scheme. This scheme implies a relatively high numerical diffusion but allows a quick and implicit solution of the equations and has therefore been chosen in the ENVI-met model. To solve the Navier-Stokes equations, a splitting method after Patinos and Kistler (1977) is used. Here, the prognostic equations for a mass-conserving wind field $u_i^{t+\Delta t}$ are split into an auxiliary flow field (u^{aux}) and a pressure field (p) as presented in the following equation (40):

2. Case study area & Methodology development

$$\frac{\partial \mathbf{u}_i^{t+\Delta t}}{\partial t} = \frac{\partial \mathbf{u}_i^{\text{aux}}}{\partial t} + \frac{1}{\rho} \nabla p \quad (40)$$

The pressure variable is then removed from the prognostic equations (1a-c), leading to a set of three prognostic equations for an auxiliary flow field:

$$\frac{\partial \mathbf{u}^{\text{aux}}}{\partial t} + \mathbf{u}_i \frac{\partial \mathbf{u}^{\text{aux}}}{\partial x_i} = \mathbf{K}_m \left(\frac{\partial^2 \mathbf{u}^{\text{aux}}}{\partial x_i^2} \right) + \mathbf{f}(\mathbf{v} - \mathbf{v}_g) - \mathbf{S}_u \quad (41a)$$

$$\frac{\partial \mathbf{v}^{\text{aux}}}{\partial t} + \mathbf{u}_i \frac{\partial \mathbf{v}^{\text{aux}}}{\partial x_i} = \mathbf{K}_m \left(\frac{\partial^2 \mathbf{v}^{\text{aux}}}{\partial x_i^2} \right) + \mathbf{f}(\mathbf{u} - \mathbf{u}_g) - \mathbf{S}_v \quad (41b)$$

$$\frac{\partial \mathbf{w}^{\text{aux}}}{\partial t} + \mathbf{u}_i \frac{\partial \mathbf{w}^{\text{aux}}}{\partial x_i} = \mathbf{K}_m \left(\frac{\partial^2 \mathbf{w}^{\text{aux}}}{\partial x_i^2} \right) + g \frac{\theta(z)}{\theta_{\text{ref}}(z)} - \mathbf{S}_w \quad (41c)$$

This flow field contains the correct vorticity, but is not mass conserving, which means that it does not fulfil the filter condition (2). However, the matching pressure field can be obtained by solving the Poisson equation (42), using the iterative Simultaneous Over Relaxation (SOR) method.

$$\nabla^2 p = \frac{\rho}{\Delta t} \nabla \cdot \mathbf{u}_i^{\text{aux}} \quad (42)$$

Finally, the correct and approximately mass-conserving flow field can be calculated from the following equation (43):

$$\mathbf{u}_i^{t+\Delta t} = \mathbf{u}_i^{\text{aux}} - \frac{\Delta t}{\rho} \frac{\partial p}{\partial x_i} \quad (43)$$

The steep pressure gradients occurring in microscale simulations with obstacles require very small time steps to solve the set of wind field equations. Therefore, the wind field is not treated as a “normal” prognostic variable in ENVI-met, but is updated after a given time interval to take into account changes in turbulence and thermal stratification. Using the wind field as a normal variable is technically possible, but too time consuming on recent computers. Depending on the problem, the total size of the three dimensional model x , y and z , as well as the resolution of the

2. Case study area & Methodology development

grid can be selected within a wide range. By default the spacing Δx , Δy and Δz is equidistant in each direction which means that only the lowest grid cell above ground is normally split into 5 sub-cells with size $\Delta z_g = 0.2\Delta z$ to increase accuracy in calculating surface processes. The three dimensional model is nested into a one-dimensional model which extends up to 2500 m height. The values of the one dimensional model are used as reference values as well as inflow profiles and top boundary conditions for the three-dimensional model.

Chapter 3rd

3. Scenarios description

The evaluated scenarios included the replacement of the basic pavement material of the study area as well as different types of tree planting along the sidewalks. For all scenarios, the duration of the simulation is always 24 hours and the initial conditions of temperature, relative humidity, wind speed and direction, and roughness remain unchanged.

3.1 CS1-Cool Pavements

For the first scenario, all the pavements were replaced with cool materials (see Table 4). Cool pavements are a class of pavement technologies that can be used to mitigate urban heat island effects. They reduce heat being released later in the day and at night by two main principles: increased reflectivity and convection. Some cool pavement technologies utilize both principles. By increasing the reflectivity of pavements, less solar energy can be absorbed leading to less heat being available for later release. Cool pavements are made with different surfaces to increase albedo, thereby reflecting ultraviolet radiation out of the atmosphere. Increasing albedo reduces heat transfer to the surface and creates local cooling. In the Figure below (Figure 19), it is displayed the placement area of the cool pavements.



Figure 19: Implementation of cool pavements in the case study area.

3.2 CS2-Green Pavements

For the simulation process of this scenario, all the pavements have been replaced with a surface consisting of a 10 cm dense grass. Green pavements are considered to be a beneficial NBS solution which fits perfectly with any street scene, providing extra benefits when it comes to spatial effects, drainage and even traffic signalling. The greenery ensures that some of the water evaporates while some of it is absorbed (Figure 20). Green pavements decrease heat absorbed and can lower surface temperatures. This decrease in surface temperatures can temporarily offset warming caused by greenhouse gases. In the Figure 21, the placement area of the green pavements is displayed.



Figure 20: Example on green pavements and its implementation.



Figure 21: Implementation of green pavements in the case study area.

3.3 CS3-Combination Cool and Green Pavements

In this case scenario a combination of the two previous methods has been implemented. Both Cool and Green pavements were used in a 4:1 ratio, to investigate the efficiency of a mixed approach, including all the co-benefits from the two materials mentioned above. More specifically, 5 meters of Green Pavements were placed after every 20 meters of Cool Pavements, thus accounting for the different albedo values for each surface during the simulation process.

3.4 F2 Street Trees Scenario

Planting vegetation on streets creates shade and evapotranspiration and therefore has a cooling effect. At this scenario, strategically positioned deciduous trees have been placed every 5 meters along the roads. The height of the trees has been considered 10 meters.

3.5 K2 Street Trees Scenario

In order to compare the results on temperature reduction among two types of trees, conifer trees have been placed along the roads every 5 meters in this scenario. In this case, the height of the trees has also been considered 10 meters. In the figure below (Figure 22), the placement area of the street trees is displayed for both two scenarios.



Figure 22: Implementation of street trees in the case study area.

3.6 Green Canopy Scenario

A green canopy is selected to be located on the main pedestrian road of the selected area. This road extends in front of a four buildings school complex. This NBS type, except from the heat island phenomenon mitigation, focuses on the effect of green canopy on the psychology of pedestrians and urban design quality. In the figure below, the placement area of the green canopy is displayed (Figure 23).

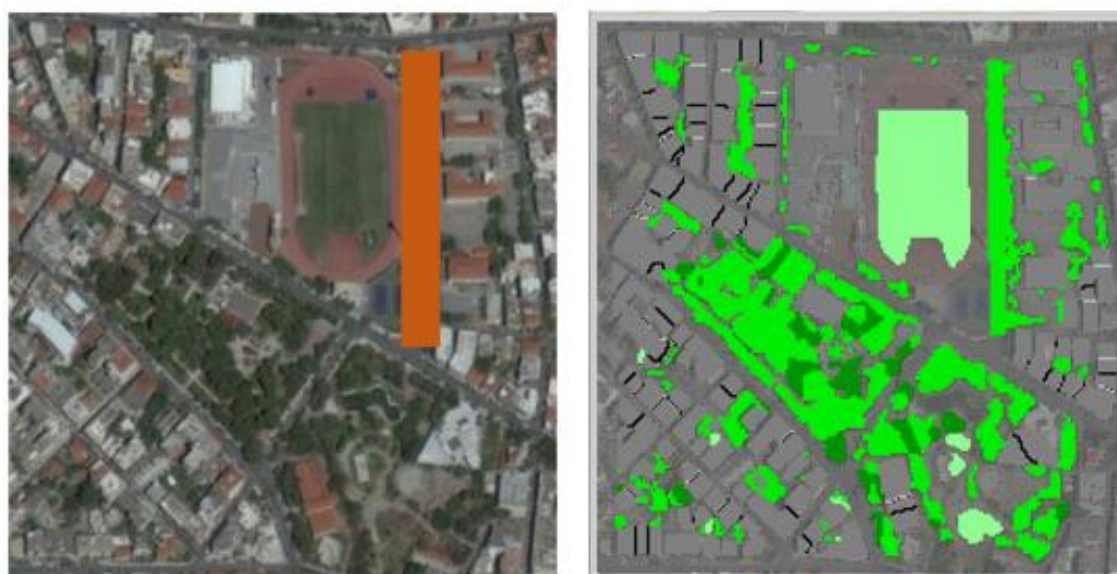


Figure 23: Implementation of green canopy in the case study area.

Chapter 4th

4. Simulation Results

4.1 Baseline scenario results

Figure 24 shows the Air Temperature of the baseline scenario at 14:00 o'clock. Areas A and B are close to the average temperature which has been used as an initial input. Noted that, although the area B represents the garden of Chania and it should act enhancing the cool island effect, it is observed that appears very high temperature. Figure 25 presents the Surface Temperature of the Baseline Scenario at 14:00 o'clock. Areas A and B have high temperature as they deal with concrete pavement and asphalt. Area C (garden of Chania) is cooler and still close to the initial average temperature (input temperature).

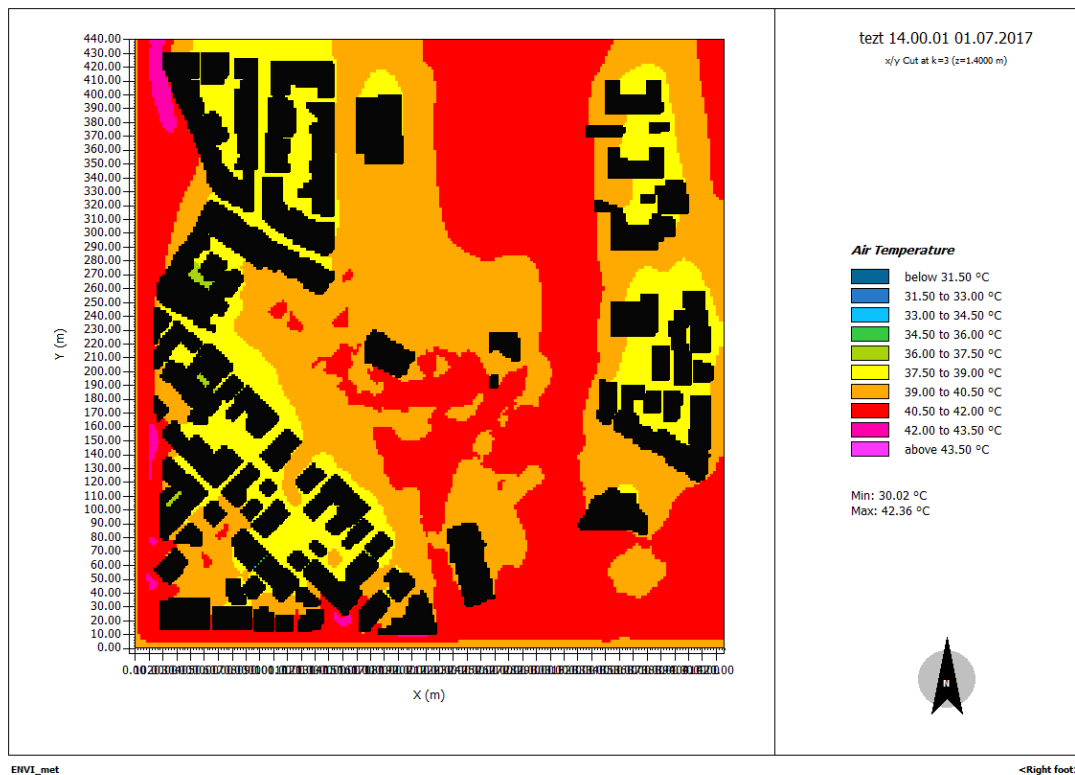


Figure 24: Baseline Scenario - Air Temperature (Time 14:00).

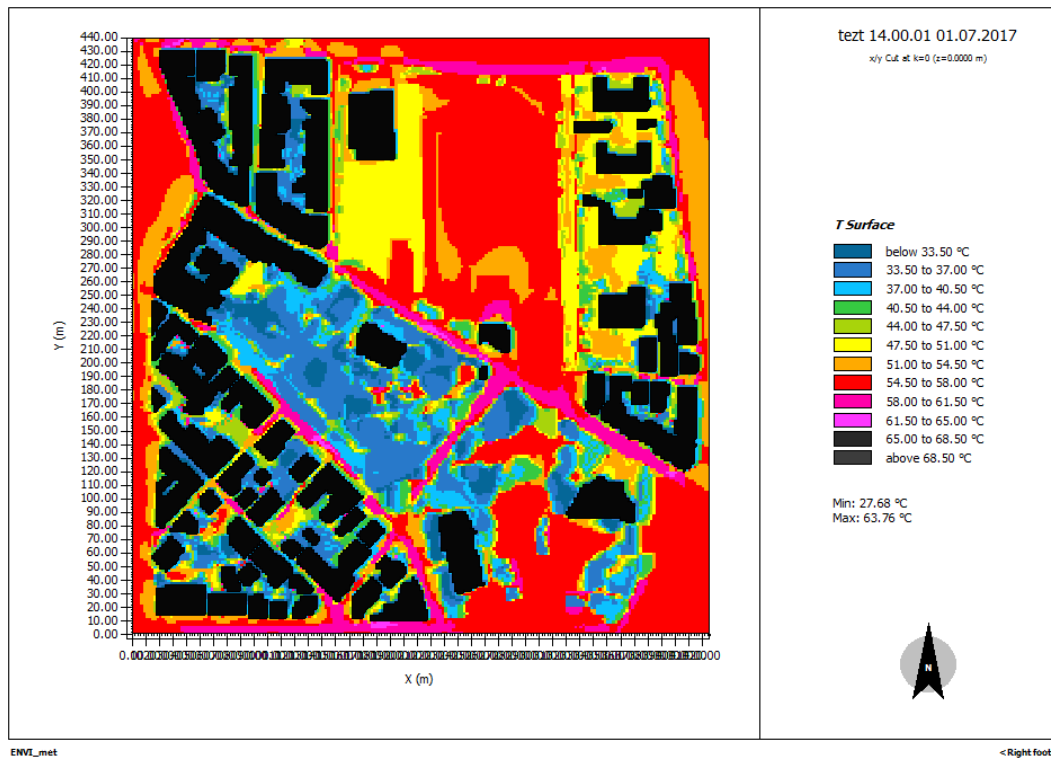


Figure 25: Baseline Scenario - Surface Temperature (Time 14:00).

4.2 Cool Pavement scenario results

The following figures illustrate the Air Temperature of the Cool Pavement Scenario at 14:00 o'clock (Figure 26) and the comparison between the Cool Pavement Scenario – Baseline Scenario concerning the Air Temperature at 14:00 o'clock (Figure 27). For all the examined areas, minor changes were observed in some very small and specific spots. For areas A and B the baseline's temperatures are ranged between 39°C – 40.5°C, while in the cool pavement scenario the temperatures are lower, ranged between 37.5°C – 39°C. More surface from areas A and B decrease temperature from the orange coloured range to yellow coloured. In case of area C the baseline's temperatures are between 40.5°C – 42°C, while in the cool pavement scenario the temperatures decrease in the specific spots are between 39°C – 40.5°C. More surface from area C decrease temperature from the red coloured range to orange coloured.

The Figures 28 and 29 show the Surface Temperature of the Cool Pavement Scenario at 14:00 o'clock and the comparison between the Cool Pavement Scenario – Baseline Scenario concerning the Surface Temperature at 14:00 o'clock, respectively. In the case of baseline scenario, areas A and B appears remarkable changes. More specifically, the baseline's temperatures ranged between 47.5°C - 51°C and 51°C – 54.5°C, while in the cool pavement scenario the temperatures decrease between 40,5°C - 44°C and 44°C – 47.5°C, respectively. In area C the changes are also evident. At the baseline scenario temperatures are between 54.5°C - 58°C, while at the cool pavement scenario the temperatures decrease between 44°C – 47.5°C. Undoubtedly, the cool pavement scenarios lead to very satisfied results and can help with the UHI effect. At the comparison figure (Figure 29), the cool pavement scenario is set as reference scenario, both for air temperature and surface temperature.

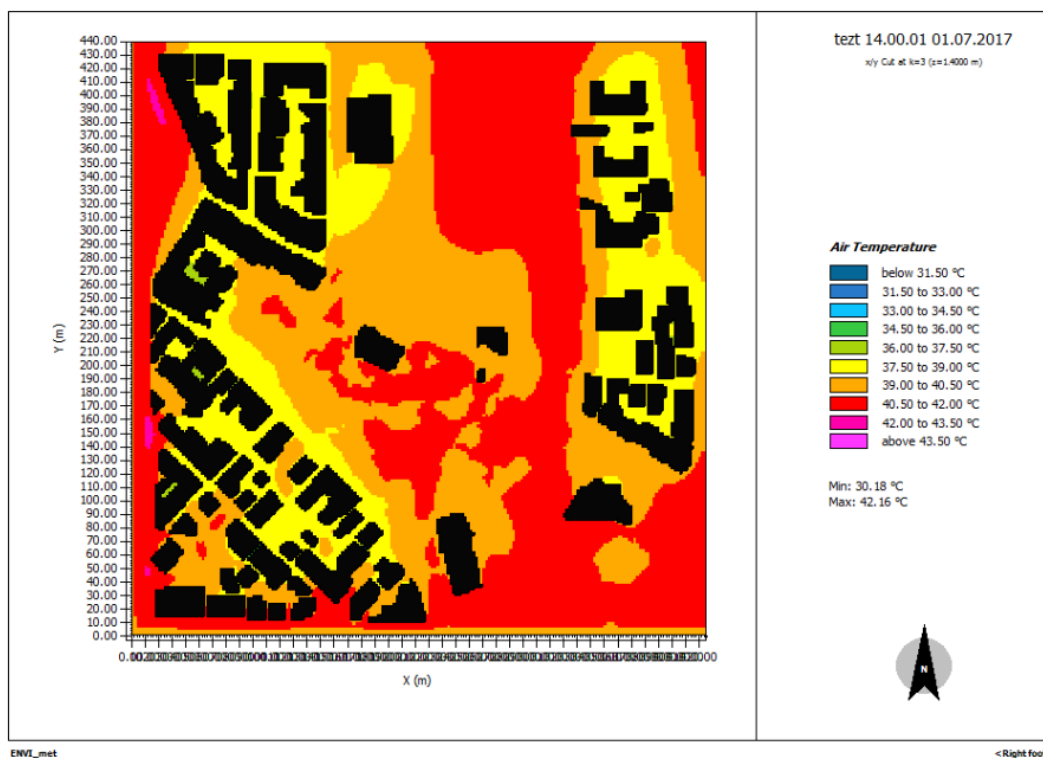


Figure 26: Cool Pavement Scenario - Air temperature (Time 14:00).

4. Results Presentation

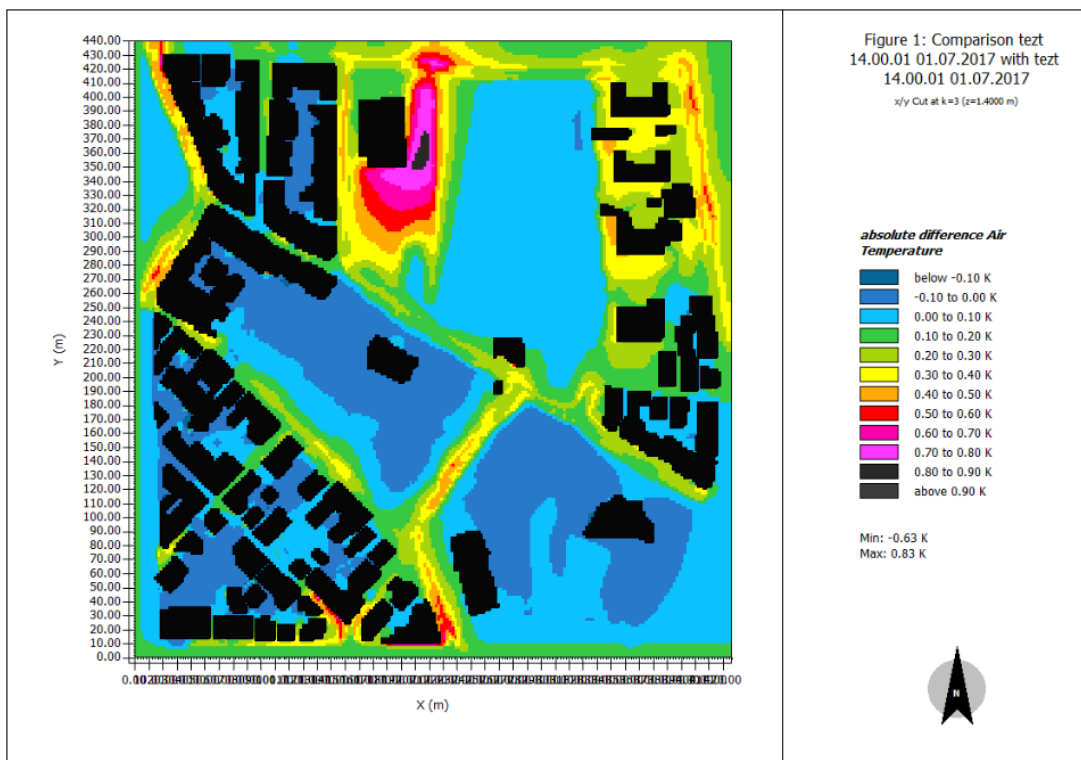


Figure 27: Comparison Cool Pavement Scenario-Baseline Scenario Air Temperature (Time 14:00).

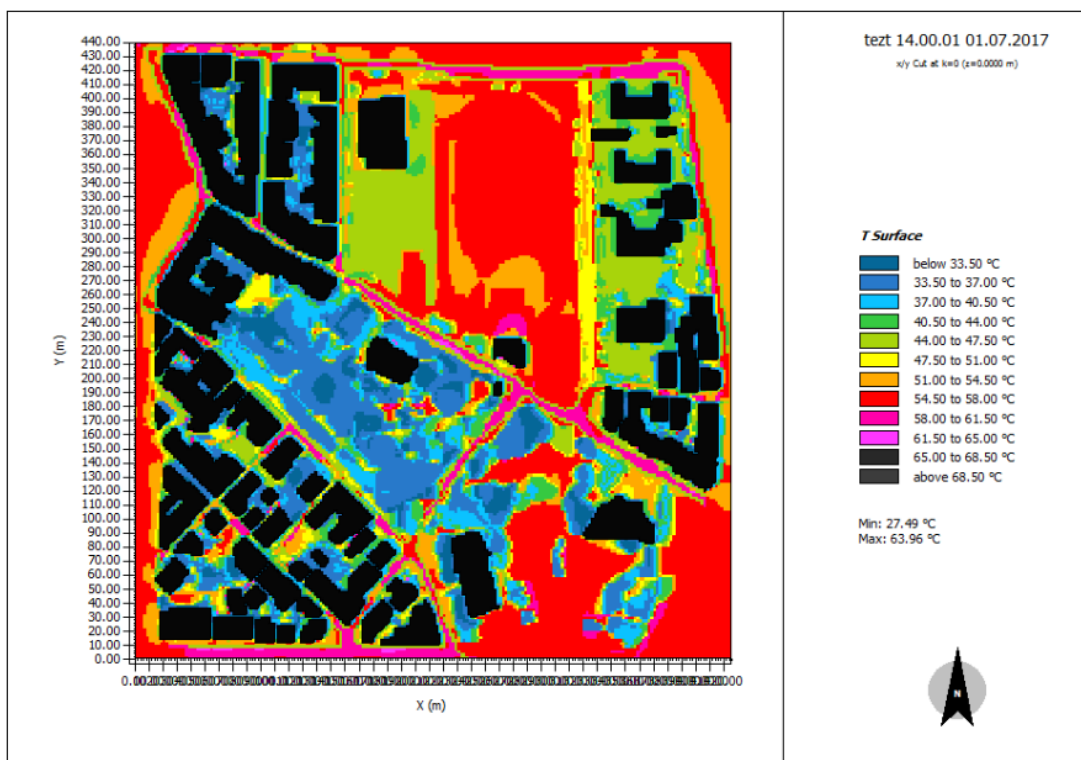


Figure 28. Cool Pavement Scenario - Surface Temperature (Time 14:00).

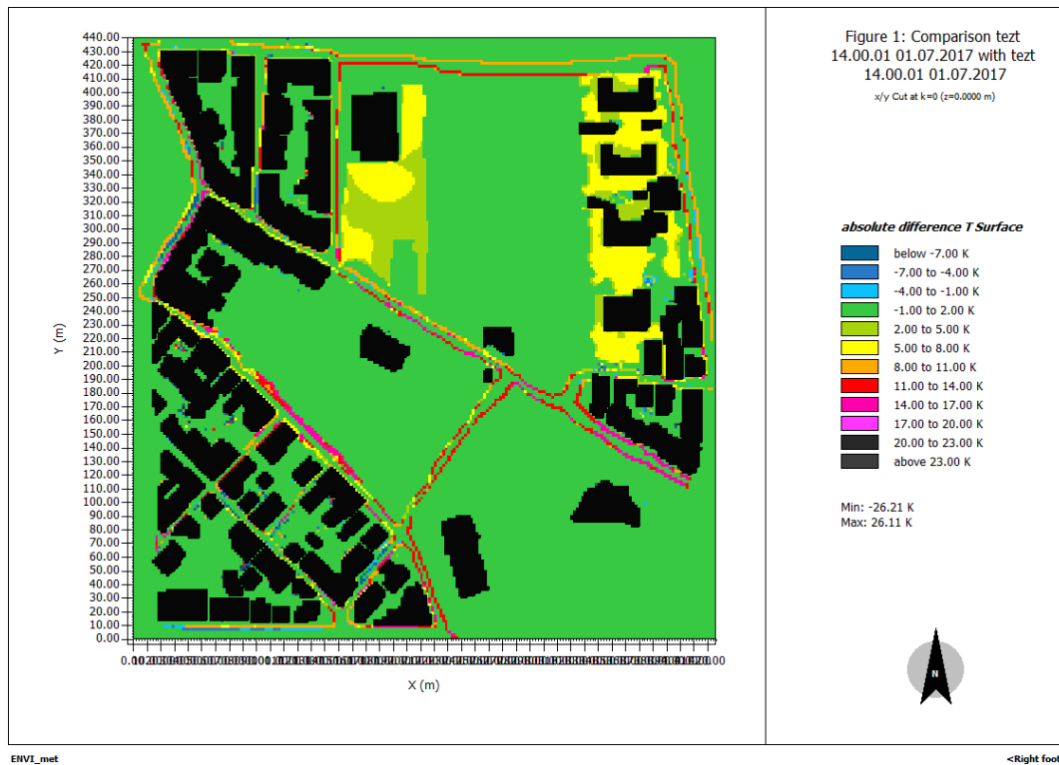


Figure 29: Comparison Cool Pavement Scenario-Baseline Scenario Surface Temperature (Time 14:00).

4.3 Green Pavements scenario results

The Air Temperature of the Green Pavement Scenario at 14:00 o'clock and the comparison between the Green Pavement Scenario – Baseline Scenario concerning the Air Temperature at 14:00 o'clock are illustrated in Figures 29 and 31, respectively. The baseline's temperatures of areas A and B ranged between 37.5°C – 39°C, while in the green pavement scenario the temperatures increase between 39°C – 40.5°C. More surface from area A and area B increase temperature from the yellow coloured range to orange coloured. In some parts of the area C the baseline's temperatures are between 37.5°C – 39°C, while in the green pavement scenario the temperatures increase between 39°C – 40.5°C. In other parts the baseline's temperatures ranged between 39°C – 40.5°C, while in the green pavement scenario the temperatures increase between 40°C – 42°C. In the first case more surface from area C increase temperature from the yellow coloured range to orange coloured range

and in the second case more surface from area C increase temperature from the orange coloured range to red coloured.

The Surface Temperature of the Green Pavement Scenario at 14:00 o'clock and the comparison between the Green Pavement Scenario – Baseline Scenario, concerning the Surface Temperature at 14:00 o'clock, are illustrated in Figures 30 and 31, respectively. The baseline's temperatures of areas A and B ranged between 47.5°C – 51°C, while in the green pavement scenario the temperatures increase between 51°C – 54.5°C. More surface from area A increase temperature from the yellow coloured range to orange coloured range. Evident changes in case of area C are noticed only in some very small spots. In the case of the baseline scenario temperatures are between 58°C – 61.5°C, while in the green pavement scenario the temperatures decrease between 51°C – 54.5°C and 47.5 °C – 51°C. More surface from area C decrease temperature from the purple coloured range to yellow and orange coloured.

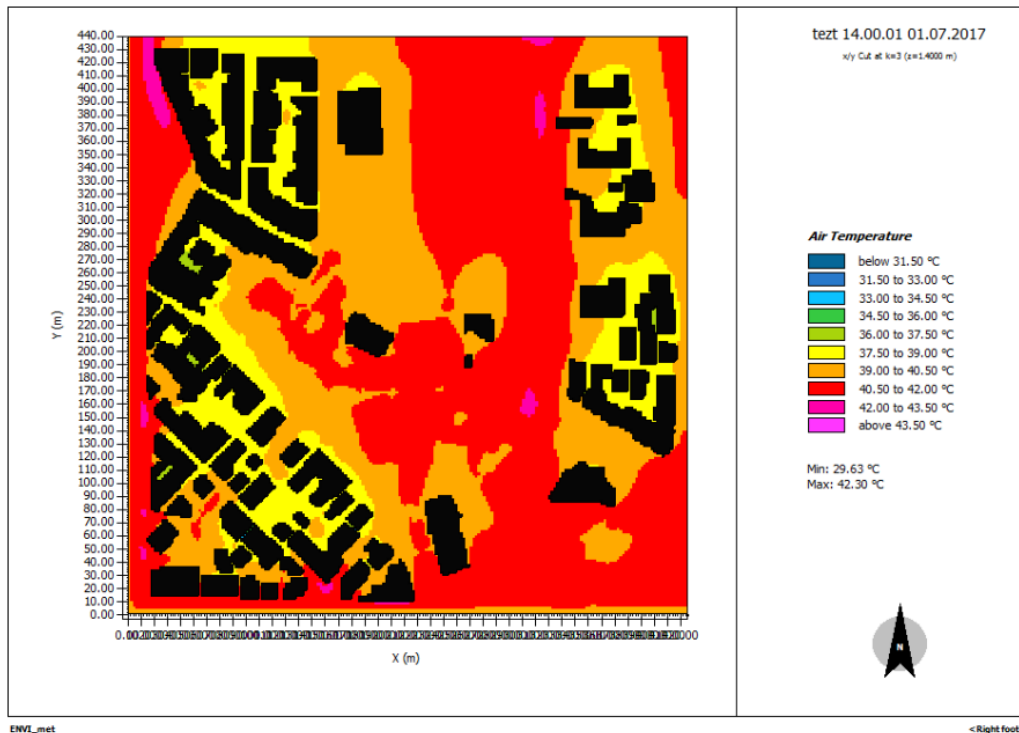


Figure 30: Green Pavement Scenario - Air temperature (Time 14:00).

4. Results Presentation

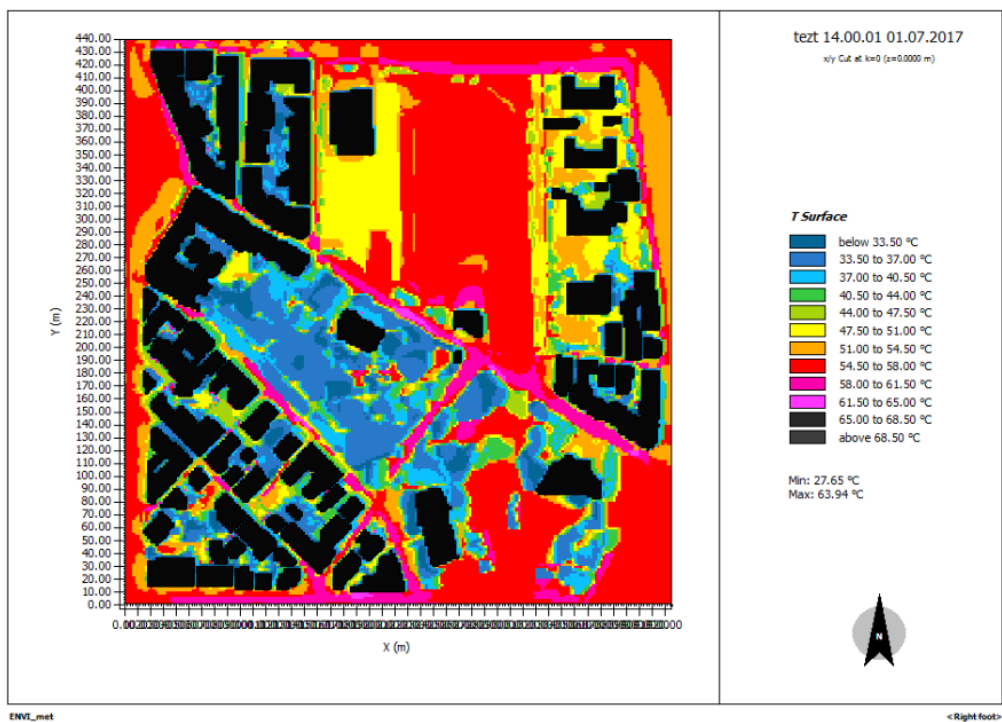


Figure 31: Green Pavement Scenario - Surface Temperature (Time 14:00).

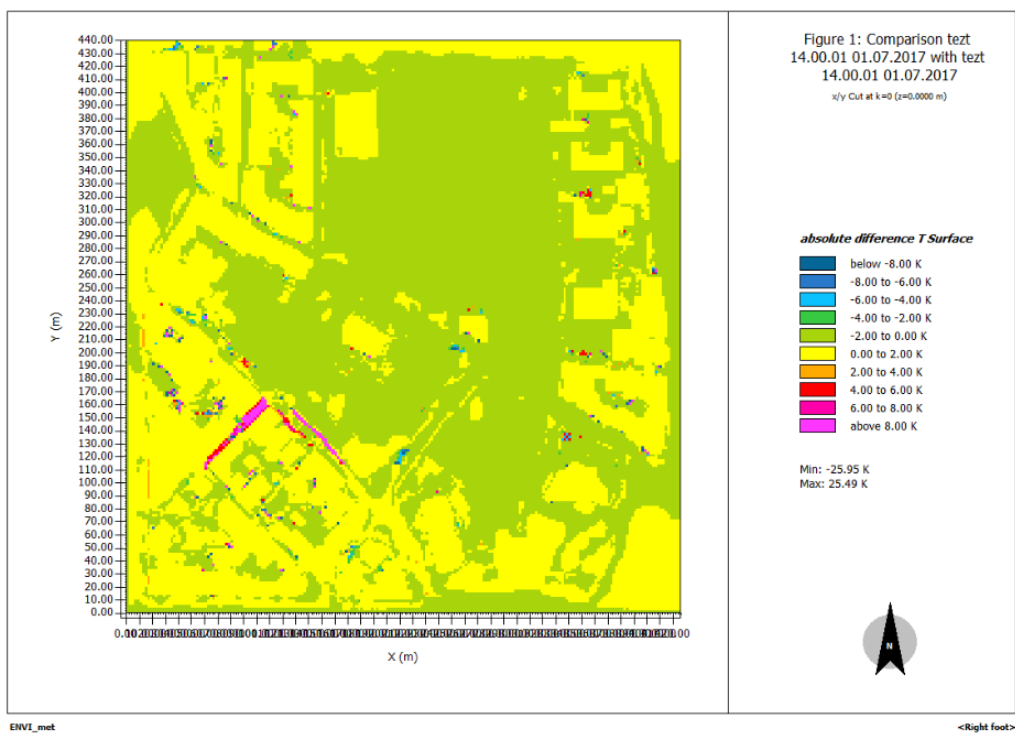


Figure 32: Comparison Green Pavement Scenario - Baseline Scenario Surface Temperature (Time 14:00).

4.4 Combination of Cool and Green Pavements scenario results

The Figures 33 and 34 illustrate the Air Temperature of the Cool and Green Pavement Scenario at 14:00 o'clock and the comparison between the Cool and Green Pavement Scenario – Baseline Scenario concerning the Air Temperature at 14:00 o'clock, respectively. For the areas A and B we can observe some small changes in specific spots. In particular, the baseline's temperatures are between 39°C – 40.5°C while in the cool and green pavement scenarios decreasing of the temperatures, ranged between 37.5°C – 39°C, was observed at the same spots. More surface from area A and B decrease temperature from the orange coloured range to yellow coloured. For the area C we can notice some small changes in specific spots. More specific the baseline's temperatures are between 40.5°C – 42°C while in the cool and green pavement scenarios decreasing of the temperatures ranged, between 37.5°C – 39°C was observed at the same spots. More surface from area A, area B decrease temperature from the red coloured range to orange coloured.

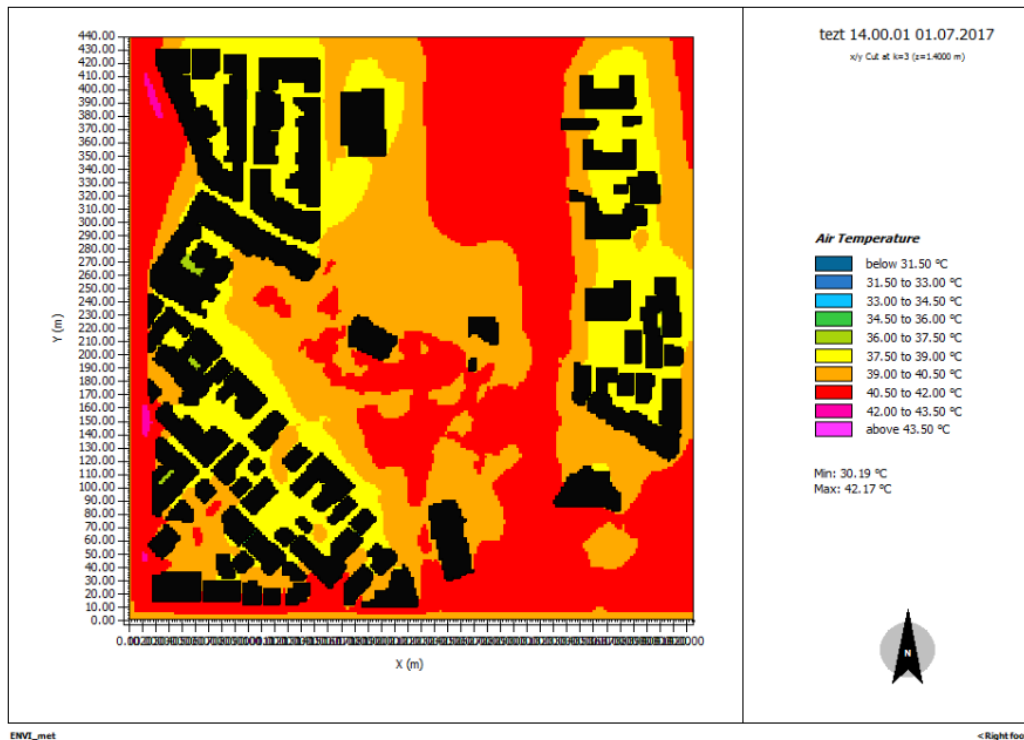


Figure 33: Cool and Green Pavement Scenario - Air temperature (Time 14:00).

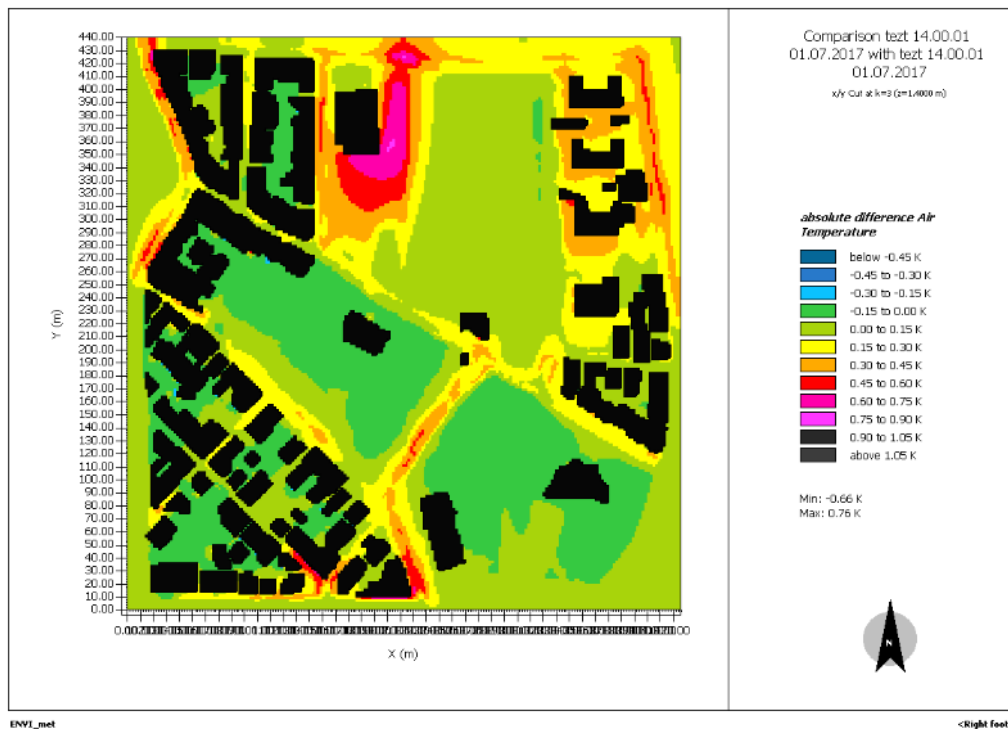


Figure 34: Comparison Cool and Green Pavement Scenario - Baseline Scenario Air Temperature (Time 14:00).

The Figures 35 and 36 illustrate the Surface Temperature of the Cool and Green Pavement Scenario at 14:00 o'clock and the comparison between the Cool and Green Pavement Scenario – Baseline Scenario concerning the Surface Temperature at 14:00 o'clock respectively. For the area A and area B we see that the changes are remarkable. For area A the baseline's temperatures are between 51°C – 54.5°C and between 47.5°C – 51°C while in the cool and green pavement scenario decreasing of the temperatures ranged between 44°C – 47.5°C and between 40.5°C – 44°C. More surface from area A decrease temperature from the yellow and orange coloured range to green and light green coloured. For area B the baseline's temperatures are between 47.5°C – 51°C while in the cool and green pavement scenario decreasing of the temperatures ranged between 44°C – 47.5°C. More surface from area B decrease temperature from the yellow coloured range to light green coloured. For the area C the changes are also evident. At the baseline scenario temperatures are between 54.5°C - 58°C while in the cool and green pavement scenario decreasing of the temperatures ranged between 44°C – 47.5°C. More surface from area C decrease temperature from the red coloured range to light green coloured. Reprehensively the

cool and green pavement scenarios have very satisfied results and can help with the UHI effect.

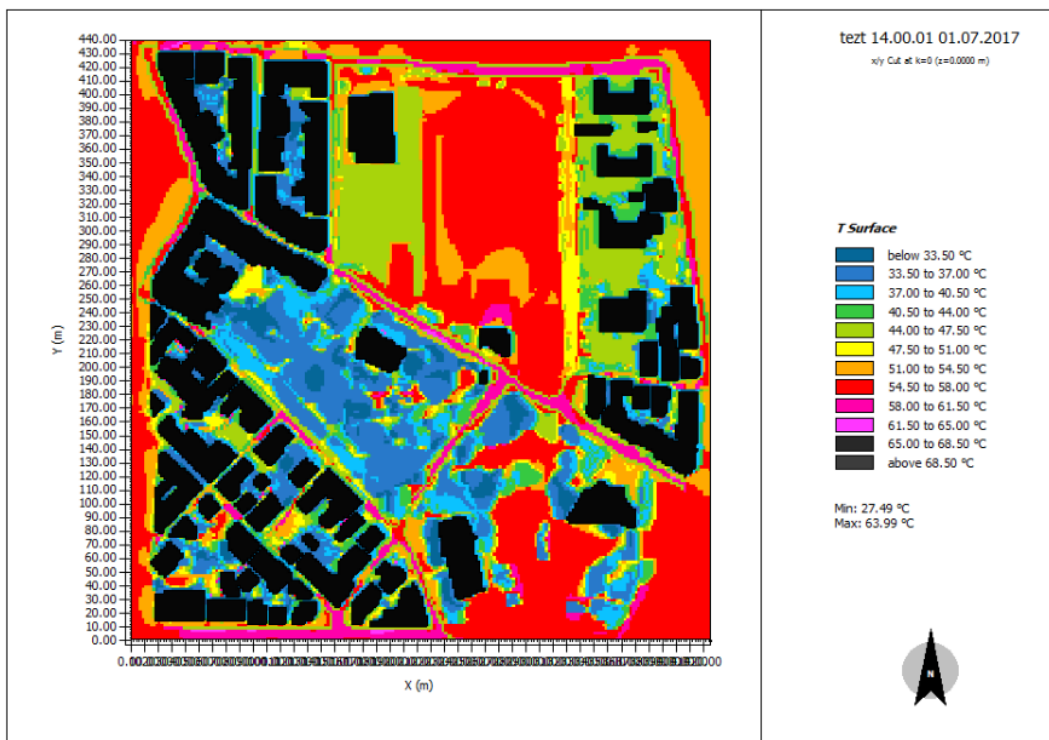


Figure 35: Cool and Green Pavement Scenario - Surface Temperature (Time 14:00).



Figure 36: Comparison Cool and Green Pavement Scenario - Baseline Scenario Surface Temperature (Time 14:00).

The Figures 37, 38 and 39 illustrate the Air Temperature of the Cool Pavements Scenario and Cool and Green Pavement Scenario at 14:00 o'clock and the comparison between the Cool Pavement Scenario - Cool and Green Pavement Scenario concerning the Air Temperature at 14:00 o'clock respectively. For area A the cool pavements temperatures are identical with cool and green pavement scenario. It something we were expecting for due to the fact that in this area we have cool pavement in both scenarios. For area B we can see changes in some specific areas. In these areas the cool pavements scenario temperatures are between 37.5°C – 39°C while in the cool and green pavement (only green pavement application) scenario increasing of the temperatures ranged between 39°C – 40.5°C, changing from the orange coloured range to yellow coloured. For the area C we can see minor changes in some very small and specific spots. More specific the cool pavements temperatures in the areas we care about are between 37.5°C – 39°C while in the cool and green pavement scenario increasing of the temperatures ranged between 39°C – 40.5°C changing from the yellow colour range to orange colour range. So, the cool pavement scenario is better than the cool and green pavement scenario in details as a solution for the UHI mitigation.

4. Results Presentation

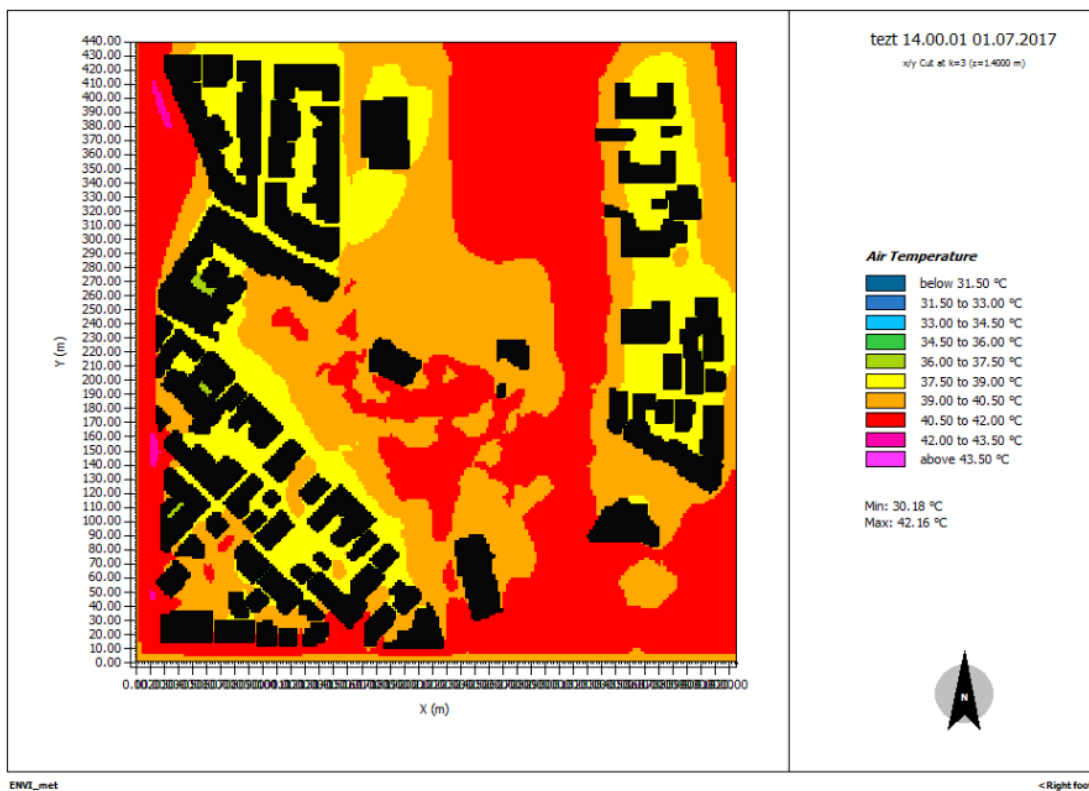


Figure 37: Cool Pavement Scenario - Air temperature (Time14:00).

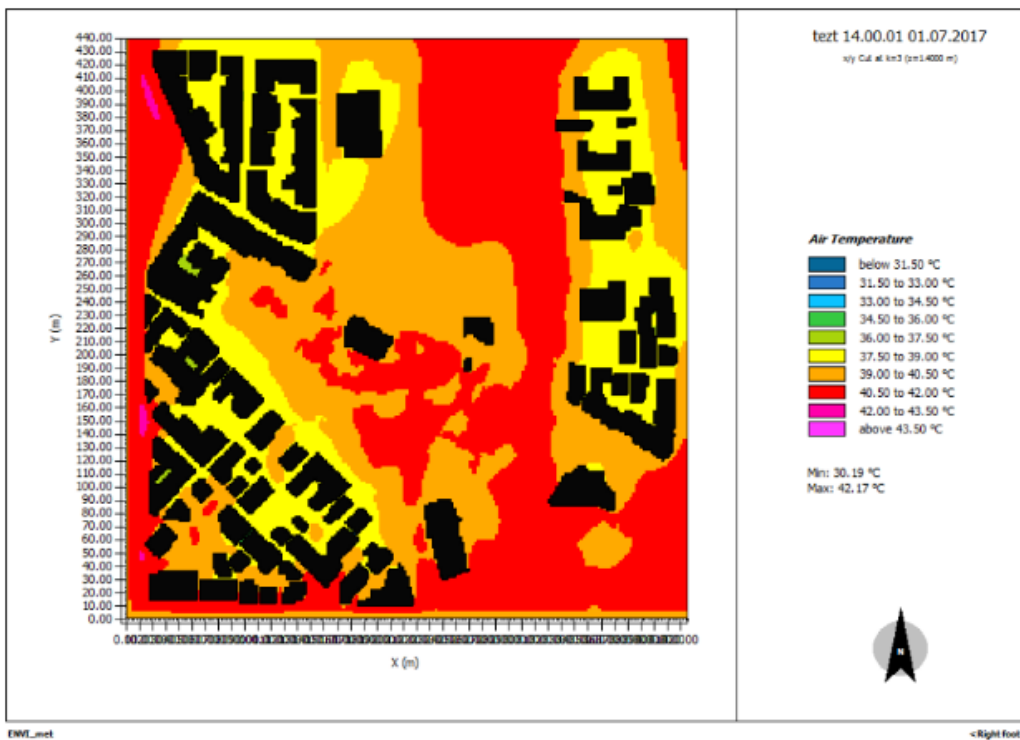


Figure 38: Cool and Green Pavement Scenario - Air temperature (Time14:00).

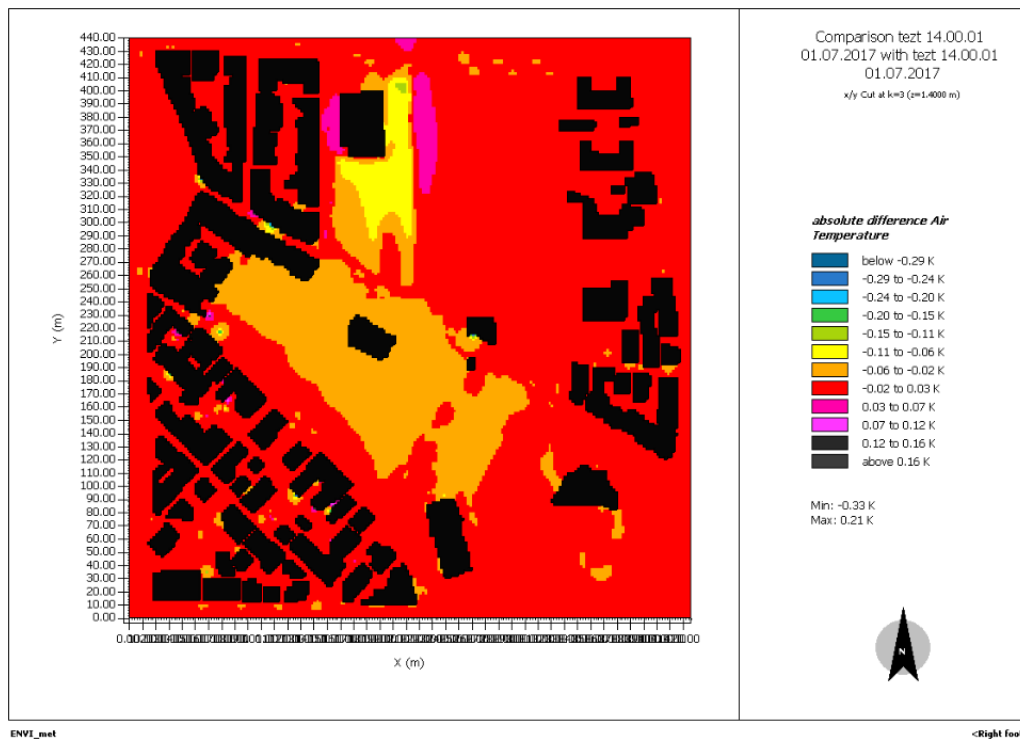


Figure 39: Comparison Cool Pavement Scenario - Cool and Green Pavement Scenario Air Temperature (Time 14:00).

The Figures 40, 41 and 42 illustrate the Surface Temperature of the Cool Pavements Scenario and Cool and Green Pavement Scenario at 14:00 o'clock and the comparison between the Cool pavement Scenario - Green Pavement Scenario concerning the Surface Temperature at 14:00 o'clock respectively. For area A the cool pavements temperatures are identical with cool and green pavement scenario. It something we were expecting for due to the fact that in this area we have cool pavement in both scenarios. For area B we can see changes in some specific areas. In these areas the cool pavements scenario temperatures are between 40.5°C – 44°C while in the cool and green pavement (only green pavement application) scenario increasing of the temperatures ranged between 44°C – 47.5°C, changing from the orange coloured range to yellow coloured. For area C the cool pavements temperatures are identical with cool and green pavement scenario. So, the cool pavement scenario is better than the cool and green pavement scenario in details as a solution for the UHI mitigation.

4. Results Presentation

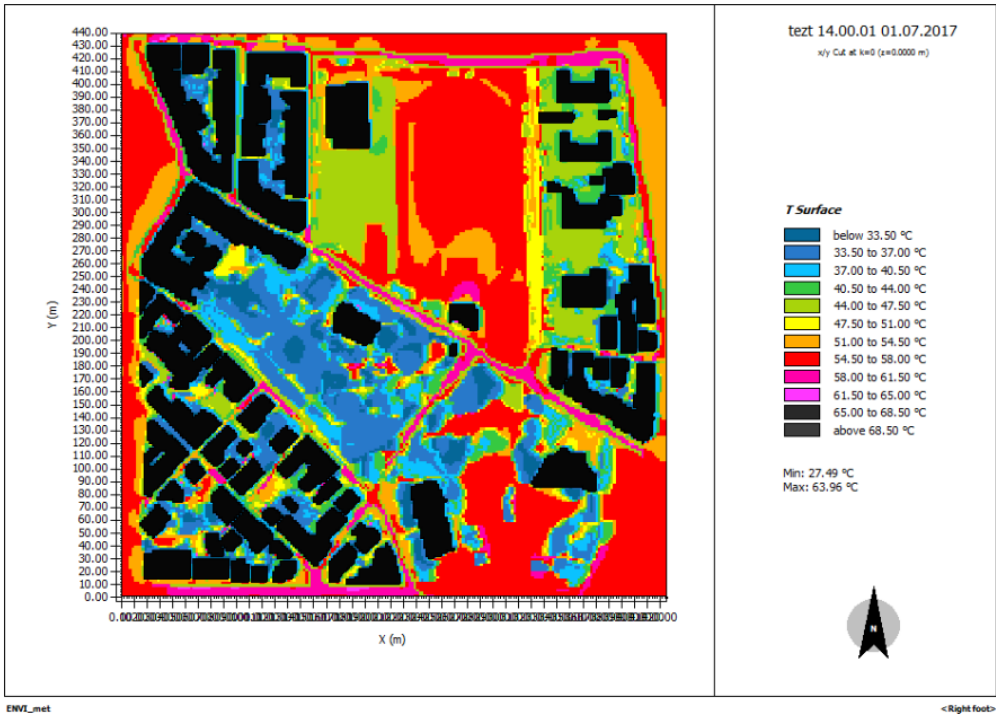


Figure 40: Cool Pavement Scenario - Surface Temperature (Time 14:00).

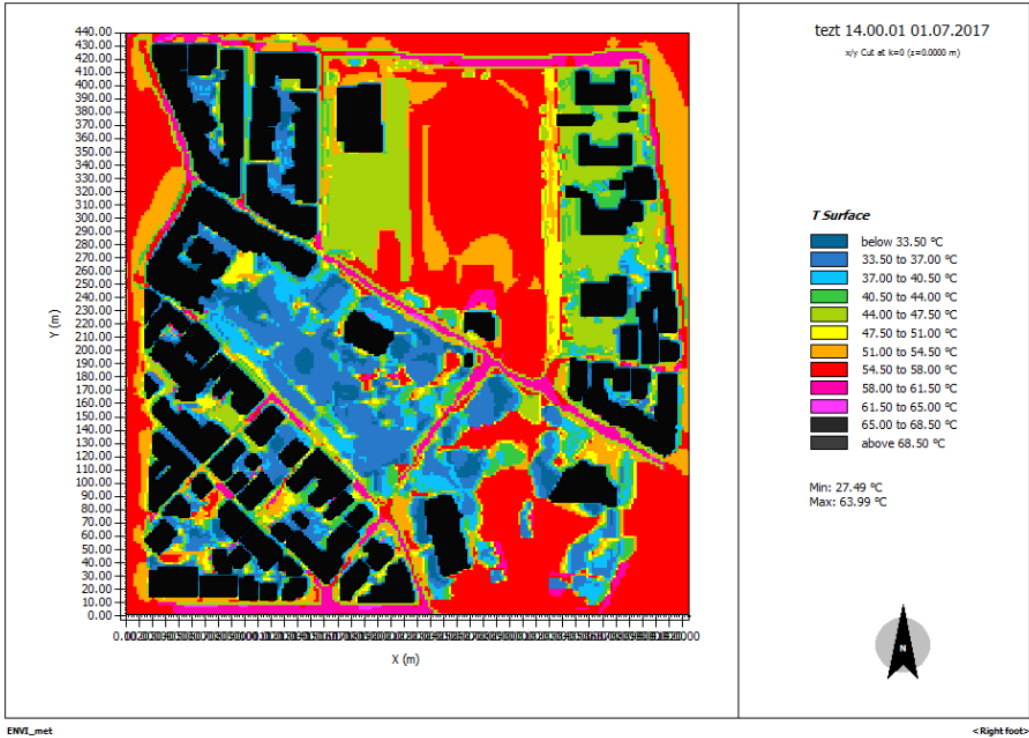


Figure 41: Cool and Green Pavement Scenario - Surface Temperature (Time 14:00).

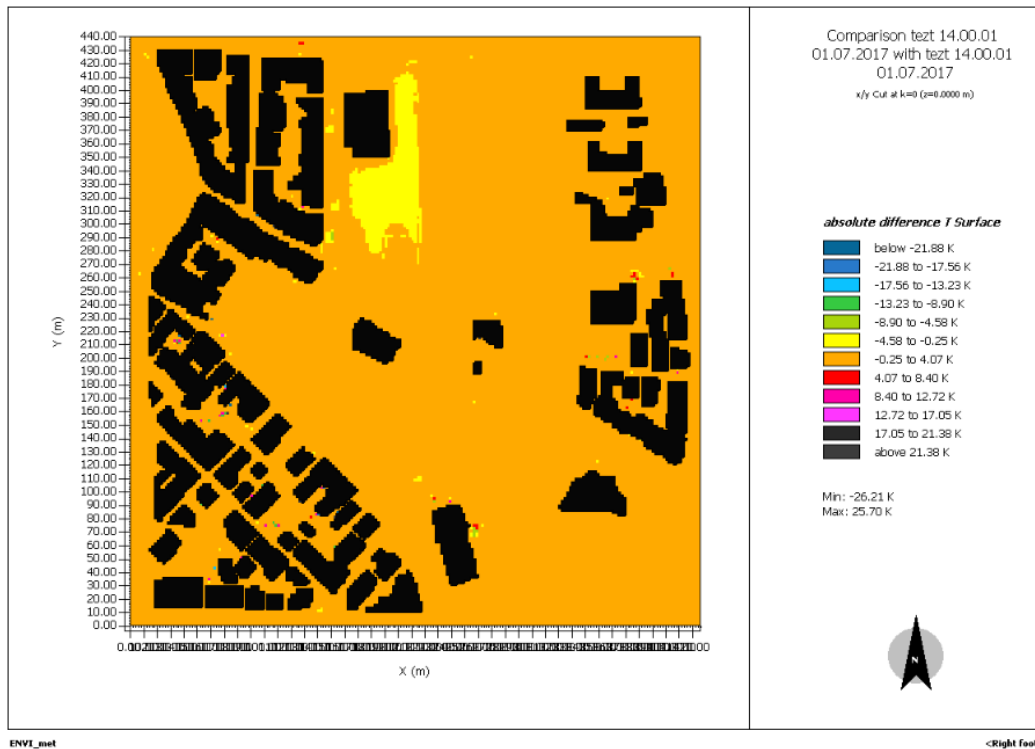


Figure 42: Comparison Cool Pavement Scenario - Cool and Green Pavement Scenario Surface Temperature (Time 14:00).

4.5 F2 Street Trees Scenario

The Figures 43 and 44 illustrate the Air Temperature of the F2 trees scenario at 14:00 o'clock and the comparison between the F2 trees scenario – Baseline concerning the Air Temperature at 14:00 o'clock, respectively. For the areas A, B and C we can observe some minor changes in specific spots. For the area A the baseline's temperatures are between 40.5°C – 42°C while in the F2 trees scenario decreasing of the temperatures, ranged between 39°C – 40.5°C, was observed at the same spots. More surface from area A decrease temperature from the red coloured range to orange coloured. Also in some spots, the baseline's temperatures are between 37.5°C – 39°C while in the F2 Trees scenario increasing of the temperatures ranged between 39°C – 40.5°C. More surface from area A increase temperature from the yellow coloured range to orange coloured. For the area B the baseline's temperatures are between 40.5°C – 42°C while in the F2 Trees scenario decreasing of the temperatures, ranged between 39°C – 40.5°C. More surface from area B decrease temperature from the red coloured range to orange coloured. Also in some spots the baseline's temperatures are

4. Results Presentation

between 39°C – 40.5°C while in the F2 Trees scenario increasing of the temperatures ranged between 40.5°C – 42°C. More surface from area A decrease temperature from the orange coloured range to red coloured. For the area C the baseline's temperatures are between 39°C – 40.5°C and 37.5°C – 39°C while in the F2 Trees scenario decreasing of the temperatures, ranged between 37.5°C – 39°C and 36°C – 37.5°C. More surface from area C decrease temperature from the orange and yellow coloured range to yellow and green coloured.

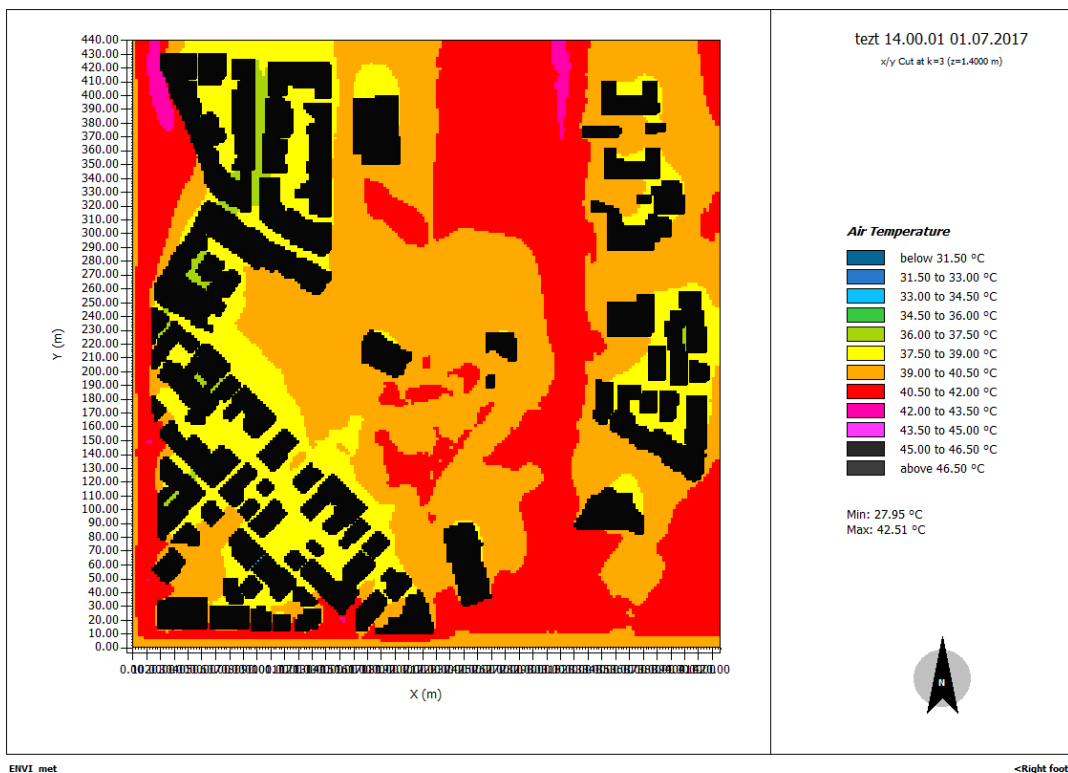


Figure 43: F2 Trees Scenario - Air Temperature (Time 14:00).

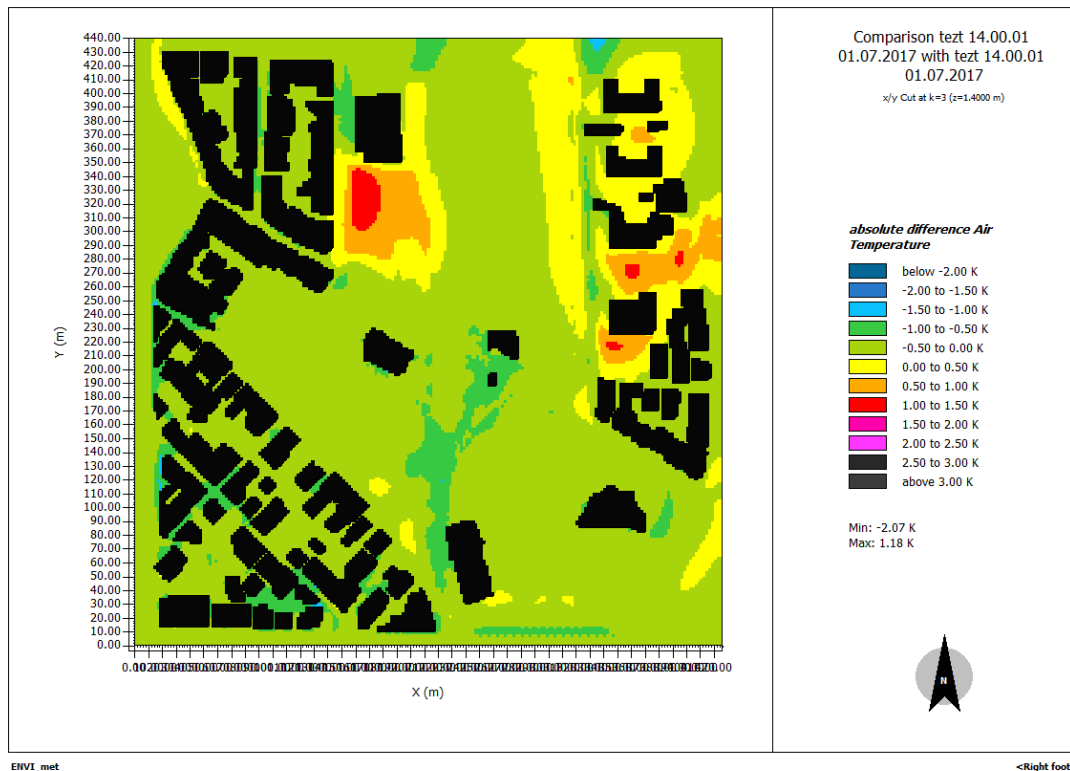


Figure 44: Comparison F2 Trees Scenario - Baseline Scenario Air Temperature (Time 14:00).

The Figures 45 and 46 illustrate the surface temperature of the F2 Trees Scenario at 14:00 o'clock and the comparison between the F2 Trees Scenario – Baseline Scenario, concerning the Air Temperature at 14:00 o'clock, respectively. For the areas A, B and C we can observe that the changes are remarkable. For area A the baseline's temperatures are between 51°C – 54.5°C, 47.5°C – 51°C and 44°C – 47.5°C while in the F2 Trees scenario decreasing of the temperatures ranged between 37°C – 40.5°C, 33.5°C – 37°C and below 33.5°C. More surface from area A decrease temperature from the orange, yellow and green coloured range to light blue, blue and dark blue coloured. For area B the baseline's temperatures are between 47.5°C – 51°C while in the F2 Trees scenario decreasing of the temperatures ranged between 37°C – 40.5°C and 33.5°C – 37°C. More surface from area B decrease temperature from the yellow coloured range to light blue and blue coloured. For area C the baseline's temperatures are between 54°C – 58°C and 51°C – 54.5°C while in the F2 Trees scenario decreasing of the temperatures ranged between 47.5°C – 51°C and 44°C – 47.5°C. More surface from area C decrease temperature from the red and orange coloured range to yellow and green coloured.

4. Results Presentation

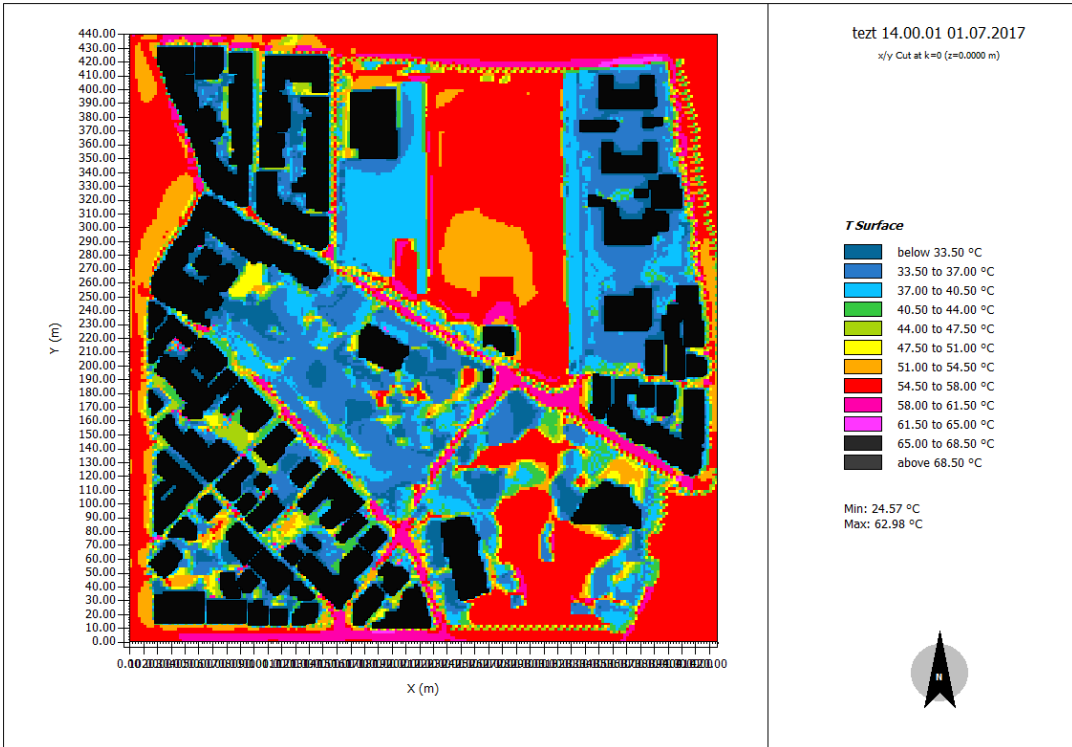


Figure 45: F2 Trees Scenario - Surface Temperature (Time 14:00).

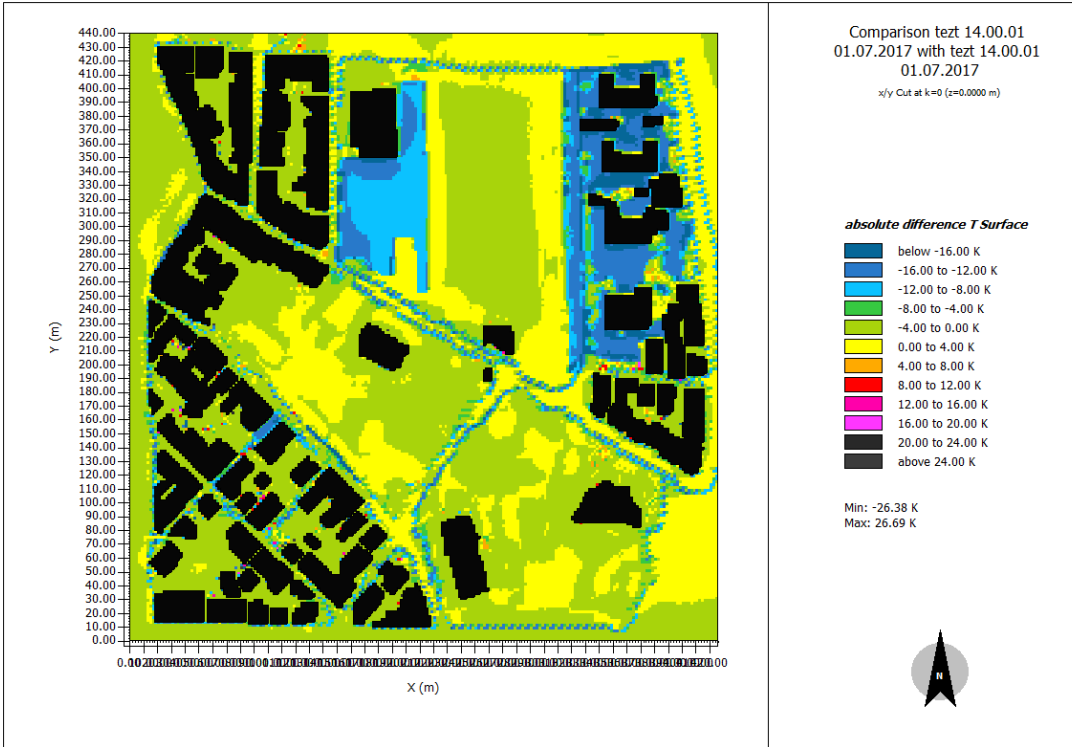


Figure 46: Comparison F2 Trees Scenario - Baseline Scenario Surface Temperature (Time 14:00).

4.6 K2 Street Trees Scenario

The Figures 47 and 48 illustrate the Air Temperature of of the K2 Trees Scenario at 14:00 o'clock and the comparison between the K2 Trees Scenario – Baseline Scenario, concerning the Air Temperature at 14:00 o'clock, respectively. For the areas A, B and C we can observe that the changes are remparkable. For the area A, area B and area C we can notice some changes in some very specific areas. For area A the baseline's temperatures are between 40.5°C – 42°C, 39°C – 40.4°C and 37.5°C – 39°C while in the K2 Trees scenario decreasing of the tempertures ranged between 39°C – 40.5°C, 37.5°C – 39°C and 36°C – 37.5°C. More surface from area A decrease temperature from the red, orange and yellow coloured range to orange, yellow and light green coloured range respectively. For the area B the baseline's temperatures are between 39°C – 40.5°C while in the K2 Trees scenario decreasing of the temperatures ranged between 37.5°C – 39°C and 36°C – 37.5°C. More surface from area B decrease temperature from the orange coloured range to yellow and light green coloured. For the area C the baseline's temperatures are between 40.5°C – 42°C, 39°C – 40.5°C and 37.5°C – 39°C while in the K2 Trees scenario decreasing of the temperatures ranged between 39°C – 40.5°C, 37.5°C – 39°C and 36°C – 37.5°C. More surface from area C decrease temperature from the red, orange and yellow coloured range to orange, yellow and light green coloured respectively.

4. Results Presentation

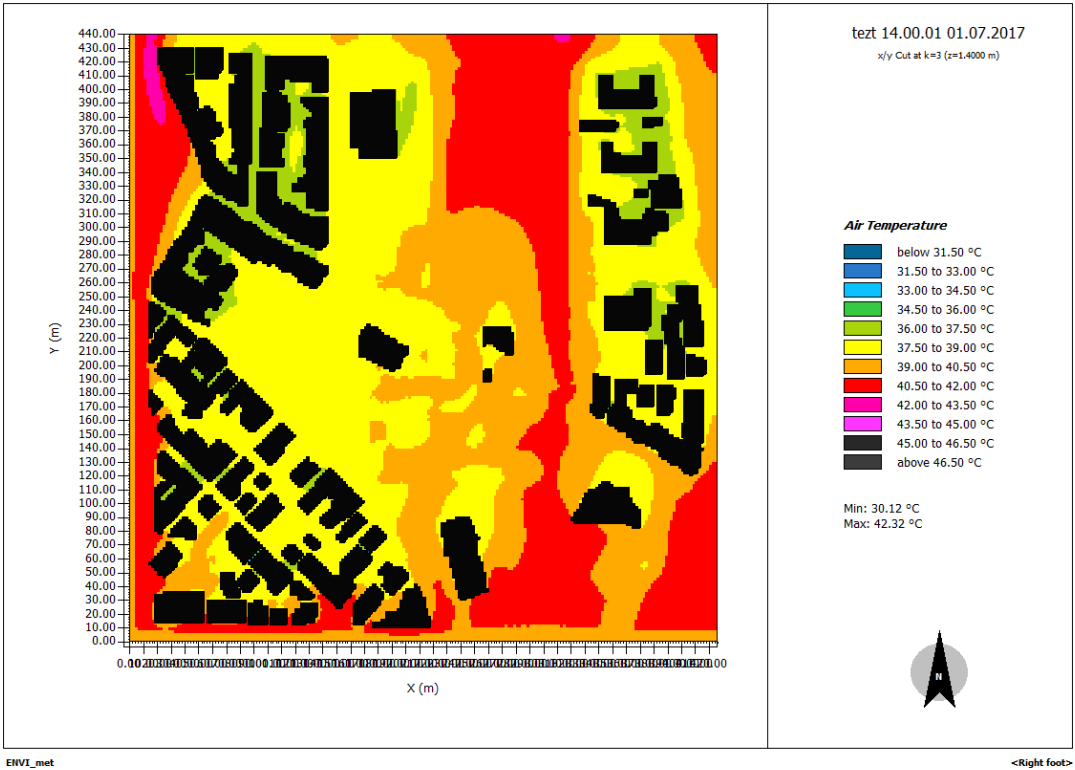


Figure 47: K2 Trees Scenario - Air temperature (Time 14:00).

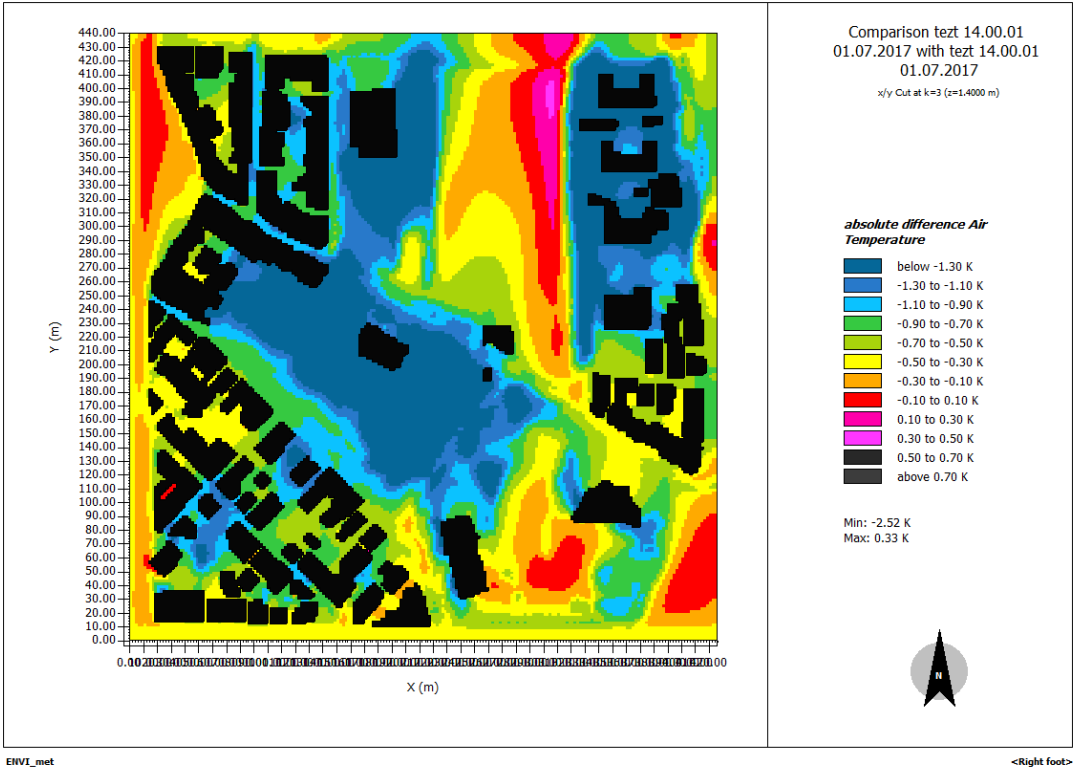


Figure 48: Comparison K2 Trees Scenario - Baseline Scenario Air Temperature (Time 14:00).

The Figures 49 and 50 illustrate the Surface Temperature of the K2 Trees Scenario at 14:00 o'clock and the comparison between the K2 Trees Scenario – Baseline Scenario concerning the Surface Temperature at 14:00 o'clock. For Areas A, B and C we can observe remarkable changes. For area A the baseline's temperatures are between 51°C – 54.5°C, 47.5°C – 51°C and 44°C – 47.5°C while in the K2 Trees scenario decreasing of the temperatures ranged between 37°C – 40.5°C, 33.5°C – 37°C and below 33.5°C. More surface from area A decrease temperature from the orange, yellow and green coloured range to light blue, blue and dark blue coloured. For area B the baseline's temperatures are between 47.5°C – 51°C while in the K2 Trees scenario decreasing of the temperatures ranged between 37°C – 40.5°C, 33.5°C – 37°C. More surface from area B decrease temperature from the yellow colour range to light blue and blue coloured. For area C the baseline's temperatures are between 58°C – 61.5°C and 54.5°C – 58°C and 51°C – 54.5°C while in the K2 Trees scenario decreasing of the temperatures ranged between 47.5°C – 51°C and 44°C – 47.5°C, 37°C – 40.5°C and 33.5°C – 37°C. More surface from area C decrease temperature from the rose, red and orange coloured range to yellow, light green, light blue and blue coloured.

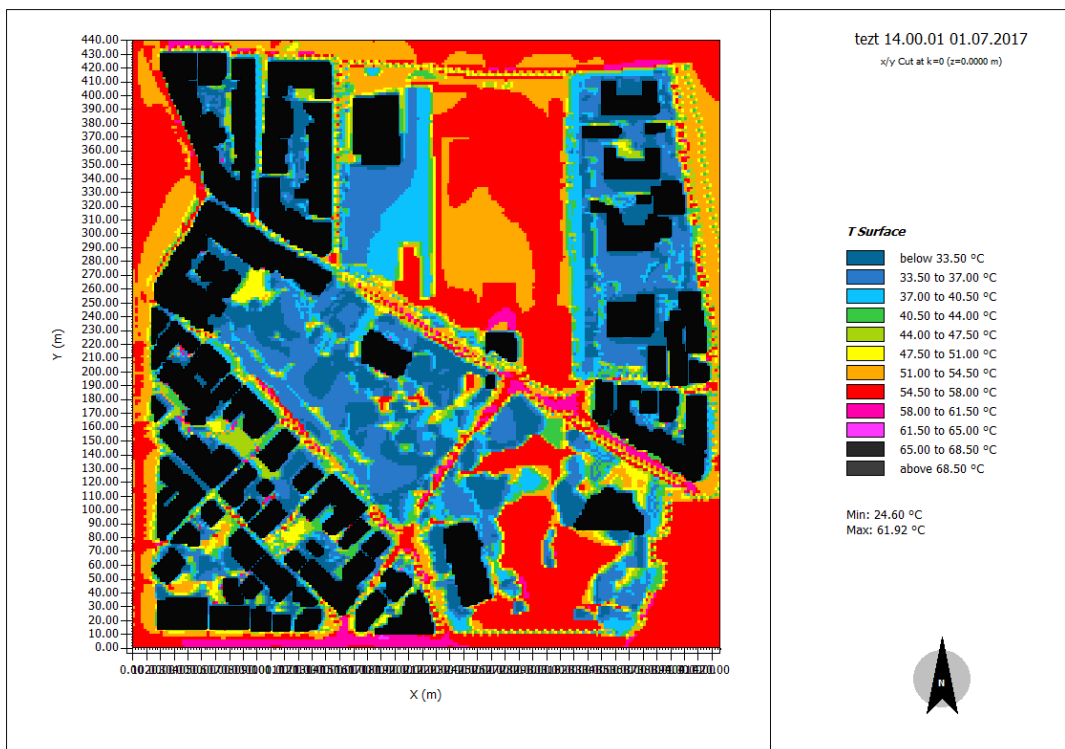


Figure 49: K2 Trees Scenario - Surface Temperature (Time 14:00).



Figure 50: Comparison K2 Trees Scenario - Baseline Scenario Surface Temperature (Time 14:00).

4.7 Green Canopy Scenario

The Figures 51 and 52 illustrate the Air Temperature of the Green Canopy Scenario at 14:00 o'clock and the comparison between Green Canopy Scenario – Baseline Scenario concerning the Air Temperature at 14:00 o'clock. For area A the baseline's temperatures are between 40.5°C – 42°C while in the Green Canopy scenario decreasing of the temperatures ranged between 39°C – 40.5°C. More surface from area A decrease temperature from the red coloured range to orange coloured respectively.

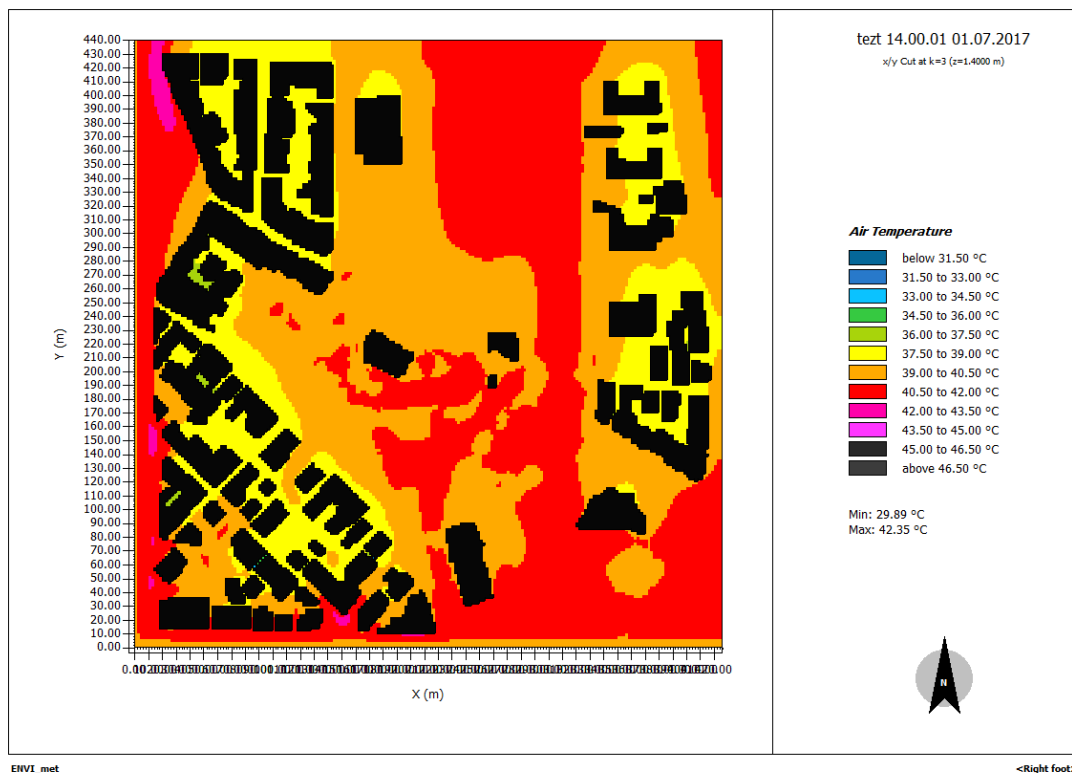


Figure 51: Green Canopy Scenario - Air Temperature (Time 14:00).

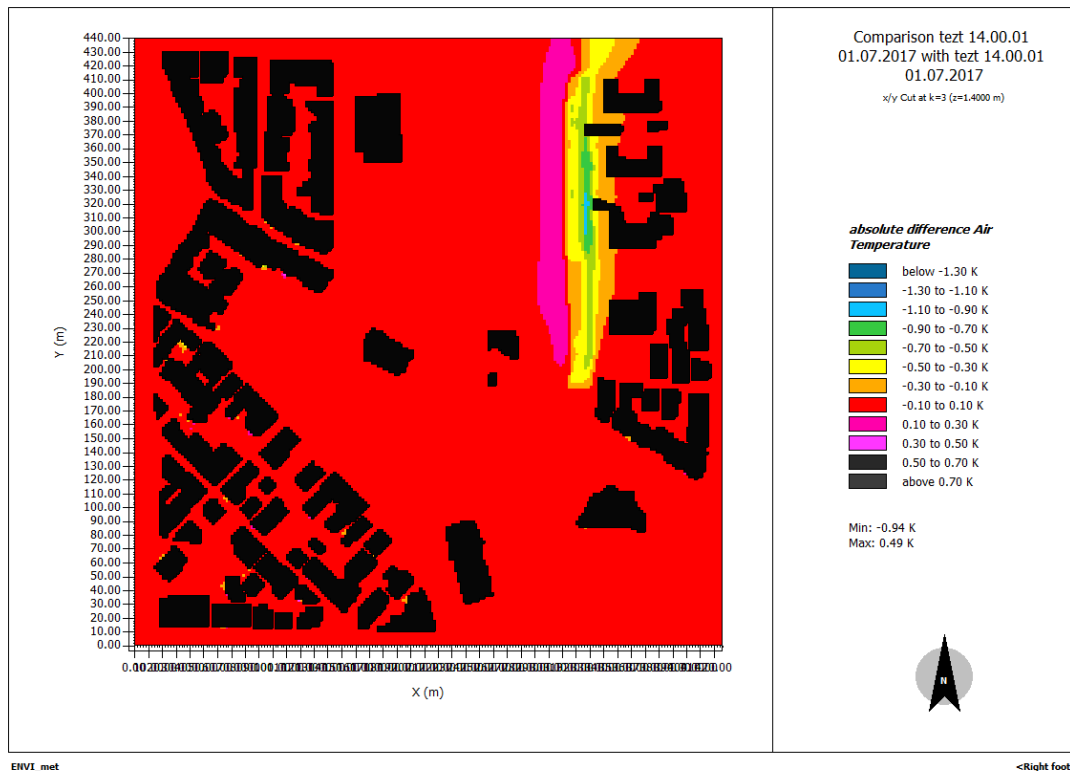


Figure 52: Comparison Green Canopy Scenario - Baseline Scenario Air Temperature (Time 14:00).

The Figures 53 and 54 illustrate the Surface Temperature of the Green Canopy Scenario at 14:00 o'clock and the comparison between the Green Canopy Scenario – Baseline Scenario concerning the Surface Temperature at 14:00 o'clock. For the area A we see that the changes are remarkable. For area A the baseline's temperatures are between 51°C – 54.5°C, 47.5°C – 51°C while in the Green Canopy scenario decreasing of the temperatures ranged between 37°C – 40.5°C, 33.5°C – 37°C. More surface from area A decrease temperature from the orange and yellow coloured range to light blue and blue coloured.

4. Results Presentation

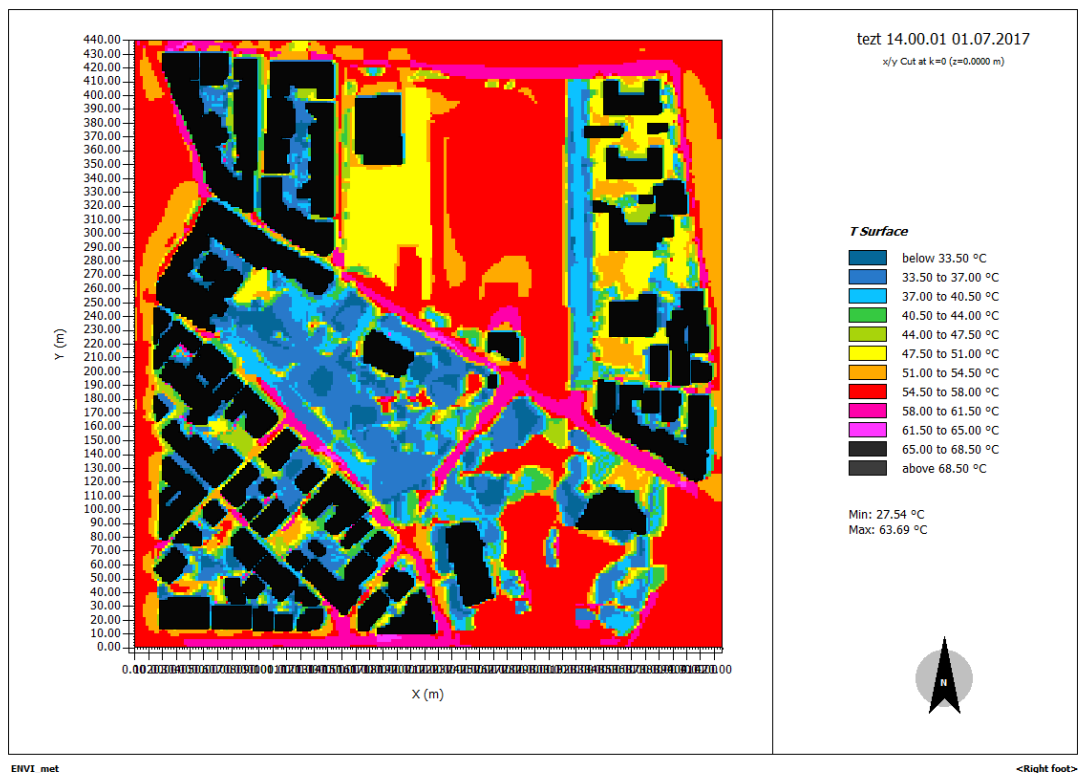


Figure 53: Green Canopy Scenario - Surface Temperature (14:00).

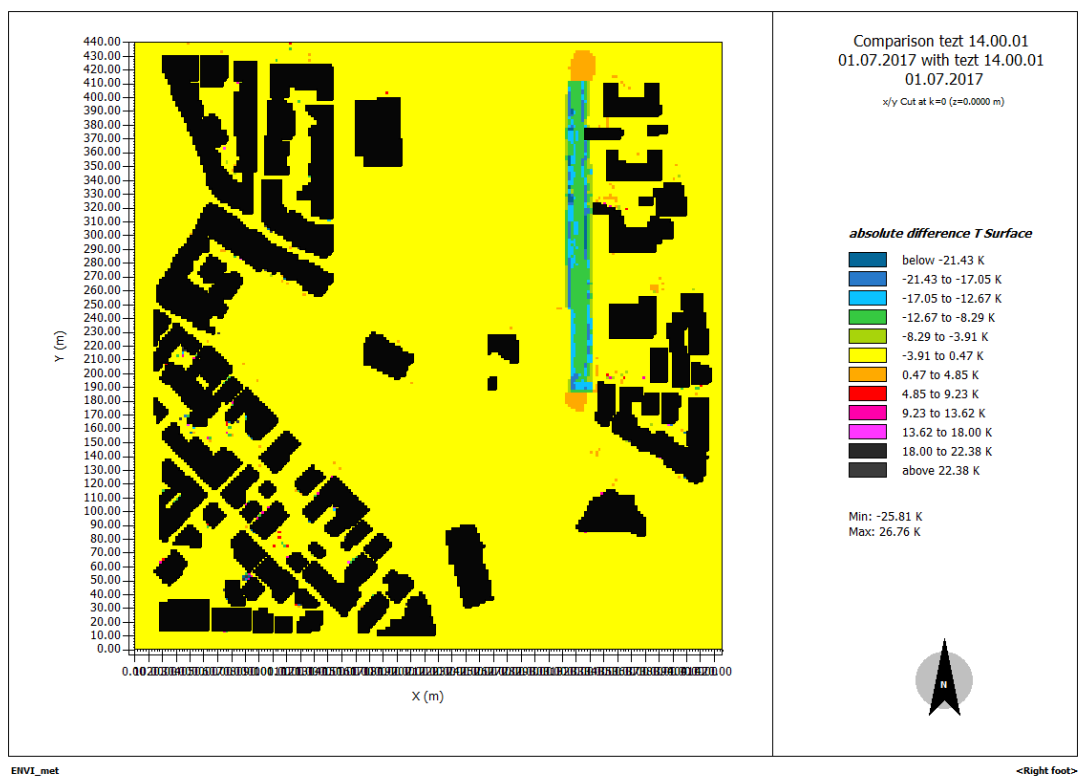


Figure 54: Comparison Green Canopy - Baseline Scenario Surface Temperature (Time 14:00).

The Figures 56, 55 and 57 illustrate the Air Temperature of the K2 Trees Scenario and F2 Trees Scenario at 14:00 o'clock and the comparison between the K2 Trees Scenario – F2 Trees Scenario concerning the Air Temperature at 14:00 o'clock respectively. For Areas A, B and C we can notice changes in specific spots. For the area A the F2 Trees scenario temperatures are between 40.5°C – 42°C, 39°C – 40.5°C and 37.5°C – 39°C while in the K2 Trees scenario decreasing of the temperatures between 39°C – 40.5°C and 36°C – 37.5°C changing from the red, orange and yellow coloured range to yellow and light green coloured. For area B the F2 Trees scenario temperatures are between 40.5°C – 42°C, 39°C – 40.5°C while in the K2 Trees scenario decreasing of the temperatures ranged between 37.5°C – 39°C and 36°C – 37.5°C, changing from the red and orange coloured range to yellow and light green coloured. For the area C the F2 Trees Scenario temperatures are between 40.5°C – 42°C, 39°C – 40.5°C and 37.5°C – 39°C while in the K2 Trees scenario decreasing of the temperatures ranged between 39°C – 40.5°C, 37.5°C – 39°C and 36°C – 37.5°C changing from the red, orange and yellow coloured range to orange, yellow and light green coloured. So, the K2 Trees Scenario is better than the F2 Trees scenario in details as a solution for the UHI mitigation.

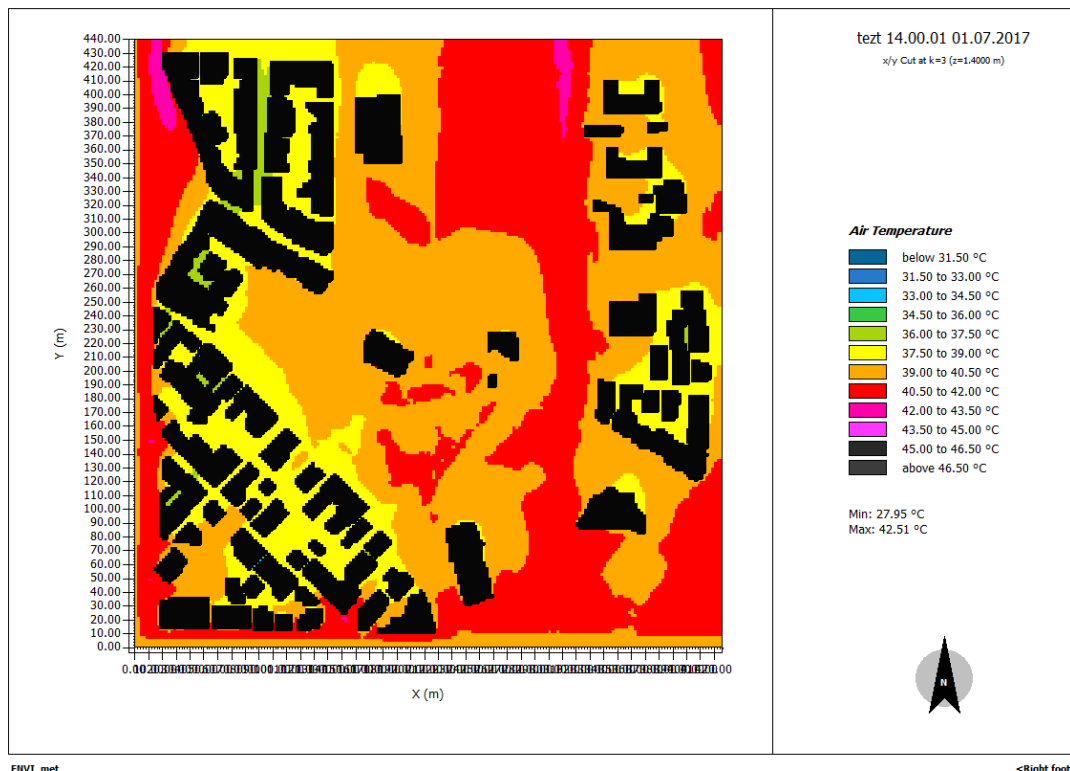


Figure 55: F2 Trees Scenario - Air Temperature (Time 14:00).

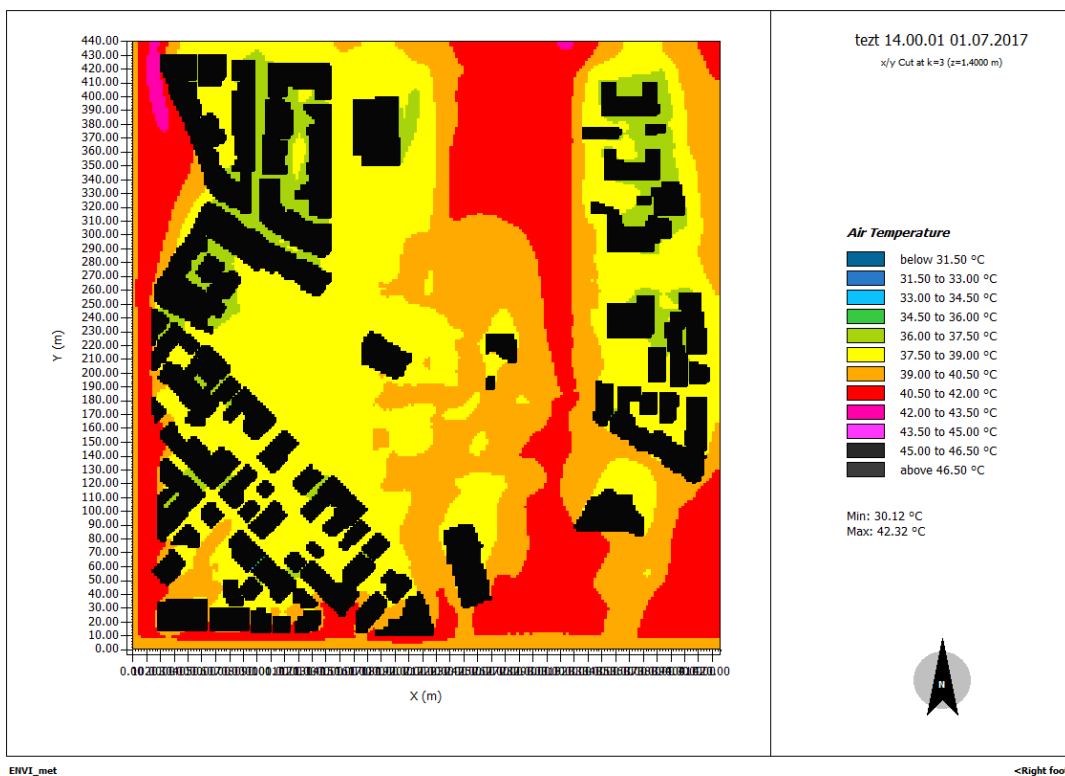


Figure 56: K2 Trees Scenario - Air Temperature (Time 14:00).

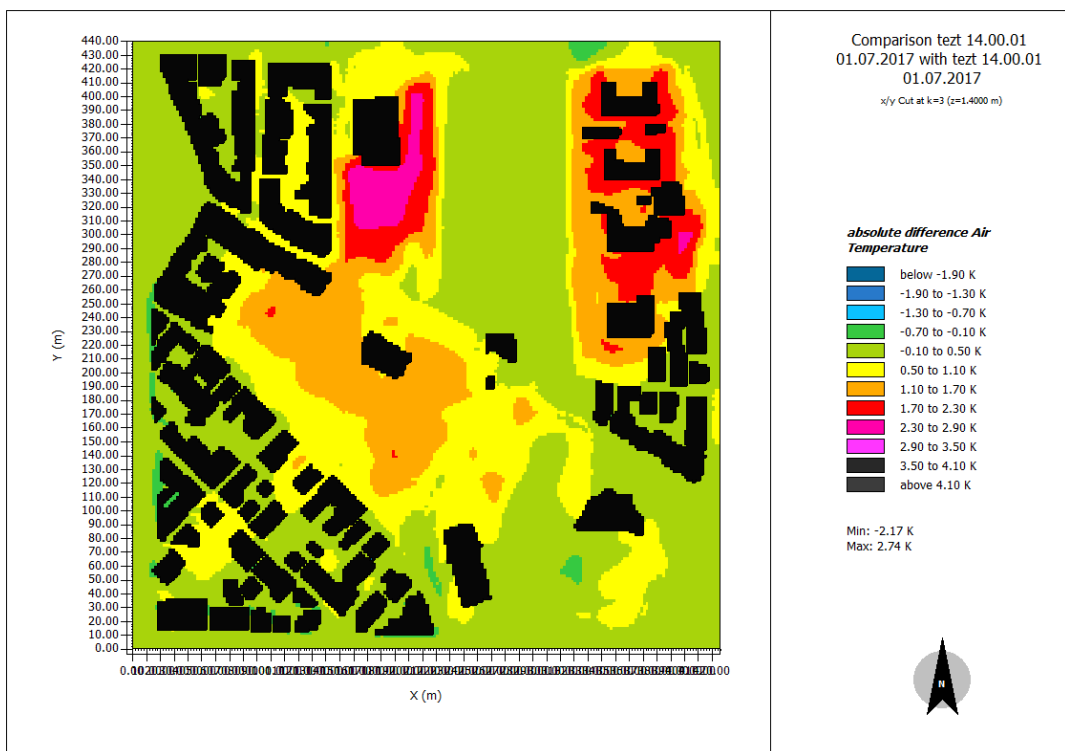


Figure 57: Comparison K2 Trees Scenario - F2 Trees Scenario Air Temperature (Time 14:00).

The Figures 58, 59 and 60 illustrate the Surface Temperature of the F2 Trees Scenario and Cool and K2 Trees Scenario at 14:00 o'clock and the comparison between the F2 Trees Scenario – K2 Trees Scenario concerning the Surface Temperature at 14:00 o'clock respectively. For area A, B and C we can see changes in some specific areas. For area A the F2 Trees scenario temperatures are between 47.5°C – 51°C, 44C – 47.5°C and 40.5°C – 44°C while in the K2 Trees scenario decreasing of the temperatures ranged between 40.5°C – 44°C and 37°C – 40.5°C changing from the yellow, light green and green coloured range to green and light blue coloured. For area B the F2 Trees scenario temperatures are between 37°C – 40.5°C while in the K2 Trees scenario decreasing of the temperatures ranged between 33.5°C – 37°C, changing from the light blue coloured range to blue coloured. For area C F2 Trees scenario temperatures are between 58°C – 61.5°C, 54.5°C – 58°C while in the K2 Trees scenari decreasing of the temperatures ranged between 51.5°C – 54°C, 47.5°C – 51°C and 37°C – 40.5°C changing from the rose and red coloured range to orange, yellow and light blue coloured. So, the F2 Trees Scenario is better than the K2 Trees scenario in details as a solution for the UHI mitigation.

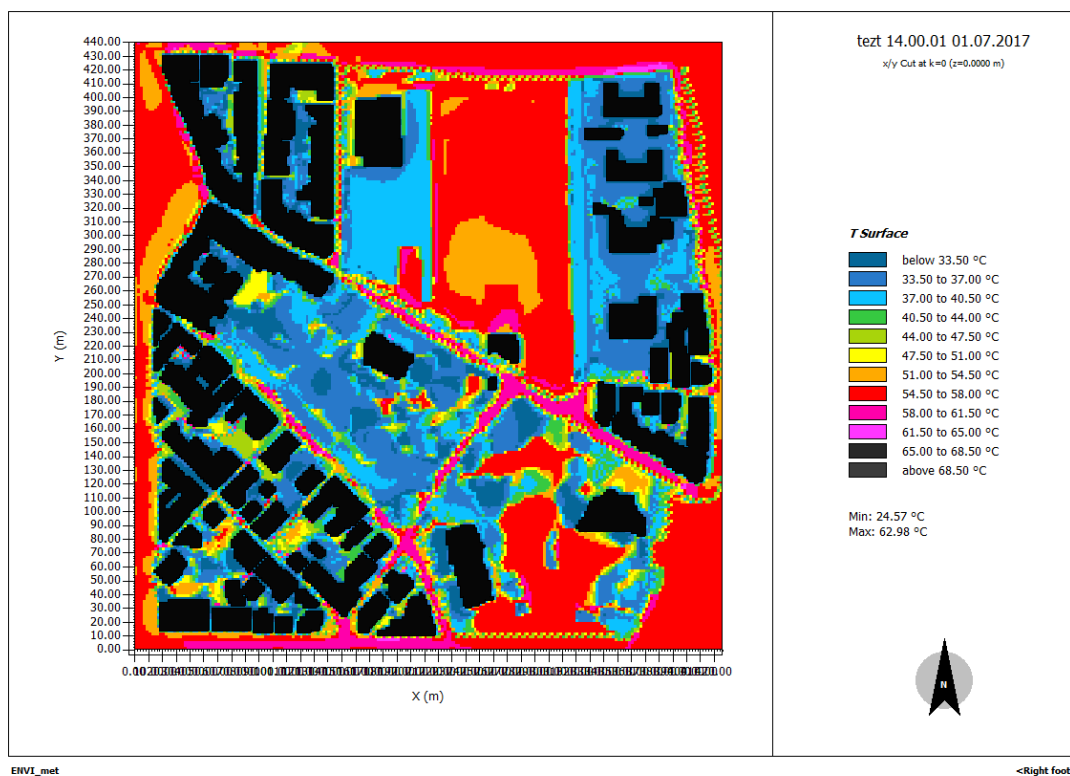


Figure 58: F2 Trees Scenario - Surface Temperature (Time 14:00).

4. Results Presentation

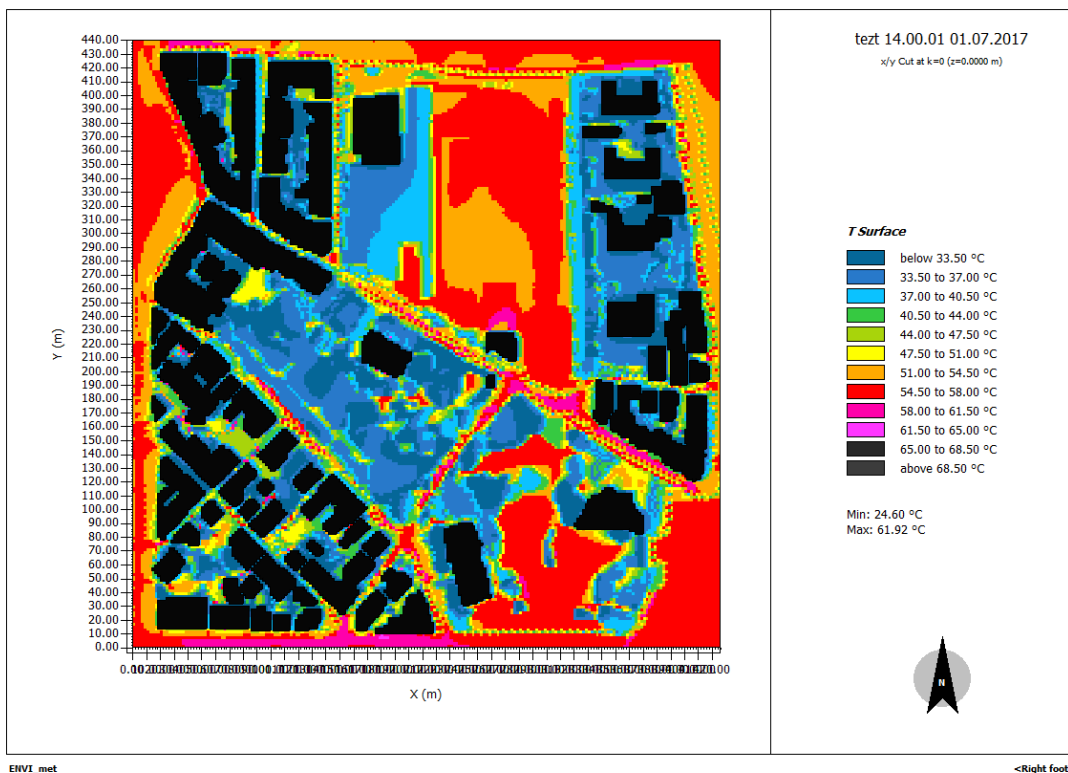


Figure 59: K2 Trees Scenario - Surface Temperature (Time 14:00).

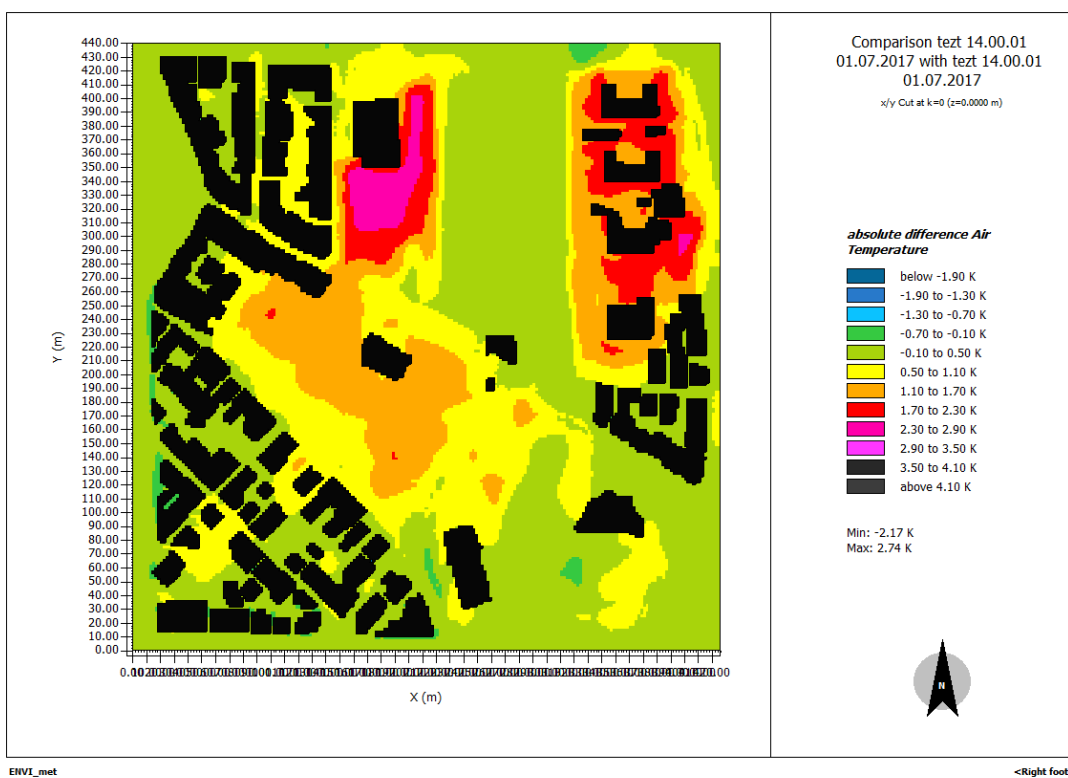


Figure 60: Comparison K2 Trees Scenario - F2 Trees Scenario Surface Temperature (Time 14:00).

Chapter 5th

5. Discussion

All the evaluated scenarios, presented in detail in Chapter 4, included the replacement of the basic pavement material of the study area as well as the planting of different types of trees along the sidewalks. Summarizing their results, we observe that the replacement of the basic materials of all the pavements with cool materials (i.e. CS1 scenario) resulted in a decrease of 1.5 °C in the air temperature and 7°C in the surface temperature of the areas A and B, compared to the baseline scenario. The corresponding air and surface temperature reductions achieved by applying the same scenario in region C were 1.5°C and 10.5°C respectively. The implementation of green pavements (i.e. CS2) led to an 1.5°C increase in the air temperature of all regions (i.e. A,B and C) compared to the baseline scenario. Regarding to the surface temperature, an increase of 3.5°C was observed in areas A and B while a decrease of 7°C was obtained in area C during the simulation of the CS2 scenario. Compared to the baseline scenario, the implementation of a combination of cool and green pavement materials (i.e. CS3), entailed a 1.5°C reduction in the air temperature of the regions A and B and a 3°C air temperature reduction in region C. The same combination also resulted in a 3.5°C reduction in the surface temperature of the regions A and B and a 10.5°C surface temperature reduction in region C.

Table 5. Comparison of different material pavement scenarios to the baseline scenario.

<i>Scenarios</i>	<i>Effect on air temperature</i>		<i>Effect on surface temperature</i>	
CS1	A	-1.5°C	A	-7°C
	B	-1.5°C	B	-7°C
	C	-1.5°C	C	-10.5°C
CS2	A	+1.5°C	A	+3.5°C
	B	+1.5°C	B	+3.5°C
	C	+1.5°C	C	-7°C
CS3	A	-1.5°C	A	-3.5°C
	B	-1.5°C	B	-3.5°C
	C	-3°C	C	-10.5°C

According to these results, we observe that the CS1 and the CS3 scenarios have satisfied effect on both the air and surface temperature reduction of the study area, while during the application of the CS2 scenario a surface temperature mitigation was

achieved only in the case of region C and its surroundings. In addition, comparing the CS1 scenario to the CS3 we observe that they contribute equally to the reduction of both the air temperature and the surface temperature of area A. However, the CS3 scenario leads to a 1.5°C increase in the air temperature of areas B and C and a 3.5°C increase in the surface temperature of region B, compared to the CS1 scenario. These differences indicate that cool materials are more effective at mitigating both the air and surface temperature of the study area than grass. Under the examined simulation circumstances, greenery seems to lower the surface temperature while its contribution to the reduction of the air temperature is limited. The above explains the lower temperature reductions achieved when using only grass on the sidewalk as well as during the implementation of the mixed approach (i.e. CS3-cool and green pavements in a 4:1 ratio). Worth to note that the microclimate conditions of each restricted area has a significant effect on temperature mitigation yield achieved by greenery coverage. For instance, it has been found that increases in grass and tree coverage ratios were effective on UHI mitigation especially in hot climates (Kim et al., 2018). Furthermore, in a study conducted in London (Vaz Monteiro et al., 2016), eight city centre parks with areas ranging from 0.2 ha to 12.1 ha were studied to determine the impact of park size. In short, this study showed that green spaces with areas of 0.5-2 ha can only cause up to 0.3°C temperature reduction over 40m distance, but the temperature reduction caused by green spaces with areas of 3-5 ha can extend over a 70-120 m distance and reach as low as 0.7°C. Thus, given the specific microclimatic characteristics of the study area and the simulation conditions used, the CS1 scenario could proposed as more effective UHI mitigation strategy.

Regarding the scenarios that took into account the tree planting along the sidewalks it was found that when deciduous trees were placed every 5 meters along the roads (i.e. F2 scenario) the air temperature of all areas was decreased by 1.5°C and the surface temperature of areas A, B and C was decreased by 14°C, 11.5°C and 7°C, respectively, compared to the baseline scenario. The same decrease in air temperature was observed when conifer trees placement along the roads every 5 meters was simulated (i.e. K2 scenario). Also, in case of K2 scenario the surface temperature of areas A, B and C was decreased by 14°C, 10.5°C and 11.5°C, respectively, compared to the baseline scenario. Furthermore, when a green canopy was selected to be located

5. Conclusions – Proposal for future research

on the main pedestrian road of the study area (i.e. Green Canopy scenario), a decrease in air and surface temperature only of area A of about 1.5°C and 15°C degrees, respectively, was observed.

Table 6. Comparison of different tree planting scenarios to the baseline scenario.

<i>Scenarios</i>	<i>Effect on air temperature</i>		<i>Effect on surface temperature</i>	
F2	A	-1.5°C	A	-14°C
	B	-1.5°C	B	-11.5°C
	C	-1.5°C	C	-7°C
K2	A	-1.5°C	A	-14°C
	B	-1.5°C	B	-10.5°C
	C	-1.5°C	C	-11.5°C
Green canopy	A	-1.5°C	A	-14°C
	B	Not affected	B	Not affected
	C	Not affected	C	Not affected

It is evident that the implementation of green canopy could not serve as a satisfied solution to reverse the overall temperature rise of the study area. Compared to the F2 scenario, the simulation of scenario K2 resulted in a greater reduction of the air temperature of areas A, B and C by 1.5°C, 3°C and 1.5°C, respectively. Besides that, the surface area of areas A, B and C was observed to be cooler by 7°C, 3.5°C and 6.5°C, respectively. Thus, among these two tree planting approaches, the K2 appears to be more suitable as an UHI mitigation solution for the given study area.

The results of this work converge with conclusions of other published works in which ENVI-met simulations have been employed to predict the cooling effect of green spaces with different shapes, dimensions, and placements in different scenarios. In a study conducted in 2012, where the impact of replacing Hong Kong sidewalk pavements with green materials was simulated in various climatic scenarios, was found that planting sidewalk trees in urban spaces result in a better cooling effect than building green surfaces (Ng and Ren, 2018). A similar study in Manchester also found that mature trees have a significant impact on the pavement surface temperature. The simulation results showed that adding 5% mature tree density would reduce the surface temperature by 1°C, and even adding 5% density saplings would result in 0.5°C temperature reduction in urban areas (Skelhorn, C, Lindley, S & Levermore, 2013). These temperature reductions are similar to those observed in the present study.

In summary we can conclude that to achieve a greener effect and a better UHI effect mitigation in the present study, the simply removing the occasional paver from the pavements is not sufficient (UrbanGreenUp, 2018). However a mixed approach, combining the replacement of the basic pavement material with cool material of high reflectivity and the planting of conifer trees along the sidewalks, could be a sustainable, environmentally friendly and at the same time affordable solution to reverse the study area temperature rise and mitigate the UHI effect.

Suggestions for future research

In general, the results of all the examined scenarios in this study are quite satisfactory as they lead to a reduction in the local temperature of the study area. However, it was observed that in the certain urban area the combination of different NBS strategies was not the most efficient solution to reverse the overall temperature rise, as expected. For instance, the replacement of all pavements with cool materials (i.e. CS1 scenario) caused greater decrease in both the air and the surface temperature of the study area than the approach of the green pavements consisting of grass (i.e. CS2). Hence, the implementation of CS3 scenario, proposing the combined use of both cool and green pavements, did not improve the temperature conditions of the study area. The lower efficiency of the mixed approach could be attributed to the reduction of the surface coverage of pavements with cool materials due to the implementation of grass. It is therefore understood that, depending on the particular microclimatic characteristics of each region, the implementation of a single strategy sometimes brings better results.

In the present study only some of the existing temperature mitigation solutions were proposed and examined. Therefore, the effectiveness of others available NBS solutions (e.g. green walls, gardens, tree-lined streets, urban parks, etc.) as well as combination of them in UHI mitigation could be explored in future studies concerning the certain area. In addition, since the selected type of vegetation did not cause a significant reduction in air temperature, implementation of different tree species or appropriate combination and space arrangement of them could also be investigated in

5. Conclusions – Proposal for future research

order to clarify which forms of greenery are more efficient for the examined urban area.

Furthermore, it is evident that the application of advanced cool materials with improved abilities in field studies could also hold as an important research area. However, to preserve a long-term high efficiency of the various cool materials applied in UHI mitigation strategies, not only the selection of the appropriate material but also its maintenance plays a crucial role.

Finally, it is worth to note that until today all the above proposed NBS strategies are implemented worldwide as UHI mitigation and adaptation measures in most of the urban centers. In many cases the later implementation or integration of NBS into urban fabric requires extensive space rearrangement, which is a quite expensive process and often does not bring the desired results. Thus, the costly later urban interventions could have been avoided if sustainable climate change mitigation measures, like NBS, have been taken into account in the technical aspects of the urban planning right from the beginning.

References

- Akbari, H., Cartalis, C., Kolokotsa, D., Muscio, A., Pisello, A.L., Rossi, F., Santamouris, M., Synnefa, A., Wong, N.H., Zinzi, M., 2016. Local climate change and urban heat island mitigation techniques - The state of the art. *J. Civ. Eng. Manag.* 22, 1–16. <https://doi.org/10.3846/13923730.2015.1111934>
- Alexandri, E., Jones, P., 2008. Temperature decreases in an urban canyon due to green walls and green roofs in diverse climates. *Build. Environ.* 43, 480–493. <https://doi.org/10.1016/j.buildenv.2006.10.055>
- Andersson, E., Borgström, S., McPhearson, T., 2017. Double Insurance in Dealing with Extremes: Ecological and Social Factors for Making Nature-Based Solutions Last. Springer, Cham, pp. 51–64. https://doi.org/10.1007/978-3-319-56091-5_4
- Arifwidodo, S., Chandrasiri, O., 2015. Urban Heat Island and Household Energy Consumption in Bangkok, Thailand, in: *Energy Procedia*. Elsevier Ltd, pp. 189–194. <https://doi.org/10.1016/j.egypro.2015.11.461>
- Asaeda, T., Ca, V.T., 1993. The subsurface transport of heat and moisture and its effect on the environment: A numerical model. *Boundary-Layer Meteorol.* 65, 159–179. <https://doi.org/10.1007/BF00708822>
- Badiu, D.L., Iojă, C.I., Pătroescu, M., Breuste, J., Artmann, M., Niță, M.R., Grădinaru, S.R., Hossu, C.A., Onose, D.A., 2016. Is urban green space per capita a valuable target to achieve cities' sustainability goals? Romania as a case study. *Ecol. Indic.* 70, 53–66. <https://doi.org/10.1016/j.ecolind.2016.05.044>
- Bai, X., Dawson, R.J., Ürge-Vorsatz, D., Delgado, G.C., Salisu Barau, A., Dhakal, S., Dodman, D., Leonardsen, L., Masson-Delmotte, V., Roberts, D.C., Schultz, S., 2018. Six research priorities for cities and climate change. *Nature*. <https://doi.org/10.1038/d41586-018-02409-z>
- Baró, F., Chaparro, L., Gómez-Baggethun, E., Langemeyer, J., Nowak, D.J., Terradas, J., 2014. Contribution of ecosystem services to air quality and climate change mitigation policies: The case of urban forests in Barcelona, Spain. *Ambio* 43, 466–479. <https://doi.org/10.1007/s13280-014-0507-x>
- Baró, F., Haase, D., Gómez-Baggethun, E., Frantzeskaki, N., 2015. Mismatches between ecosystem services supply and demand in urban areas: A quantitative assessment in five European cities. *Ecol. Indic.* 55, 146–158. <https://doi.org/10.1016/j.ecolind.2015.03.013>
- Bruse, M., 2004. ENVI-met 3.0: Updated Model Overview.
- Bruse, M., Fleer, H., 1998. Simulating surface-plant-air interactions inside urban environments with a three dimensional numerical model. *Environ. Model. Softw.* 13, 373–384. [https://doi.org/10.1016/S1364-8152\(98\)00042-5](https://doi.org/10.1016/S1364-8152(98)00042-5)
- Calautit, J.K., Hughes, B.R., Nasir, D.S., 2017. Climatic analysis of a passive cooling technology for the built environment in hot countries. *Appl. Energy* 186, 321–335. <https://doi.org/10.1016/j.apenergy.2016.05.096>
- Calfapietra, C., Peñuelas, J., Niinemets, Ü., 2015. Urban plant physiology: Adaptation-mitigation strategies under permanent stress. *Trends Plant Sci.* <https://doi.org/10.1016/j.tplants.2014.11.001>
- Cameron, R.W.F., Taylor, J.E., Emmett, M.R., 2014. What's "cool" in the world of green façades? How plant choice influences the cooling properties of green walls. *Build.*

- Environ. 73, 198–207. <https://doi.org/10.1016/j.buildenv.2013.12.005>
- Clapp, R.B., Hornberger, G.M., 1978. Empirical equations for some soil hydraulic properties. *Water Resour. Res.* 14, 601–604. <https://doi.org/10.1029/WR014i004p00601>
- Cohen-Shacham, E; Walters, G; Janzen, C; Maginnis, S., 2016. Nature-based solutions to address global societal challenges. IUCN International Union for Conservation of Nature. <https://doi.org/10.2305/iucn.ch.2016.13.en>
- Cohen, M., Baudoin, R., Palibrk, M., Persyn, N., Rhein, C., 2012. Urban biodiversity and social inequalities in built-up cities: New evidences, next questions. The example of Paris, France. *Landsc. Urban Plan.* 106, 277–287. <https://doi.org/10.1016/j.landurbplan.2012.03.007>
- Cohen, P., Potchter, O., Matzarakis, A., 2012. Daily and seasonal climatic conditions of green urban open spaces in the Mediterranean climate and their impact on human comfort. *Build. Environ.* 51, 285–295. <https://doi.org/10.1016/j.buildenv.2011.11.020>
- Davies, Z.G., Edmondson, J.L., Heinemeyer, A., Leake, J.R., Gaston, K.J., 2011. Mapping an urban ecosystem service: Quantifying above-ground carbon storage at a city-wide scale. *J. Appl. Ecol.* 48, 1125–1134. <https://doi.org/10.1111/j.1365-2664.2011.02021.x>
- Deardorff, J.W., 1978. Efficient prediction of ground surface temperature and moisture, with inclusion of a layer of vegetation. *J. Geophys. Res.* 83, 1889. <https://doi.org/10.1029/jc083ic04p01889>
- Demuzere, M., Orru, K., Heidrich, O., Olazabal, E., Geneletti, D., Orru, H., Bhave, A.G., Mittal, N., Feliu, E., Faehnle, M., 2014. Mitigating and adapting to climate change: Multi-functional and multi-scale assessment of green urban infrastructure. *J. Environ. Manage.* 146, 107–115. <https://doi.org/10.1016/j.jenvman.2014.07.025>
- Depietri, Y., McPhearson, T., 2017. Integrating the Grey, Green, and Blue in Cities: Nature-Based Solutions for Climate Change Adaptation and Risk Reduction. Springer, Cham, pp. 91–109. https://doi.org/10.1007/978-3-319-56091-5_6
- Emilsson, T., Ode Sang, Å., 2017. Impacts of Climate Change on Urban Areas and Nature-Based Solutions for Adaptation. Springer, Cham, pp. 15–27. https://doi.org/10.1007/978-3-319-56091-5_2
- European Commission, 2016. Nature-based solutions | European Commission.
- European Commission, 2015. Towards an EU Research and Innovation policy agenda for Nature-Based Solutions & Re-Naturing Cities. <https://doi.org/10.2777/765301>
- Filho, W.L., Icaza, L.E., Emanche, V.O., Al-Amin, A.Q., 2017. An evidence-based review of impacts, strategies and tools to mitigate urban heat islands. *Int. J. Environ. Res. Public Health* 14. <https://doi.org/10.3390/ijerph14121600>
- Gaitani, N., Spanou, A., Saliari, M., Synnefa, A., Vassilakopoulou, K., Papadopoulou, K., Pavlou, K., Santamouris, M., Papaioannou, M., Lagoudaki, A., 2011. Improving the microclimate in urban areas: a case study in the centre of Athens. *Build. Serv. Eng. Res. Technol.* 32, 53–71. <https://doi.org/10.1177/0143624410394518>
- Giannico, V., Laforteza, R., John, R., Sanesi, G., Pesola, L., Chen, J., 2016. Estimating Stand Volume and Above-Ground Biomass of Urban Forests Using LiDAR. *Remote Sens.* 8, 339. <https://doi.org/10.3390/rs8040339>
- Gill, S.E., Handley, J.F., Ennos, A.R., Pauleit, S., 2007. Adapting cities for climate change: The role of the green infrastructure. *Built Environ.* 33, 115–133. <https://doi.org/10.2148/benv.33.1.115>
- Goddard, M.A., Dougill, A.J., Benton, T.G., 2010. Scaling up from gardens: biodiversity conservation in urban environments. *Trends Ecol. Evol.*

- <https://doi.org/10.1016/j.tree.2009.07.016>
- Gómez-Baggethun, E., Barton, D.N., 2013. Classifying and valuing ecosystem services for urban planning. *Ecol. Econ.* 86, 235–245.
<https://doi.org/10.1016/j.ecolecon.2012.08.019>
- Hartig, T., Mitchell, R., de Vries, S., Frumkin, H., 2014. Nature and Health. *Annu. Rev. Public Health* 35, 207–228. <https://doi.org/10.1146/annurev-publhealth-032013-182443>
- Hathway, E.A., Sharples, S., 2012. The interaction of rivers and urban form in mitigating the Urban Heat Island effect: A UK case study. *Build. Environ.* 58, 14–22.
<https://doi.org/10.1016/j.buildenv.2012.06.013>
- Huthoff, F., Schielen, R., Daggenvoorde, R., Wegman, C., 2018. Evaluating Nature-Based Solutions Best practices, frameworks and guidelines Final report.
- Iojă, C.I., Grădinaru, S.R., Onose, D.A., Vânău, G.O., Tudor, A.C., 2014. The potential of school green areas to improve urban green connectivity and multifunctionality. *Urban For. Urban Green.* 13, 704–713. <https://doi.org/10.1016/j.ufug.2014.07.002>
- Jacobs, C.M.J., De Bruin, H.A.R., 1997. Predicting Regional Transpiration at Elevated Atmospheric CO₂: Influence of the PBL-Vegetation Interaction, *Journal of Applied Meteorology*. American Meteorological Society. [https://doi.org/10.1175/1520-0450\(1997\)036<1663:PRTAEA>2.0.CO;2](https://doi.org/10.1175/1520-0450(1997)036<1663:PRTAEA>2.0.CO;2)
- Kabisch, N., Frantzeskaki, N., Pauleit, S., Naumann, S., Davis, M., Artmann, M., Haase, D., Knapp, S., Korn, H., Stadler, J., Zaunberger, K., Bonn, A., 2016. Nature-based solutions to climate change mitigation and adaptation in urban areas: Perspectives on indicators, knowledge gaps, barriers, and opportunities for action. *Ecol. Soc.* 21.
<https://doi.org/10.5751/ES-08373-210239>
- Kabisch, N., Haase, D., 2014. Green justice or just green? Provision of urban green spaces in Berlin, Germany. *Landsc. Urban Plan.* 122, 129–139.
<https://doi.org/10.1016/j.landurbplan.2013.11.016>
- Kabisch, N., Korn, H., Stadler, J., Bonn, A., 2017. Nature-Based Solutions to Climate Change Adaptation in Urban Areas—Linkages Between Science, Policy and Practice. Springer, Cham, pp. 1–11. https://doi.org/10.1007/978-3-319-56091-5_1
- Karlessi, T., Santamouris, M., 2013. Improving the performance of thermochromic coatings with the use of UV and optical filters tested under accelerated aging conditions. *Int. J. Low-Carbon Technol.* 10, 45–61. <https://doi.org/10.1093/ijlct/ctt027>
- Keniger, L.E., Gaston, K.J., Irvine, K.N., Fuller, R.A., 2013. What are the benefits of interacting with nature? *Int. J. Environ. Res. Public Health.*
<https://doi.org/10.3390/ijerph10030913>
- Kim, H., Gu, D., Kim, H.Y., 2018. Effects of Urban Heat Island mitigation in various climate zones in the United States. *Sustain. Cities Soc.* 41, 841–852.
<https://doi.org/10.1016/j.scs.2018.06.021>
- Kolokotsa, D., Psomas, A., Karapidakis, E., 2009. Urban heat island in southern Europe: The case study of Hania, Crete. *Sol. Energy* 83, 1871–1883.
<https://doi.org/10.1016/j.solener.2009.06.018>
- Kolokotsa, D., Santamouris, M., Zerefos, S.C., 2013. Green and cool roofs' urban heat island mitigation potential in European climates for office buildings under free floating conditions. *Sol. Energy* 95, 118–130. <https://doi.org/10.1016/j.solener.2013.06.001>
- Krasny, M.E., Lundholm, C., Kabori, H., 2013. Urban landscapes as learning arenas for biodiversity and ecosystem services management, in: *Urbanization, Biodiversity and Ecosystem Services: Challenges and Opportunities: A Global Assessment*. Springer Netherlands, pp. 629–664. https://doi.org/10.1007/978-94-007-7088-1_30

- Kronenberg, J., Bergier, T., Maliszewska, K., 2017. The Challenge of Innovation Diffusion: Nature-Based Solutions in Poland. pp. 291–305. https://doi.org/10.1007/978-3-319-56091-5_17
- La Rosa, D., Spyra, M., Inostroza, L., 2016. Indicators of Cultural Ecosystem Services for urban planning: A review. *Ecol. Indic.* <https://doi.org/10.1016/j.ecolind.2015.04.028>
- Lai, L.W., Cheng, W.L., 2010. Urban heat island and air pollution-an emerging role for hospital respiratory admissions in an urban area. *J. Environ. Health.*
- Lauder, B.E., Spalding, D.B., 1974. The numerical computation of turbulent flows. *Comput. Methods Appl. Mech. Eng.* 3, 269–289. [https://doi.org/10.1016/0045-7825\(74\)90029-2](https://doi.org/10.1016/0045-7825(74)90029-2)
- Lee, T.W., Choi, H.S., Lee, J., 2014. Generalized scaling of urban heat island effect and its applications for energy consumption and renewable energy. *Adv. Meteorol.* 2014. <https://doi.org/10.1155/2014/948306>
- Lee, Y.Y., Md Din, M.F., Ponraj, M., Noor, Z.Z., Iwao, K., Chelliapan, S., 2017. Overview of Urban Heat Island (UHI) phenomenon towards human thermal comfort. *Environ. Eng. Manag. J.* 16, 2097–2112. <https://doi.org/10.30638/eemj.2017.217>
- Lehmann, I., Mathey, J., Röbber, S., Bräuer, A., Goldberg, V., 2014. Urban vegetation structure types as a methodological approach for identifying ecosystem services - Application to the analysis of micro-climatic effects. *Ecol. Indic.* 42, 58–72. <https://doi.org/10.1016/j.ecolind.2014.02.036>
- Leuzinger, S., Vogt, R., Körner, C., 2010. Tree surface temperature in an urban environment. *Agric. For. Meteorol.* 150, 56–62. <https://doi.org/10.1016/j.agrformet.2009.08.006>
- Li, H., Meier, F., Lee, X., Chakraborty, T., Liu, J., Schaap, M., Sodoudi, S., 2018. Interaction between urban heat island and urban pollution island during summer in Berlin. *Sci. Total Environ.* 636, 818–828. <https://doi.org/10.1016/j.scitotenv.2018.04.254>
- Li, X., Zhou, Y., Yu, S., Jia, G., Li, H., Li, W., 2019. Urban heat island impacts on building energy consumption: A review of approaches and findings. *Energy.* <https://doi.org/10.1016/j.energy.2019.02.183>
- Lin, B., Meyers, J., Barnett, G., 2015. Understanding the potential loss and inequities of green space distribution with urban densification. *Urban For. Urban Green.* 14, 952–958. <https://doi.org/10.1016/j.ufug.2015.09.003>
- Liu, J., Chen, J.M., Black, T.A., Novak, M.D., 1996. E - ϵ modelling of turbulent air flow downwind of a model forest edge. *Boundary-Layer Meteorol.* 77, 21–44. <https://doi.org/10.1007/BF00121857>
- Lundgren-Kownacki, K., Hornyanszky, E.D., Chu, T.A., Olsson, J.A., Becker, P., 2018. Challenges of using air conditioning in an increasingly hot climate. *Int. J. Biometeorol.* 62, 401–412. <https://doi.org/10.1007/s00484-017-1493-z>
- Mak, C., Scholz, M., James, P., 2017. Sustainable drainage system site assessment method using urban ecosystem services. *Urban Ecosyst.* 20, 293–307. <https://doi.org/10.1007/s11252-016-0593-6>
- Maragkogiannis, K., Kolokotsa, D., Maravelakis, E., Konstantaras, A., 2014. Combining terrestrial laser scanning and computational fluid dynamics for the study of the urban thermal environment. *Sustain. Cities Soc.* 13, 207–216. <https://doi.org/10.1016/j.scs.2013.12.002>
- Meli, P., Benayas, J.M.R., Balvanera, P., Ramos, M.M., 2014. Restoration enhances wetland biodiversity and ecosystem service supply, but results are context-dependent: A meta-analysis. *PLoS One* 9. <https://doi.org/10.1371/journal.pone.0093507>
- Mensah, C.A., 2014. Destruction of Urban Green Spaces: A Problem Beyond Urbanization in

- Kumasi City (Ghana). *Am. J. Environ. Prot.* 3, 1.
<https://doi.org/10.11648/j.ajep.20140301.11>
- Ng, E., Ren, C., 2018. China's adaptation to climate & urban climatic changes: A critical review. *Urban Clim.* 23, 352–372. <https://doi.org/10.1016/j.uclim.2017.07.006>
- Nuruzzaman, M., 2015. Urban Heat Island: Causes, Effects and Mitigation Measures - A Review. *Int. J. Environ. Monit. Anal.* 3, 67.
<https://doi.org/10.11648/j.ijema.20150302.15>
- Oral, H.V., Carvalho, P., Gajewska, M., Ursino, N., Masi, F., Hullebusch, E.D. van, Kazak, J.K., Exposito, A., Cipolletta, G., Andersen, T.R., Finger, D.C., Simperler, L., Regelsberger, M., Rous, V., Radinja, M., Buttiglieri, G., Krzeminski, P., Rizzo, A., Dehghanian, K., Nikolova, M., Zimmermann, M., 2020. A review of nature-based solutions for urban water management in European circular cities: a critical assessment based on case studies and literature. *Blue-Green Syst.* 2, 112–136.
<https://doi.org/10.2166/bgs.2020.932>
- Pauleit, S., Zölch, T., Hansen, R., Randrup, T.B., Konijnendijk van den Bosch, C., 2017. Nature-Based Solutions and Climate Change – Four Shades of Green. pp. 29–49.
https://doi.org/10.1007/978-3-319-56091-5_3
- Pielke, R.A., 2013. *Mesoscale Meteorological Modeling*, Mesoscale Meteorological Modeling. Elsevier Inc. <https://doi.org/10.1016/C2009-0-02981-X>
- Pino, J., Marull, J., 2012. Ecological networks: Are they enough for connectivity conservation? A case study in the Barcelona Metropolitan Region (NE Spain). *Land use policy* 29, 684–690. <https://doi.org/10.1016/j.landusepol.2011.11.004>
- Qiu, G.Y., Zou, Z., Li, X., Li, H., Guo, Q., Yan, C., Tan, S., 2017. Experimental studies on the effects of green space and evapotranspiration on urban heat island in a subtropical megacity in China. *Habitat Int.* 68, 30–42.
<https://doi.org/10.1016/j.habitatint.2017.07.009>
- Rahman, M.A., Armson, D., Ennos, A.R., 2015. A comparison of the growth and cooling effectiveness of five commonly planted urban tree species. *Urban Ecosyst.* 18, 371–389.
<https://doi.org/10.1007/s11252-014-0407-7>
- Rao, V.L., 2014. Effects of Urban Heat Island on Air pollution Concentrations, *Int.J.Curr.Microbiol.App.Sci.*
- Raymond, Christopher M, Berry, P., Breil, M., Nita, M.R., Kabisch, N., de Bel, M., Enzi, V., Frantzeskaki, N., Geneletti, D., Cardinaletti, M., Lovinger, L., Basnou, C., Monteiro, A., Robrecht, H., Sgrigna, G., Munari, L., Calfapietra, C., Associations, W., del Vallès, C., 2017. An impact evaluation framework to support planning and evaluation of nature-based solutions projects Prepared by the EKLIPSE Expert Working Group on Nature-based Solutions to Promote Climate Resilience in Urban Areas European Federation of Green Roof IFLA.
- Raymond, Christopher M., Frantzeskaki, N., Kabisch, N., Berry, P., Breil, M., Nita, M.R., Geneletti, D., Calfapietra, C., 2017. A framework for assessing and implementing the co-benefits of nature-based solutions in urban areas. *Environ. Sci. Policy* 77, 15–24.
<https://doi.org/10.1016/j.envsci.2017.07.008>
- Santamouris, M., Ding, L., Fiorito, F., Oldfield, P., Osmond, P., Paolini, R., Prasad, D., Synnefa, A., 2017. Passive and active cooling for the outdoor built environment – Analysis and assessment of the cooling potential of mitigation technologies using performance data from 220 large scale projects. *Sol. Energy* 154, 14–33.
<https://doi.org/10.1016/j.solener.2016.12.006>
- Santamouris, M., Gaitani, N., Spanou, A., Saliari, M., Giannopoulou, K., Vasilakopoulou, K.,

- Kardomateas, T., 2012. Using cool paving materials to improve microclimate of urban areas - Design realization and results of the flisvos project. *Build. Environ.* 53, 128–136. <https://doi.org/10.1016/j.buildenv.2012.01.022>
- Santamouris, M., Synnefa, A., Karlessi, T., 2011. Using advanced cool materials in the urban built environment to mitigate heat islands and improve thermal comfort conditions. *Sol. Energy.* <https://doi.org/10.1016/j.solener.2010.12.023>
- Santamouris, M., Synnefa, A., Kolokotsa, D., Dimitriou, V., Apostolakis, K., 2008. Passive cooling of the built environment - Use of innovative reflective materials to fight heat islands and decrease cooling needs. *Int. J. Low Carbon Technol.* 3, 71–82. <https://doi.org/10.1093/ijlct/3.2.71>
- Schilling, V.K., 1991. A parameterization for modelling the meteorological effects of tall forests - A case study of a large clearing. *Boundary-Layer Meteorol.* 55, 283–304. <https://doi.org/10.1007/BF00122581>
- Schipperijn, J., Ekholm, O., Stigsdotter, U.K., Toftager, M., Bentsen, P., Kamper-Jørgensen, F., Randrup, T.B., 2010. Factors influencing the use of green space: Results from a Danish national representative survey. *Landsc. Urban Plan.* 95, 130–137. <https://doi.org/10.1016/j.landurbplan.2009.12.010>
- Seddon, N., Chausson, A., Berry, P., Girardin, C.A.J., Smith, A., Turner, B., 2020. Understanding the value and limits of nature-based solutions to climate change and other global challenges. *Philos. Trans. R. Soc. B Biol. Sci.* <https://doi.org/10.1098/rstb.2019.0120>
- Shahmohamadi, P., Che-Ani, A.I., Etesam, I., Maulud, K.N.A., Tawil, N.M., 2011a. Healthy environment: The need to mitigate urban heat island effects on human health, in: *Procedia Engineering*. Elsevier, pp. 61–70. <https://doi.org/10.1016/j.proeng.2011.11.139>
- Shahmohamadi, P., Che-Ani, A.I., Maulud, K.N.A., Tawil, N.M., Abdullah, N.A.G., 2011b. The Impact of Anthropogenic Heat on Formation of Urban Heat Island and Energy Consumption Balance. *Urban Stud. Res.* 2011, 1–9. <https://doi.org/10.1155/2011/497524>
- Skelhorn, C, Lindley, S & Levermore, G., 2013. The impact of vegetation types on air and surface temperatures in a temperature city: A fine scale assessment in Manchester, UK The impact of vegetation types on air and surface temperatures in a temperature city: A fine scale assessment in Manchester, UK. *Landsc. Urban Plan.* 121, 129–140.
- Song, J., Wang, Z.H., 2015. Impacts of mesic and xeric urban vegetation on outdoor thermal comfort and microclimate in Phoenix, AZ. *Build. Environ.* 94, 558–568. <https://doi.org/10.1016/j.buildenv.2015.10.016>
- Stovin, V., 2010. The potential of green roofs to manage Urban Stormwater. *Water Environ. J.* 24, 192–199. <https://doi.org/10.1111/j.1747-6593.2009.00174.x>
- Taha, H., 1997. Urban climates and heat islands: Albedo, evapotranspiration, and anthropogenic heat. *Energy Build.* 25, 99–103. [https://doi.org/10.1016/s0378-7788\(96\)00999-1](https://doi.org/10.1016/s0378-7788(96)00999-1)
- Tamosiunas, A., Grazuleviciene, R., Luksiene, D., Dedele, A., Reklaitiene, R., Baceviciene, M., Vencloviene, J., Bernotiene, G., Radisauskas, R., Malinauskiene, V., Milinaviciene, E., Bobak, M., Peasey, A., Nieuwenhuijsen, M.J., 2014. Accessibility and use of urban green spaces, and cardiovascular health: Findings from a Kaunas cohort study. *Environ. Heal. A Glob. Access Sci. Source* 13. <https://doi.org/10.1186/1476-069X-13-20>
- Tjernström, M., 1989. Some tests with a surface energy balance scheme, including a bulk parameterisation for vegetation, in a mesoscale model. *Boundary-Layer Meteorol.* 48, 33–68. <https://doi.org/10.1007/BF00121782>

- Tomlinson, C.J., Chapman, L., Thornes, J.E., Baker, C.J., 2011. Including the urban heat island in spatial heat health risk assessment strategies: A case study for Birmingham, UK. *Int. J. Health Geogr.* 10, 42. <https://doi.org/10.1186/1476-072X-10-42>
- Tsitoura, M., Tsoutsos, T., Daras, T., 2014. Evaluation of comfort conditions in urban open spaces. Application in the island of Crete. *Energy Convers. Manag.* 86, 250–258. <https://doi.org/10.1016/j.enconman.2014.04.059>
- UrbanGreenUp, 2018. Urban Green Up NBS Catalogue.
- US EPA, O., 2008. Reducing Urban Heat Islands: Compendium of Strategies Urban Heat Island Basics — Climate-ADAPT [WWW Document]. URL <https://climate-adapt.eea.europa.eu/metadata/publications/reducing-urban-heat-islands-compendium-of-strategies-urban-heat-island-basics> (accessed 4.22.20).
- van Ham, C., Klimmek, H., 2017. Partnerships for Nature-Based Solutions in Urban Areas – Showcasing Successful Examples. Springer, Cham, pp. 275–289. https://doi.org/10.1007/978-3-319-56091-5_16
- van Vuuren, D.P., Isaac, M., Kundzewicz, Z.W., Arnell, N., Barker, T., Criqui, P., Berkhout, F., Hilderink, H., Hinkel, J., Hof, A., Kitous, A., Kram, T., Mechler, R., Scrieciu, S., 2011. The use of scenarios as the basis for combined assessment of climate change mitigation and adaptation. *Glob. Environ. Chang.* 21, 575–591. <https://doi.org/10.1016/j.gloenvcha.2010.11.003>
- Vaz Monteiro, M., Doick, K.J., Handley, P., Peace, A., 2016. The impact of greenspace size on the extent of local nocturnal air temperature cooling in London. *Urban For. Urban Green.* 16, 160–169. <https://doi.org/10.1016/j.ufug.2016.02.008>
- Wang, Y., Li, Y., Sabatino, S. Di, Martilli, A., Chan, P.W., 2018. Effects of anthropogenic heat due to air-conditioning systems on an extreme high temperature event in Hong Kong. *Environ. Res. Lett.* 13, 034015. <https://doi.org/10.1088/1748-9326/aaa848>
- Watkin, Ruangpan, Vojinovic, Weesakul, Torres, 2019. A Framework for Assessing Benefits of Implemented Nature-Based Solutions. *Sustainability* 11, 6788. <https://doi.org/10.3390/su11236788>
- Wilson, J.D., 1988. A second-order closure model for flow through vegetation. *Boundary-Layer Meteorol.* 42, 371–392. <https://doi.org/10.1007/BF00121591>
- Yamada, T., 1982. A Numerical Model Study of Turbulent Airflow in and Above a Forest Canopy. *J. Meteorol. Soc. Japan. Ser. II* 60, 439–454. https://doi.org/10.2151/jmsj1965.60.1_439
- Yamada, T., Mellor, G., 1975. A Simulation of the Wangara Atmospheric Boundary Layer Data, *Journal of the Atmospheric Sciences*. American Meteorological Society. [https://doi.org/10.1175/1520-0469\(1975\)032<2309:ASOTWA>2.0.CO;2](https://doi.org/10.1175/1520-0469(1975)032<2309:ASOTWA>2.0.CO;2)
- YUE Wenze, 岳文泽, XU Lihua, 徐丽华, 2013. Thermal environment effect of urban water landscape. *Acta Ecol. Sin.* 33, 1852–1859. <https://doi.org/10.5846/stxb201112141915>
- Zaragoza, A., Bartolom, C., 2012. Albedo Effect and Energy Efficiency of Cities, in: *Sustainable Development - Energy, Engineering and Technologies - Manufacturing and Environment*. InTech. <https://doi.org/10.5772/29536>
- Zheng, D., Ducey, M.J., Heath, L.S., 2013. Assessing net carbon sequestration on urban and community forests of northern New England, USA. *Urban For. Urban Green.* 12, 61–68. <https://doi.org/10.1016/j.ufug.2012.10.003>